UNIVERSITA' DEGLI STUDI DI PAVIA

FACOLTA' DI INGEGNERIA
DIPARTIMENTO DI INGEGNERIA INDUSTRIALE E DELL'INFORMAZIONE

DOTTORATO DI RICERCA IN BIOINGEGNERIA E BIOINFORMATICA
XXXII CICLO - 2019

A PHYSIOLOGICALLY BASED PHARMACOKINETIC MODELLING FRAMEWORK TO SUPPORT INHALED DRUG DEVELOPMENT FROM THE EARLY TO THE LATE STAGES

PhD Thesis by

SILVIA GRANDONI

Advisor:
Prof. Paolo Magni

PhD Program Chair:
Prof. Riccardo Bellazzi

UNIVERSITA' DEGLI STUDI DI PAVIA

FACOLTA' DI INGEGNERIA
DIPARTIMENTO DI INGEGNERIA INDUSTRIALE E DELL'INFORMAZIONE

DOTTORATO DI RICERCA IN BIOINGEGNERIA E BIOINFORMATICA
XXXII CICLO - 2019

A PHYSIOLOGICALLY BASED PHARMACOKINETIC MODELLING FRAMEWORK TO SUPPORT INHALED DRUG DEVELOPMENT FROM THE EARLY TO THE LATE STAGES

PhD Thesis by
SILVIA GRANDONI

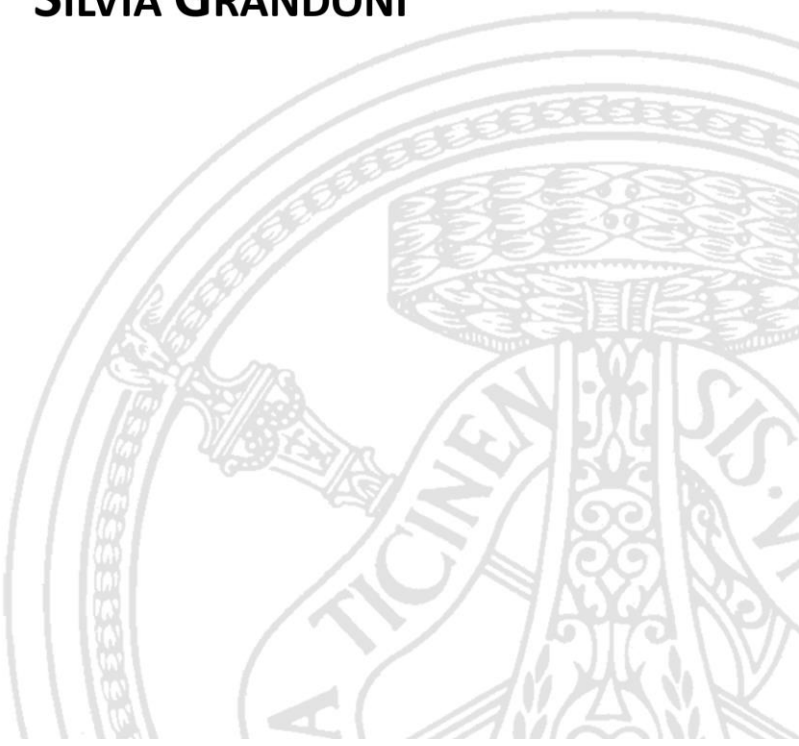

Advisor:
Prof. Paolo Magni

PhD Program Chair:
Prof. Riccardo Bellazzi

"To know how to wonder and question is the first step of the mind toward discovery".

L. Pasteur

Acknowledgments

What an incredible experience this PhD period! The years of several firsts, for me: first project, first office desk, first car, first flight, first conference, first intercontinental flight and intercontinental conference! These firsts have for me a special meaning, and the people close to me know why.

First of all, I want to express my gratitude to Prof. Paolo Magni, present in every step of this route, who believed in me from the beginning, a person of huge expertise, he motivates and supports the students as a father. It was lucky to have the opportunity of working with him.

Another thank you to the preclinical DMPK group members of Chiesi S.p.A, Dr. Nicola Cesari and Dr. Giandomenico Brogin, with whom I started this project, for their knowledge sharing.

An affectionate thought also for my colleagues, some of them companions of the firsts mentioned above, I wish them to achieve their personal goals.

A special thank you to Dr. Laura Matti, with her great professionalism gives me the instruments for fully experience my life.

Last but not least, the acknowledgments to my family.

The first thank you to my parents, Raffaella and Paolo, who continuously support me with infinite love and an endless courage and strength. They are always my safe haven.

Thank you also to my life partner Christian who always takes care of me with a naturalness and a joy that make me feel loved and protected every day.

Abstract (Italiano)

Il processo di ricerca e sviluppo di un farmaco è estremamente lungo e complesso ed ha come obiettivo di fornire delle terapie sicure ed efficaci ai pazienti nel più breve tempo possibile.
L'industria farmaceutica è alla continua ricerca di strategie per ottimizzare tale processo, cercando di predire con anticipo quali composti hanno la maggiore probabilità di fallire e di consentire ai candidati più promettenti di proseguire nello sviluppo in modo veloce ed efficiente.
A tale scopo, le aziende stanno sempre più frequentemente adottando l'uso di modelli matematici lungo l'intero processo di sviluppo, questa strategia è stata definita dalla comunità scientifica come *Model Informed Drug Disvovery and Development* (MI3D). Questo lavoro, svolto durante il Dottorato di Ricerca, si colloca nel contesto del MI3D per supportare lo studio della farmacocinetica dei composti somministrati per inalazione con azione locale, durante tutto il processo del loro sviluppo. Per farmacocinetica si intende lo studio dell'assorbimento, distribuzione, metabolismo ed escrezione.
L'uso della via inalatoria è ormai ben consolidato ed ha numerosi vantaggi nel trattamento locale delle patologie dell'apparato respiratorio, infatti, consente di ottenere alte concentrazioni nel tessuto target, rapidità di azione e di ridurre l'esposizione sistemica associata ad effetti indesiderati. Lo studio della farmacocinetica dei composti somministrati per inalazione è più complesso rispetto alle vie di somministrazione più comunemente usate quali quella orale o intravenosa. Il suo obiettivo è determinare la relazione tra la dose somministrata, la concentrazione

del farmaco nel tessuto polmonare e quella in un fluido facilmente accessibile quale il sangue, che viene generalmente campionato in tali studi.
Sfortunatamente, la misurazione dell'esposizione polmonare è difficilmente realizzabile, ma particolarmente importante per studiare la farmacocinetica e come questa influenza la farmacodinamica, ovvero la relazione quantitativa tra la concentrazione del farmaco e la risposta farmacologica.
Tra gli approcci di modellistica possibili, uno in particolare ha le caratteristiche per poter essere applicato durante tutte le fasi di sviluppo dei farmaci inalatori, quello basato sulla fisiologia, chiamato Physiologically Based Pharmacokinetic (PBPK) modelling. In esso, l'organismo è descritto come una serie di compartimenti che corrispondono ad organi e tessuti, connessi dalla circolazione sanguigna e l'andamento nel tempo della concentrazione del farmaco in ciascuno di essi è descritto attraverso bilanci di massa. Questo significa che possono essere utilizzati per descrivere e predire la concentrazione nel polmone, che è all'atto pratico difficilmente monitorabile. Inoltre, la loro struttura consente di integrare diverse informazioni composto-specifiche e fisiologiche man mano che queste diventano disponibili.
Lo scopo di questo lavoro è lo sviluppo di un framework basato su modelli PBPK per predire la farmacocinetica *in vivo* dei composti somministrati per inalazione, nel ratto e nell'uomo, che possa essere applicato sin dalle prime fasi di sviluppo, sfruttando le informazioni *in silico* e *in vitro* che vengono tipicamente ottenute negli stadi iniziali di ricerca per la loro caratterizzazione.
Nel Capitolo 1, saranno presentate una panoramica sullo sviluppo del farmaco e un'introduzione al sistema respiratorio, necessaria per comprendere il ruolo dei farmaci inalatori e la loro farmacocinetica. Saranno inoltre riportate le principali problematiche legate allo

studio di quest'ultima e come i modelli PBPK possono supportarlo.
Nel Capitolo 2, lo sviluppo e la valutazione di un modello PBPK, per simulare somministrazioni intravenose e orali in due specie precliniche e nell'uomo, saranno mostrati. Esso sarà la base per una successiva integrazione di un modello polmonare basato sulla fisiologia che consenta di simulare somministrazioni inalatorie.
Nel Capitolo 3, sono presentati il modello polmonare e la validazione del modello PBPK finale, con esso integrato, per predire la cinetica *in vivo* dei composti inalatori, in polmone ed in plasma, nel ratto. Nel Capitolo 4, viene invece presentata la valutazione del modello per la predizione della farmacocinetica dopo inalazione nell'uomo, su volontari sani e, come per il ratto, a partire dalle informazioni *in silico* e *in vitro* sui composti, ottenute nelle prime fasi di sviluppo. Nel Capitolo 5 sono invece riportate le conclusioni del lavoro.

Abstract (English)

Drug research and development is a long, complicated and expensive process with the aim of bringing safe and effective new treatments to patients as fast as possible. Pharmaceutical companies are making efforts to optimize this process, predicting in advance compounds with high probability of failure and making the development of the most promising candidate drugs faster and more effective. In order to address this issue, they are continuously increasing the use of modelling and simulation along the entire drug development process, this strategy has been defined as *model informed drug discovery and development* (MI3D). In this context, this PhD work deals with the application of mathematical modelling approaches to support the study of the pharmacokinetics (PK) i.e., the study of absorption, distribution, metabolism, and excretion, of locally acting inhaled drugs during their development.

Drug delivery by inhalation has been a well-established practice over the years and remains an interesting route of delivery for local treatment since it allows the obtainment of high concentrations in the target tissue, the lung, rapid action and the reduction of the systemic exposure, generally associated with undesired effects.

The study of the PK of inhaled drugs presents a greater number of challenges compared to other popular routes of administration such as intravenous (IV) and oral (PO). Its goal is to understand the relationship between the delivered dose, the drug concentration at the site of

action and that in an easily accessible fluid such as blood. Unfortunately, measuring the pulmonary exposure is technically challenging since the lung tissue is not easily accessible, even if it is important to understand the PK and how it influences the pharmacodynamics (PD), i.e. the quantitative relationship between the drug concentration and the pharmacological response.

Among the existing modelling approaches, one has a great potential of being applied along the whole development process of inhaled drugs: Physiologically Based Pharmacokinetic (PBPK) modelling. In PBPK models, the living organism is described as a set of compartments corresponding to organs and tissues, connected by the blood circulation, in which the time course of the drug concentration is described as a series of mass balance equations. This means that PBPK models can be used to describe and predict the inhaled drug concentration in the hardly accessible lung tissue. Furthermore, their structure allows to integrate several drug-specific and physiological information as they become available during the drug development.

The aim of this PhD work is to build and evaluate a PBPK modelling framework that can be applied from the early stages of drug development, to predict *in vivo* lung and plasma disposition of orally inhaled compounds in rats and in man, from the *in vitro* and *in silico* information routinely collected at the beginning of the development process.

In Chapter 1, after an overview on the drug discovery and development, an introduction to the respiratory system, necessary to understand orally inhaled therapeutics and their PK, is presented. The main challenges related to the study of the PK and how PBPK models can help with this are also reported. In Chapter 2, the development and evaluation of a PBPK model representing the whole organism, to simulate IV and PO administrations in two preclinical species and

in man, is presented. It constitutes the base for the subsequent integration of a physiologically based pulmonary model to study the PK of inhaled drugs. In Chapter 3, the pulmonary model and the evaluation of the final whole body PBPK model to predict the lung and plasma PK of inhaled drugs in rats, are presented. In Chapter 4, its ability to prospectively predict the plasma PK in healthy volunteers has been evaluated, given the model structure previously defined and, as for rats, the *in silico* and the *in vitro* drug-specific information collected during the early stages of drug development. In Chapter 5 the overall conclusions are reported.

Contents

List of Abbreviations

ACAT	Advanced Compartmental Absorption model
ADMET	Absorption Distribution Metabolism Excretion Toxicity
AUC	Area Under Curve
B	Bell
BCS	Biopharmaceutical Classification System
BP	Blood to Plasma Ratio
BW	Body Weight
C	Central
DPI	Dry Powder Inhaler
ELF	Epithelial Lining Fluid
EMA	European Medicine Agency
ET	Extra Thoracic
EV	Extra Vascular
FDA	Food and Drug Administration
FE	Fold Error
FIH	First In Human
FPE	First Pass Effect
FPF	Fine Particle Fraction
GI	Gastrointestinal
GSA	Global Sensitivity Analysis
GSD	Geometric Standard Deviations
HLM	Human Liver Microsomes
HPGL	Hepatocytes per Gram of Liver
HR	Highly Retained
HS	Highly Soluble
IT	Intratracheal
IV	Intravenous
IVIVE	In Vitro In Vivo Extrapolation

LTB	Lung Tissue Binding
MBDD	Model Based Drug Development
MDI	Metered Dosed Inhaler
MI3D	Model Informed Drug Discovery and Development
MMAD	Mass Median Aerodynamic Diameter
MPPGL	Milligram of Protein per Gram of Liver
MRT	Mean Residence Time
MW	Molecular Weight
NB	Narrow Bell
NCA	Non Compartmental Analysis
P	Peripheral
PBPK	Physiologically Based Pharmacokinetic
PD	Pharmacodynamics
PK	Pharmacokinetics
pMDI	pressurized Metered Dosed Inhaler
PO	Per Os, Oral
PPB	Plasma Protein Binding
PR	Poorly Retained
PS	Poorly Soluble
PSD	Particle Size Distribution
SDDPI	Single Dose Dry Powder Inhaler
SLF	Simulated Lung Fluid
SLFB	Simulated Lung Fluid Binding
TEER	Transepithelial Electrical Resistance
THL	Terminal Half Life
UL	U shaped Left skewed
UR	U shaped Right skewed
US	U Shaped
VASC	Vascular

List of Figures

List of Tables

Chapter 1

Introduction

1.1. Drug discovery and development

Drug discovery and development is a long, complicated and expensive process with the aim of bringing safe and effective new treatments to the patients. The entire process can be divided into different phases [1], as summarized in Figure 1-1, however, the entire process is highly integrated, with overlap and sharing of information across the various phases [1] that are described hereinafter.

Figure 1-1 The drug discovery and development process.

A drug *discovery* program begins when for a disease or medical condition suitable medical products do not

exist or they are not satisfactory. To justify a drug discovery effort, in a pre-discovery phase, the disease or condition is studied and basic research activities are performed in order to develop the hypothesis that the inhibition or activation of a certain protein or pathway will elicit a therapeutic effect. In the first phase of drug discovery, the so-called *target identification*, scientists work to find a target. A good target must be efficacious, safe and "druggable", i.e., accessible to the compound and upon binding it must produce a biological response. Subsequently, screening assays are developed and used for the identification of compounds with a desired activity at the target, called "hits", this is the *hit identification* phase. During the *hit to lead* phase compounds are further evaluated and go through a series of tests to obtain information regarding Absorption, Distribution, Metabolism, Excretion and Toxicological (ADMET) properties and efficacy on the target. The studies are performed *in vitro*, some properties are evaluated in living cells and via computational models. Furthermore, they undergo to first refinements to produce more potent and selective compounds. In the subsequent *lead optimization* phase, the selected lead compounds are optimized to make them more effective and safer.

After the discovery process has taken place, the most promising compounds are tested in the *preclinical phase*: this is the first *in vivo* phase, with the aim of narrowing the candidate selection for subsequent evaluations in human. The compounds are tested in animals with the main aim of assessing the PK [2] and *in vitro* studies on human cells fractions or cultures are conducted. Scientists test compounds to obtain early *in vivo* information on efficacy and toxicity, the lack of these elements is considered to be the major reason for drug failures and the PK governs them to a large extent

[3]. Subsequently, during the *clinical phase* candidates are tested in human, in three different stages:

- *Phase I*: in this step the first administration in human takes place. This phase is typically conducted in healthy volunteers, in some case, if it is not possible such as in oncology, in patients. The goal is to obtain information on human tolerability and safety, hence, studies on maximum safe doses and concentrations are made. Preliminary estimates about the inter-subject variability can be obtained. Investigations on the PD, to address the proof of therapeutic concept may be also possible during this phase, using clinically relevant biomarkers.
- *Phase II*: in the first part called "II A" the main aim is to confirm the efficacy and the affirmation of safety and tolerability in patients. Maximum safe dose and plasma concentration are obtained. In the second part "II B", the evidence of efficacy is still investigated and the dosing regimen that will be administered in the larger cohort of patients in Phase III are explored.
- *Phase III*: this is a confirmatory phase, in which a larger number of patients is enrolled to provide evidence of clinical efficacy and to define a more complete profile of adverse reactions. Studies on variability in dose response due to both PK and PD are investigated to understand their sources. The information can help to define dosing regimens in special populations (e.g. patients with renal or hepatic impairments, elderly).

Before placing on the market, the drug must be approved by regulatory agencies such as European Medicine Agency (EMA) in Europe and Food and Drug

Administration (FDA) in USA. This involves several interactions between companies and agencies, that start during the development process and lead to a final submission of standardized detailed reports, containing information related to the performed studies. Regulatory reviews generally take place just before first administration to human (volunteers or patients), at the end of Phase II and III, prior to submission, but also intermittently after the drug is marketed [1].
After the approval and the launch on the market, there is the so-called *Phase IV* or *post-marketing surveillance*, the study continues, monitoring the population using the drug to evaluate long-term safety (e.g. with the adverse reaction reporting) and effectiveness.

1.2. Model informed drug discovery and development

As stated above, the drug discovery and development process requires long time and high costs. It spans from 12 to 15 years [4] with an estimate of post-approval R&D cost of about $2.8 billion, with a growth from the estimates obtained in previous studies [5]. The attrition rates are high, with an average success rate for all therapeutic areas of about 11%. The reported failure rate of compounds even at the registration stage is 23%, this means that approximately one of four compounds fails after all the trials and the full discovery and development costs incurred [6]. Therefore, pharmaceutical industries are making efforts to optimize this process, predicting in advance compounds with high probability of failure and making the development of the most promising candidate drugs faster and more effective.
The use of modelling and simulation strategies across

different fields is well accepted and the benefit in its introduction has been documented [7], it is also included in the drug discovery and development process, but has been of relative late adoption. Pharmaceutical companies are continuously increasing the use of modelling and simulation, that has been defined as "model based drug development" (MBDD) and more recently the term "model based discovery" has been introduced. This definition has been changed in the last years into *model informed drug discovery and development* (MI3D), to address the potential negative connotation of the model-based activities such as their use as a substitute of the decision maker. MI3D refers to the "application of a wide range of quantitative models aimed at improving the quality, efficiency and cost effectiveness of decision making" during drug discovery and development through "fit-for-purpose data analysis and prediction" [8]. This quantitative framework has been shown to play a strategic role in optimizing the whole process through the *learn and confirm* paradigm. The MI3D learn and confirm paradigm is shown in Figure 1-2.

As a first step, the determination of questions to be addressed with modelling is essential to start in order to understand which data and information are needed (e.g. disease mechanism information). Models are used to describe the relationship between independent variables (e.g. time, dose), dependent variables (e.g. drug, concentration, disease state) and covariates (e.g. demographics, comedications, genetic factors) with mathematical equations. To inform this relationship, knowledge about pathology, physiology, pharmacology can be used as well as statistical assumptions for the absence or limitation of data. The assumptions made need to be evaluated and if the model does not describe adequately the experimental data alternative

assumptions or models can be considered and subsequently evaluated in an iterative process.

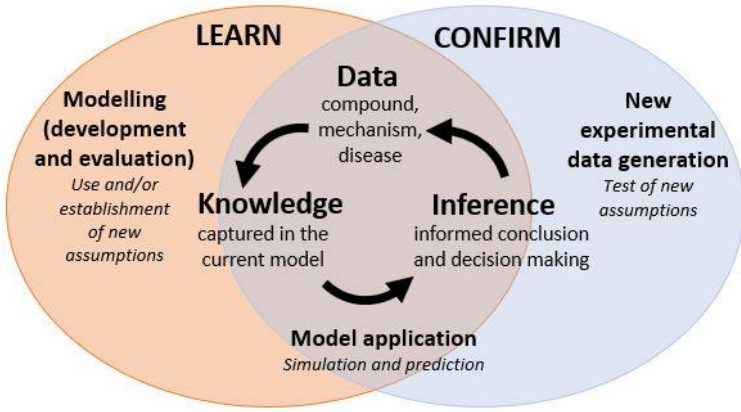

Figure 1-2 The learning and confirm paradigm in MI3D.

The questions that modelling addresses deal with many of the issues that arise during the whole drug discovery and development process [8] such as:

- *Pharmacokinetics characterization*: ADME study in a certain species and extrapolation across different species (e.g. preclinical to man) or populations (e.g. pediatric, elderly, impaired) to understand how elements like the drug formulation, the drug administration, demographics and disease state can impact on it.
- *Safety/Tolerability characterization*: study of the dose-exposure-response relationship for safety/tolerability outcomes in a certain species, population and extrapolation to other species and populations.
- *Efficacy characterization*: study of the dose-exposure-response relationship for efficacy outcomes in a certain species population and extrapolation to other species and populations.

- *Benefit/Risk studies*: definition of the therapeutic window, study of the optimal dosing regimens that allow to obtain safe and effective treatments defining and quantifying the trade-off between the safety and efficacy, integrating information from the preclinical phase and early clinical data.
- *Dose schedule selection*: definition of optimal doses and dosing regimens. Definition of alternative doses or dosing regimens, even in situations when additional confirmatory studies are difficult to conduct or require long time period that can delay the obtainment of new treatments.
- *Study design optimization*: increasing the efficiency and reducing costs, studying appropriate sample size, collecting relevant data at optimal time points to maximize the amount of information that can be achieved.

The result of a recent survey [8], targeted to clinical pharmacologist, pharmacometricians in industries and the regulatory agencies FDA and EMA, reveals that industry applications of MI3D deals mainly with PK studies, followed by efficacy, safety outcomes, study/program design, and benefit-risk assessment regulatory submissions [9], [7].

The use of the evidence generated from MI3D in regulatory submissions is rapidly increasing to the point where there is a growing interest in publication of good practices related to MI3D and in 2019 a paper [8] was published to investigate whether the industry good practice matches with regulatory expectation and to understand the current and future viewpoints on the role of MI3D in research development and regulatory review.

In summary, MI3D assists decision making along all

the phases of the drug discovery and development process, supporting internal decisions in the transitions between the different developmental phases, increasing confidence in investments, furthermore it supports labelling and inform regulatory submission.

1.3. Inhalation as a route for drug delivery

Drug delivery by inhalation has been a well-established practice over the years and remains an interesting route of delivery [10]. Essentially, a drug can be delivered via the pulmonary route for two reasons: for *local treatment* and for *systemic treatment*.
In case of *local treatment*, the objective is to obtain high concentrations in the lung tissue, rapidity of action if needed and to reduce the systemic exposure, generally associated with side effects. Indeed, this route, allows the direct application of the drug to the target tissue, that enables a rapid therapeutic response, that allows to have a similar or superior therapeutic effect at a fraction of the dose administered with other routes of administration such as the IV or the PO one [11]. In the latter case, after the oral ingestion, the action of the first pass effect (FPE) due to the drug metabolism in the liver and in the gut can reduce the systemic concentration of the drug, limiting the lung exposure via the systemic circulation. A schematic representation of how the drug can reach the lung via different routes of delivery is reported in Figure 1-3.
Examples of diseases typically treated with locally acting inhaled therapeutics are the respiratory ones such as asthma and chronic obstructive pulmonary diseases COPD [12]. Asthma is a lung disease that causes inflammation and narrowing of the airways, with recurring periods of wheezing (a whistling sound during

breathing), chest tightness, shortness of breath and coughing.

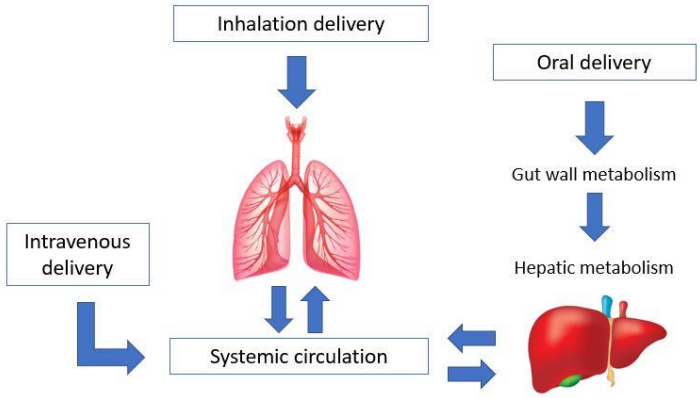

Figure 1-3 Different routes of administration and the related paths towards the lung. In this schema, the part of inhaled drug that can be swallowed undergoing to gastrointestinal absorption is neglected.

The inflammation process makes the airways swollen, very sensitive with a tendency to react strongly to certain inhaled substances, with an over production of mucus [13]. Instead, COPD is a progressive disease that causes difficulties in breathing for the reduced airflow, due to the loss of tissue elasticity in the respiratory tract that expands during inspiration to accept air, to the reduced surface available for the gas exchange and to the thickening and clogging of the airways walls for an excessive mucus production [14].

The inhaled route represents an attractive also for systemic treatment and has been investigated as a "needle-free" alternative for systemic drug administration. Its advantages lie in the anatomical and physiological characteristics of the lung such as the large surface area, the thin tissue barrier and the high vascularization level in the deepest part of the respiratory system (which allow the gas exchanges to take place) permitting a fast absorption. Furthermore,

the low local enzymatic activity and the avoidance of the FPE, prevent a reduction of the systemic drug concentration (in this case associated with both safety and efficacy). Examples of systemic administration by inhalation deal with anesthesia [15] (whose employment began in 1840s), with pain treatment and more recently with the treatment of type I and type II diabetes, in fact, in 2006, FDA and EMA approved the fast acting inhaled insulin Exubera (that was withdrawn in less than two years due to inadequate sales) [12].

1.4. The respiratory system

Knowledge about the anatomy of the respiratory system is crucial to understand and predict the PK and the PD of inhaled drugs, hence, an overview on the human one is here reported. Since in this research a mathematical model to predict the preclinical PK in rats was developed, a brief mention on the main differences between the human and the rat respiratory system is reported.

The human respiratory system can be divided in two functional zones: the conducting airways and the respiratory region [16].

The conducting airways begins with mouth and nose and comprise the trachea, bronchi bronchioles and terminal bronchioles. A representation of the conducting airways can be seen in Figure 1-4. Their role is to transport gasses to the respiratory region, furthermore they ensure that they are heated, humidified and purified to provide to the alveolar region air with similar conditions to those already present. The nose begins this process, indeed, during nasal breathing temperature and humidity adjustments take place at the nostrils and the air is filtered passing through the hair called vibrissae, then, air passes in the

nasal cavity, mostly coated with the respiratory mucosa, whose pseudostratified ciliated epithelium is covered with a mucous layer secreted by goblet cells and seromucosal glands located in the underlying connective tissue. In the nasal cavity the air is further cleaned, warmed and moistened, the mucus catches the foreign particles that once trapped, are removed by the ciliary beat toward the pharynx to be swallowed, this mechanism is called nasal mucociliary clearance.

When the airstream leaves the nasal cavity, it reaches the upper part of the pharynx, called nasopharynx, and continues vertically through the oral region of the pharynx (oropharynx) and then in the larynx and trachea. The respiratory mucosa of the nasal cavity continues into the nasopharynx and where the oropharynx and the larynx cross is substituted by a squamous epithelium.

The larynx is an air passage used for phonation, hence, it contains the vocal cords, furthermore, it contains epiglottis that prevents the food entering in the tracheal tube, since in the oropharynx the air flux crosses the food ingested and the epiglottis closes the laryngeal tube during swallowing.

The trachea is a cartilaginous tube that originates at the base of the larynx and ends at the carina where a bifurcation generates the two primary bronchi of each lung as can be seen in Figure 1-4. Not perfectly cylindrical, the trachea is flattened posteriorly and very mobile, it can extend and shorten rapidly. The inner part of the trachea, the mucosa, is in contact with the airspace and is similar to those of the lower part of the pharynx and of the bronchi. Trachea is lined by pseudostratified columnar epithelium, mainly populated by ciliated and goblet cells. Goblet cells (as submucosal glands) allow mucus formation with the production of high molecular weight glycoproteins, called mucins. Mucus is a viscoelastic gel consisting of water, mucins,

mixed with serum and cellular proteins and lipids [17], it is populated by dead cells, granulocytes, lymphocytes and a great number of macrophages. Ciliated cells are covered by mucus and their cilia transport it toward the pharynx. They are responsible for the important defense mechanism *called pulmonary mucociliary clearance*: foreign particles entering the respiratory system through the airstream can be trapped in the mucus and transported toward the oropharynx by the ciliary beating, where they can be eliminated by sputum or swallowed.

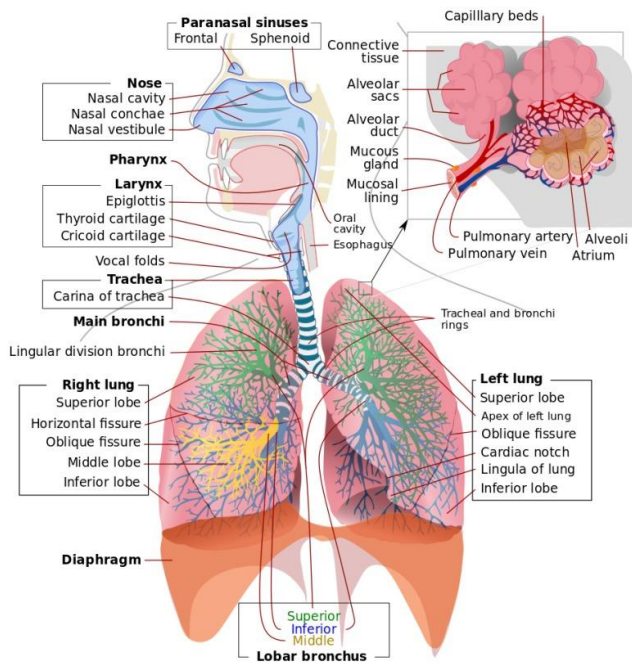

Figure 1-4 A representation of the entire human respiratory system [18].

The trachea divides at the carina into two branches called *primary bronchi*, that further divide in a dichotomous manner (with some exceptions) into daughter branches, called *bronchi,* with reduced diameter and thinner walls in a tree-like structure, this

branching allows a progressive increase in the surface area and a decrease in air speed. The tissue composition changes with branching with a decrease in the presence of cartilage and an increase of smooth muscle cells and elastic tissue.
When the diameter reduces to 1 mm and the cartilage plates disappear the airways are called *bronchioles*. The tissue composition of this airway's tract changes: the cartilage disappear, ciliated and non-ciliated cells are present, among this latter there are Clara cells, that replace the secretory cells such as the goblet ones. The Clara cells are responsible for the enzymatic degradation of xenobiotics that reaches the respiratory system. The bronchiolar epithelium is covered by respiratory mucosa and the mucociliary clearance mechanism is still present. The bronchioles further divide and form the *terminal bronchioles* that constitute the distal and smaller part of the conducting airways [19].
The *respiratory region* is the part of the respiratory system in which the gas exchanges take place. It consists of respiratory bronchioles, alveolar ducts and alveolar sacs.
The *respiratory bronchioles* structure is similar to that of the terminal bronchioles, but their walls are interrupted by the presence of the *alveoli*, sac-like structures, that represent the functional units of the respiratory system, their very thin walls allow the gas exchange. A representation of the difference in the wall thickness along the different respiratory tracts is reported in Figure 1-5.
Proceeding with the bifurcation the number of alveoli increases and the diameter decreases. Each respiratory bronchiole ends with an *alveolar duct*, that is a linear rearrangement of the alveoli, from their branching structures called *alveolar sacs* originate, they are composed of a small group of alveoli. The alveolar

epithelium is very thin and composed of two types of cells: type I pneumocytes, that represent about the 95% of the alveolar surface and type II pneumocytes that produce a substance called *surfactant* [20], whose role is to enhance lung compliance during inspiration, reducing the work of breathing and to reduce the alveolar surface tension at end expiration, avoiding a condition in which the alveoli collapse, called atelectasis. The surfactant is composed of 90% of lipids, most of them phospholipids and by about 10% of proteins [21]. The alveolar region is also populated by macrophages, that phagocyte foreign particles and eliminate them by different mechanisms such as enzymatic degradation, migration toward the bronchial region where they are transported by the mucociliary clearance or entering the lymphatic system.

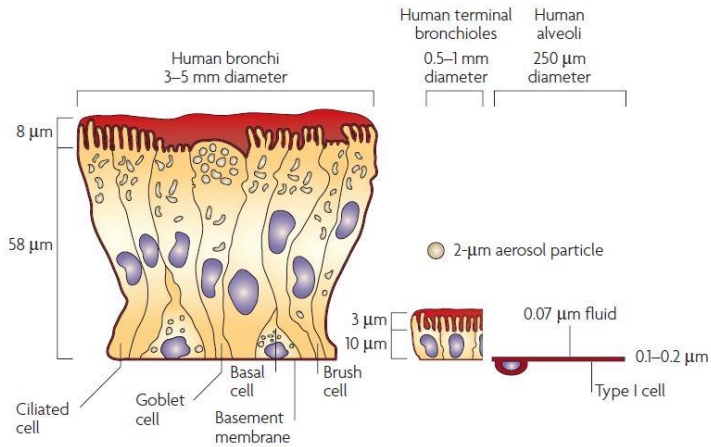

Figure 1-5 A representation of tissues in the different tracts of the respiratory system [22].

The respiratory region is supplied by an extremely rich capillary network whose blood is provided by the pulmonary artery and drained by the pulmonary vein.
As mentioned before the gas exchange takes place here, during inspiration oxygen molecules enter the respiratory system and pass through the conducting airways up to the alveolar spaces. The alveolar surface

is very large and since it is in contact with a huge number of capillaries, the available exchange surface is very large. Oxygen molecules diffuse through the blood-gas barrier, reach the capillary lumen and bind to hemoglobin of the erythrocytes forming oxyhemoglobin.

Through the *pulmonary circulation* deoxygenated blood can be oxygenated, coming from the right ventricle of the heart and carried by the pulmonary artery. Gas exchange in the respiratory system, as per other diffusion driven processes is concentration dependent and driven by different partial pressure of gases in blood and in the alveoli. Higher partial pressure of oxygen in the alveoli allow its diffusion in blood and the binding to hemoglobin. Oxygenated blood reaches the left atrium of the heart through the pulmonary vein. The *systemic circulation* allows the entire body oxygen supply, pumping the blood through the aorta.

A graphical representation of the pulmonary and systemic circulation is reported in Figure 1-6.

Oxygen moves from hemoglobin to tissues where its partial pressure is lower and can be used for metabolism. When carbon dioxide is produced due to metabolism, by the same difference of partial pressure driver, it is transferred to blood. Deoxygenated blood is carried by the vena cava to the right atrium and then to the right ventricle, from here it is pumped through the pulmonary artery and enters the pulmonary circulation to give the carbon dioxide and be oxygenated [19]. Carbon dioxide molecules leave the blood and, diffusing through the blood-gas barrier, leave alveolar spaces during inspiration.

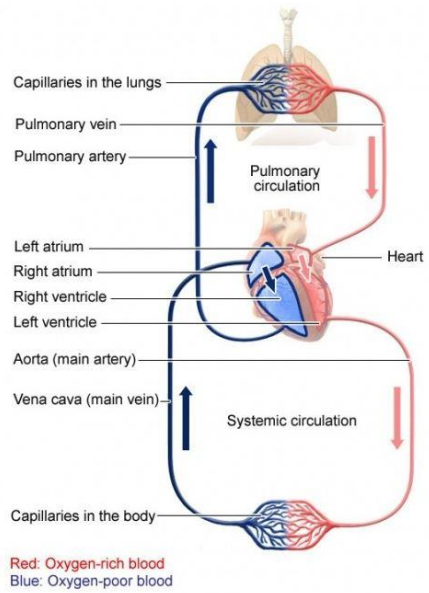

Figure 1-6 A representation of the pulmonary and systemic circulation [23].

The rodent's respiratory system

The rodent's respiratory system is similar to that of human, the division in conducting airways and respiratory region is still possible, the airway epithelial cell types present are substantially the same in rat and human (e.g. ciliated, goblet cells) but with different densities. In particular the cell composition of the bronchioles and alveolar septa is highly similar in the two species [24]. Some differences exist related to the morphology of the tree-like structure of the conducting airways that in rats is monopodial while in human is almost regular dichotomous, [25], a graphical representation of the different possible branching patterns is reported in Figure 1-7.

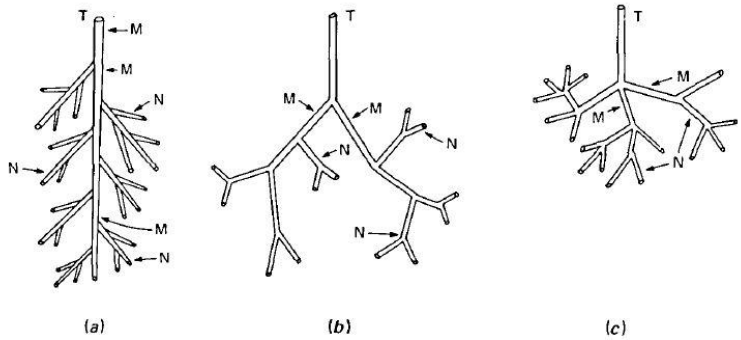

Figure 1-7 different branching patterns of the respiratory system: (a) monopodial, (b) regular dichotomous, (c) irregular polychotomous [25].

Another morphological difference concerns the transition from the conducting airways to the respiratory region, indeed, while in human this transition is smooth due to the presence of the respiratory bronchioles, in rodents the most distal zone of the conducting airways is composed of the terminal bronchioles, from which sharply open alveoli [26].

1.5. Orally inhaled drugs

Since this work deals with the development of a PBPK framework to be used in the context of inhaled drugs for topical treatment of diseases such as asthma and COPD, a brief overview on the main categories of orally inhaled drugs and on the devices for drug delivery is reported here.

The well-established treatment options for such diseases include drugs such as corticosteroids, β-agonists and anticholinergics [27].

Herein is briefly reported their mechanisms of action.

To elicit their action, corticosteroids, need to bind to the glucocorticoid receptor, located in the cytosol, forming a steroid–glucocorticoid complex. Once

activated this complex translocates from the cytosol to the nucleus of the cell where it exerts its primary anti-inflammatory effects, binding to glucocorticoid response elements (GREs), which are specific DNA sequences, this leads to the repression of pro-inflammatory cytokines and proteins gene transcription and to the up-regulation of anti-inflammatory proteins production [28].

The β2-adrenoceptor agonists, instead, exert their biological effects through cell surface β2-adrenoceptors that may be found throughout the airways on the epithelium and smooth muscle, whose greatest concentration may be found in the alveoli. The ligand binding to the active site of the receptor leads to the production of intracellular cyclic adenosine monophosphate (cAMP), and the subsequent activation of protein kinase A (PKA), which in turn phosphorylates a number of intracellular regulatory proteins [28]. The physiological responses associated with this mechanism, include bronchodilation via smooth muscle relaxation, stimulation of cells secretions, increase in ciliary beat frequency, inhibition of pro-inflammatory mediators release from lung mast cells and neutrophils, prejunctional inhibition of acetylcholine release from parasympathetic neurons in airway smooth muscle [29]. In the lungs, release of acetylcholine from parasympathetic nerves regulates the airways tone, the airway smooth muscle contraction, mucus secretions, and vasodilation through interactions with M-receptors on the airway smooth muscle, glands, and the pulmonary vasculature. The action of the anticholinergic agents resides proper in the block of M1 and M3 muscarinic receptors, reducing smooth muscle tone and leading to bronchodilation [30].

Concerning the devices for drug inhalation, three distinct categories of delivery systems exist including nebulizers, pressurized metered dose inhalers (pMDIs),

and dry powder inhalers (DPIs). Nebulizers, that have a long history for drug delivery can be defined in terms of "an aqueous solution or suspension formulation, an aerosol generating device, and an energy", the drug present in form of solution or suspension is nebulized by compressed air or ultrasounds and delivered to the patient through a mouthpiece or a ventilation mask. pMDIs (pressurized Metered Dose Inhalers) are devices wherein the drug is formulated in a volatile propellant such as hydrofluoroalkane (HFA) or chlorofluorocarbon (CFC). Upon activation, with the ejection of the propellent, an amount of the drug is delivered to the lung. Dry Powder Inhalers (DPIs), in contrast to pMDIs, are passive devices that do not include propellants, hence, the patients respiratory effort is required to disperse the drug powder and incorporate it into an airstream to be inhaled [31].

1.6. The fate of inhaled drugs

Compounds delivered by inhalation are involved in several complex mechanisms whose knowledge is essential to understand their PK. Essentially, a compound delivered by inhalation, once reached the respiratory system, deposits, dissolves in the pulmonary fluids and then can be absorbed in the blood circulation, furthermore, can be involved in several clearance mechanisms as shown in Figure 1-8. These mechanisms will be described hereinafter.

In this work *lung PK* refers to lung processes prior to the absorption in the blood circulation while *systemic PK* refers to the PK after this process occurred [32].

Once inhaled, only a certain fraction of the drug is subject to *deposition* in the respiratory system, indeed, in part can be exhaled. Another part undergoes oropharyngeal deposition and can be swallowed and

absorbed through the gastrointestinal (GI) route, with a limitation in the lung exposure and a possible increase in the systemic drug exposure. The deposition is influenced by many factors such as lung morphology, breathing patterns and particle properties. Concerning particles properties their size, in particular their aerodynamic diameter (d_{ae}) influence the deposition, it is defined as the diameter of a sphere with standard density that settles at the same terminal velocity of the particle of interest, this size measure includes particle density and shape [33].

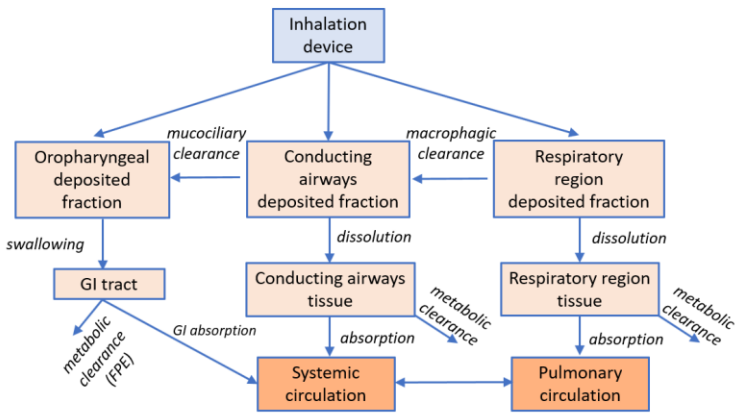

Figure 1-8 A schematic representation of the main PK processes associated with inhalation.

It is known that particles greater than 5-7 µm are deposited predominantly in the oropharyngeal zone by impaction, particles between 1 and 5 µm belong to the ideal range to allow lung deposition and particles under 1 µm do not deposit in the respiratory system because they are exhaled [27]. The main physical mechanisms associated with deposition are the following: inertial impaction, sedimentation, diffusion.

Impaction involves the larger (> 5 µm) and faster particles, unable to follow the air streamline due to

inertia, typically occur in the curvature when the airflow is deflected, in the upper tract of the conducting airways.

Sedimentation occurs in the lower bronchial region where the slower airflow imposes a weak dragging force compared to gravity, hence, the particle deposits. Typically, particles between 0.5 and 2 µm are involved in this mechanism.

Diffusion by Brownian motion increases with the decreasing in particle size and in air speed and for this reason it is relevant in the alveolar region where the air speed is reduced, it is known that particles under 0.5 µm of diameter are subject to this mechanism [31]. A representation of mechanisms acting predominantly in each zone of the respiratory system is reported in Figure 1-9, in which the number of generations, i.e. the levels of bifurcation of the respiratory tree are also reported.

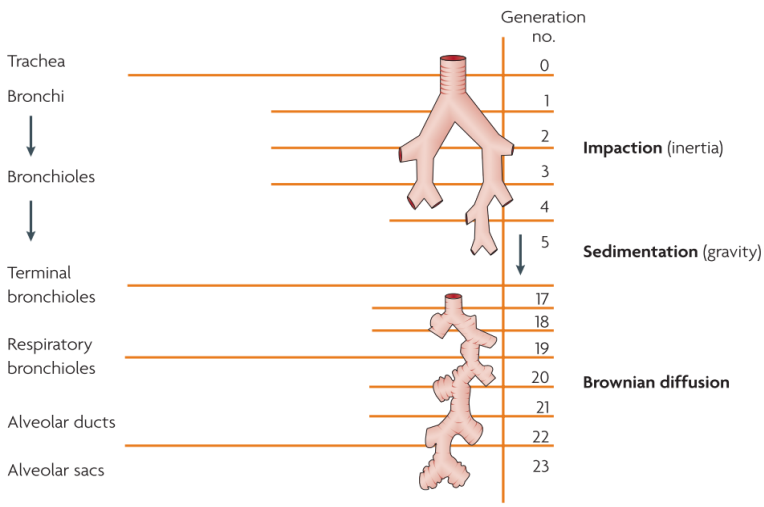

Figure 1-9 Different contributions to the deposition in the respiratory system [22].

Deposition is recognized as a relevant mechanism that impacts on both the lung and systemic PK, [32] indeed, as an example, more oropharyngeal deposition reduces

the lung exposure, furthermore, due to the heterogeneity in the respiratory system, different deposition patterns may lead to a different drug disposition, as will be explained subsequently. Since the respiratory system is one of the areas of the organism with the highest level of contact with the external environment is provided with a series of defense mechanisms to prevent the particle entering in the organism, such as cough, mucociliary clearance and macrophagic clearance (more relevant for undissolved particles [32]) furthermore foreign substances can be eliminated by the pulmonary metabolic clearance [11] (after dissolution takes place). As explained in Section 1.4 the *mucociliary clearance* acts on particles deposited on the airways mucus layer, that are transported by the ciliary beating toward the pharynx, where they can be subsequently swallowed. Mucus velocity increases from the peripheral toward the central airways, decreases with age in healthy individuals and can also be affected by airway diseases [31]. *Macrophagic clearance* acts in the alveolar region, transporting particles toward the mucociliary escalator, translocating them in the tracheobronchial lymph or by internal enzymatic degradation, these clearance processes typically act on slowly dissolving particles.

Once deposited, particles have to dissolve to be absorbed through the lung tissue. *Dissolution* depends on the properties of compounds such as lipophilicity, solubility, area of the solid-liquid interface.

Concerning solubility it depends on compound, on the formulation and physical form of the drug, as well as on composition of the dissolving media (the epithelial lining fluid, ELF), [31]. The dissolution in the lung is complex due to the heterogeneity of the respiratory system, indeed, elements controlling the dissolution vary along the respiratory system, generating different

dissolution profiles in parallel. An example of this heterogeneity regards the composition of the ELF: mucus in the airways is mainly composed of water while the surface lining fluid of the alveolar region is composed mainly by phospholipids and proteins.
Once dissolved, the drug undergoes the *absorption* process. To reach blood it has to cross the epithelium, its basement membrane, the interstitium (composed of cells, collagen, elastic fibers, interstitial fluid, and lymphatic vessels) and finally the capillary walls. There are several possible routes of drug absorption across the epithelium such as paracellular and transcellular routes, active and passive transports, pore formation, vesicular transport, and drainage into the lymphatic system. Passive diffusion is the process of solute migration from a region of higher concentration to a region with a lower concentration, the concentration gradient depends on the physicochemical properties of the drug, on the thickness of the air-blood barrier, on the rate of perfusion and on the absorption surface area. Due to the morphological heterogeneity of the respiratory system the rate of absorption by passive diffusion is region-dependent, and generally assumed to be slower in the conducting airways due to thicker walls and less perfusion and faster in the alveolar region for a larger absorption area, higher perfusion and thinner walls. Concerning active transport, it is known that different types of transporters contribute to the uptake of the compounds into the cells (such as transporters of the solute carriers, SLC) while other efflux the compounds out of the cells (such as ATP-Binding-Cassettes ABC, via ATP-dependent mechanisms) as a mechanism of defense that prevents the foreign substances entering in the systemic circulation [32], [31]. A representation of the possible routes for the transport of the substances across the lung epithelium is shown in Figure 1-10.

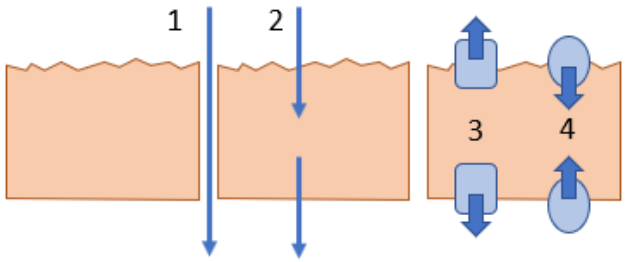

Figure 1-10 Possible transport mechanisms acting in the lung: 1) paracellular diffusion, 2), transcellular diffusion, 3) active efflux transport, 4) active uptake.

The *tissue affinity* i.e. the capability of the drug molecules to bind the different substructure of the tissue [34] such as cell membrane, target receptors and organelles, can impact on the absorption process slowing it down and hence contributing to lung retention and to a possible increase of the local effect duration [34]. Tissue affinity depends on the physicochemical and pharmacological characteristics of compounds and it has been demonstrated that cationic lipophilic molecules (generally basic amines with pKa[1]>8) are subject to accumulation in the lung tissue [34]. In the literature it has been reported that a possible explanation lies in the combination of accumulation in membranes and sequestration by lysosomes; this last mechanism is called lysosomal trapping. Lysosomes are acidic cells organelles involved in various metabolic processes such as phospholipids turnover, the breakdown of endogenous waste products such as bacteria and viruses, autophagy and apoptosis. Lysosomal trapping is a nonenzymatic and non–transporter-mediated process to which compounds are subject on the basis of their physicochemical properties [35]. It occur when a compound diffuses into lysosomes and becomes protonated due to their acidic environment; once protonated, the compound does not easily cross the lysosomal membrane and this prevents the drug diffusion back outside the lysosomes in the cytosolic space [35],

[1] Acidic dissociation constant.

[36]. Recently, lysosomal sequestration has been subject of investigation through *in vitro* and *in silico* models [36], [37] and it has been proposed that this mechanism augment the lung retention and hence the duration effect of several β2 agonist pulmonary drugs [36].

1.7. Challenges in studying the PK of inhaled drugs

The study of the PK of inhaled therapeutics presents a greater number of challenges compared to other routes of administration such as the IV and the PO ones [10]. The goal of its study is to understand the relationship between the delivered dose, the drug concentration at the sites of action and the drug concentration in an easily accessible fluid such as the blood, [38]. Whereas for IV and oral drugs the dose is known, for inhaled drug there is an uncertainty on the dose that actually reaches the lungs, in fact, as explained before, a part of the delivered drug can be exhaled and part can be swallowed and undergoing to GI absorption. Moreover, an uncertainty can exist on the amount actually delivered from the devices. The measurement of inhaled drugs lung exposure is technically challenging since the lung is not easily accessible, but it is important to understand the overall PK properties and how these influence the PD since the lung is the target organ. Blood samples, instead, help to assess the systemic compound level associated with possible on or off-target unwanted effects.
In preclinical settings it is possible to evaluate lung concentration through lung tissue homogenates, obtained by destructive samples (using one or more animals at each time point). This methodology, however, has the limitation to produce an overall measure without distinguishing between the different

lung regions that can be or not the target where the drug should elicit its effect, furthermore, it dissolves the deposited drug in the lungs, making the use of this data to establish PK/PD relationship challenging especially for poorly soluble compounds, for which the dissolution in the fluids is not instantaneous. In clinical setting, few possibilities to obtain lung measurements are available, these includes bronchial biopsy, microdialysis, induced sputum and sampling of epithelial fluid with the Broncho-Alveolar Lavage (BAL). Apart from the limitations proper of each techniques in general they are invasive, expensive and do not provide samples representative of the entire lung, since they are typically related to a single time point and/or location site and for these reasons the blood sampling very often represents the unique PK readout, [38], [10]. However, limitations reside in using plasma concentration as a surrogate of lung concentration due to several reasons [38]:

- plasma samples, collected from the venous sides, are the results of several interactions with the tissues of the body after inhalation takes place.
- plasma measurements can include the contribution of the GI absorption due to the swallowed part of inhaled compound.
- the possible presence of non-absorptive clearance.
- the lung absorption is typically multiphasic due to different regional absorption.

1.8. Modelling the PK of inhaled drugs

Historically, the development of novel inhaled therapeutics is based on experimental tests to assess

that candidates have a suitable PK profile, that they are potent enough and do not exhibit toxicity at therapeutic doses, however, as previously mentioned, the only use of experimental methods may lead to extended drug development programs with high attrition rates, especially for novel therapeutic targets [39]. As stated above, the use of mathematical modelling to inform the PK during drug development has gained more recognition over the years, however, the number of models to study of the PK of inhaled drugs is limited compared to other routes of administration [32]. Among the existing PK modelling approaches, one represents an interesting opportunity to optimize the development of inhaled products: mechanistic modelling [39].
In the next Subsection, characteristics of PBPK modelling, a widely used mechanistic modelling approach to study the PK, and the potential advantages in their use during the inhaled drugs drug development, will be presented. The state of the art in this field is also reported.

1.8.1. The role of the mechanistic modelling approach to study the PK of inhaled drugs

PBPK models are tools that allow to predict *in silico* the exposure of drug in a target organ, integrating the processes of ADME occurring in this organ. In PBPK models the living organism is described as a set of compartments representing organs and tissues connected by the blood circulation, an example of a generic PBPK model is reported in Figure 1-11. The time course of the drug concentration in each compartment is described through a mass-balance equation [40].

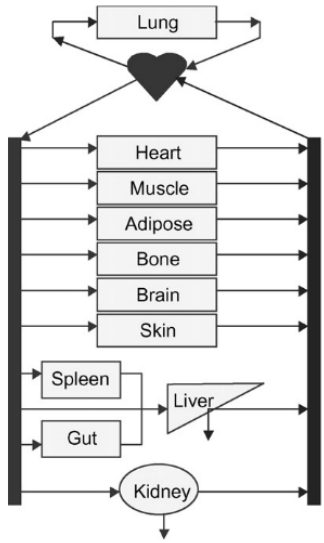

Figure 1-11 The schema of a PBPK model [41].

One of the most interesting characteristics of PBPK models is that model parameters can be divided into system-specific (e.g. organ volumes and blood fluxes) and compound-related (e.g. solubility, permeability, tissue binding). This means that it is possible to create pre-built drug-independent model structures that can be re-used for predicting the exposure to different compounds in the same species or the same compound in different species [40], [42]. In fact, one of the first and more extensive field of PBPK modelling approach application was the preclinical to clinical translation in toxicology, where for ethical reasons, the exposure of human to pollutants or toxic agents is not allowed and then it is only possible to predict the human exposure on the basis of preclinical data [43]. In particular, for what concerns the field of inhalation, a significant number of studies related to xenobiotic inhalation, based on PBPK models, were done in the past [44]. In the literature, examples of application and assessment of PBPK models of different complexity along the whole drug development process are reported. Different

type of drug-specific or physiological information can be integrated from the beginning in the PBPK mechanistic framework and gradually added, updated and refined as they are made available by the *in vitro*/*in vivo* studies. Therefore, PBPK modelling approach represents a good example of incremental strategy to the model building [45].

The use of mathematical models to study inhaled drugs PK is recent compared to other therapeutic areas and the use of PBPK models, in particular, is even more recent. Among the published models the major part of the works deals with PK compartmental models. In the compartmental modelling approach compartments do not correspond to anatomical entities are rather abstract mathematical constructs and model parameters do not directly correspond to physiological reality [44]. The parameters are estimated on PK data and the structure choice is typically based on how well fits the data. They are typically less complex than other type of models, like PBPK models, since they have less mechanistic rationale. In some cases, empirical models may have a physiology-motivated structure and some parameters can be fixed to values present in the literature acquiring a semi-physiological character. Compartmental PK models are widely used, especially in the context of clinical population PK/PD modelling, to understand the dose-exposure-effect/toxicity relationship across different populations. They are applied for several purposes such as individualized dosing regimens and clinical trial design [46].

A work published in 2015 [32], reports an overview on the possible modelling approaches to study the PK of inhaled drugs and extensively reviewed the published compartmental models, that were all applied for clinical studies and used blood PK data only, these studies report a relation between the systemic PK and the efficacy, while some of them use the systemic PK for

safety studies. In 2018, a paper of Hendrickx et. al [47], presented a compartmental modelling approach where some parameters are linked to actual physiology in order to facilitate the cross-species translation. Preclinical data of lung and plasma concentration after intratracheal (IT) administration are modelled and used as a starting point for the translation. The ability of the model to predict the human plasma profiles was investigated on 12 different bronchodilators and the PK/PD relationships were explored.

Until 2016, no PBPK models to study the PK of inhaled drugs were presented in the literature, the first published work was that of Caniga et. al, at Merck [48], presenting a PBPK model describing the processes such as drug dissolution, absorption, distribution, of inhaled drugs with a model to describe the PD response, taking as input the predicted unbound drug concentration in the lung. The model structure accounts for regional differences representing the respiratory system divided into airways and in alveolar region. This model, calibrated with *in vitro* physicochemical properties of the corticosteroid drug mometasone and the observed preclinical *in vivo* data, was able to predict the lung and systemic PK data after IT administration in rats and the drug anti-inflammatory response, evaluated with *in vivo* PD data related to inflammation in rats. Furthermore, the model, with human PBPK components was able to predict the plasma PK of mometasone, budesonide and fluticasone. Even if it described the main processes occurring when a drug is inhaled, it neglects some processes such as the mucociliary clearance mechanism that can impact on the PK of poorly soluble compounds and specific binding kinetics.

In 2016 Boger et. al at AstraZeneca published another version of PBPK model to study the PK of inhaled drugs, [49] with the aim to understand which combinations of drug and formulation properties result

in lung-selective receptor occupancy, including mechanisms neglected in the model of Caniga et. al. The model, starting from physiological information, drug physicochemical properties and calibration on preclinical lung concentration data, was able to accurately predict the PK of the poorly soluble drug fluticasone propionate, after IV administration and via nose-only inhalation in rats. It was also able to predict the target site exposure, this was evaluated using receptor occupancy measurements. The same author in 2018 presents a PBPK-PD model [50], developed from the previous one presented in 2016, describing with an increased level of details the respiratory system as composed of 24 generations. The objective of the study was to evaluate the ability of the PBPK-PD model to predict the time course of FEV1 (i.e forced expiratory volume in 1 second), a traditional clinical endpoint for the efficacy assessment of potential bronchodilators [51], after inhalation of salbutamol. This study allowed to indirectly evaluate the model prediction of local free drug concentration in the human lung, using an endpoint of efficacy that is linked to local free drug concentration levels, hardly experimentally obtainable in human. The model, once developed on rats was used for the translation of the PK to human, fixing some lung parameters tuned on rat *in vivo* data.

The same author proposed and published another approach to mechanistic modelling in 2018, in which the human respiratory system is seen as a continuum through the use of the partial differential equations [52].

Apart from the in-house developed model described above, commercial platforms exist to study inhaled drugs, in which lung models are embedded. One of these is the Gastroplus platform™ (Simulation Plus Inc.) with the Additional Dosage Routes Module, that allows to study other routes of administration beside the

traditional oral and intravenous drug administration routes for which the platform was originally developed. In this tool three different pulmonary regions are considered: the bronchial, the bronchiolar and the alveolar regions and an extra thoracic compartment. This model includes a particle deposition model based on that proposed for the human respiratory tract, from the International Commission on Radiological Protection (ICRP) in 1994 [19] and the processes of dissolution, clearance and absorption.

Another commercial PBPK modelling tool that allows to model the absorption following inhalation is the SimCyp Simulator™ (Certara), it includes a first order absorption model to describe absorption across the lung, that can be used with the full PBPK model. The user can assign the proportion of the dose which is inhaled that goes directly to the lungs where absorption is simulated, the remaining dose is swallowed and goes to the GI tract where oral absorption can be simulated using any of the Simcyp oral absorption models [53]. However, limited information is available regarding technical details of models implemented in these tools due to their commercial nature.

Chapter 2

Development of a PBPK model for intravenous and oral administration studies[2]

As stated above PBPK models are suitable to study the PK of compounds along the different phases of drug development. Starting from the early stages, possible applications deal with the prioritization of compounds before performing *in vivo* experiments. The cost to generate *in vivo* data is in fact higher than that to characterize candidates *in vitro* (e.g., their main properties can be routinely determined via high-throughput techniques). The *in vitro* compounds properties can hence be combined with physiological species-specific information to predict the *in vivo* PK in the preclinical species of interest [54], [41], [55]. Once preclinical *in vivo*

[2] Part of this Chapter is taken from S. Grandoni, N. Cesari, G. Brogin, P. Puccini and P. Magni, "Building in-house PBPK modelling tools for oral drug administration from literature information," *Admet Dmpk*, vol. 7, no. 1, pp. 4–21, 2019.

data become available for the selected candidate, the simulated profiles can be compared with experimental data to verify if some of the model assumptions were violated. If this is the case, the model can be refined following the "learn, confirm and refine" paradigm, [40].
The adjusted model can be further used and expanded, for example, for predicting other routes of administration (e.g., PO after IV) in the same species or the same route in other species. For example, PBPK models can be used to extrapolate PK from animals to man (e.g., healthy volunteers), by updating the species-specific model parameters and collecting additional compound-related *in vitro* data [55], [54]. Furthermore, within the clinical development context, PBPK models can be used to extrapolate PK from healthy volunteers to patients or can be used to predict PK in special populations, like children and elderly, integrating into the model the physiological-related changes due to the specific physiological or pathological condition [56].
In this context the aim of the first part of this work is to develop a generic basic PBPK model starting from literature information, that can be the basis for subsequent studies of specific ADME mechanisms. In this work, the mechanisms of interest are those associated with inhalation and the generic PBPK model developed will be extended with the physiologically based pulmonary model with the final aim of informing the development of inhaled drugs. The workflow followed for this part of the project is summarized in Figure 2-1.

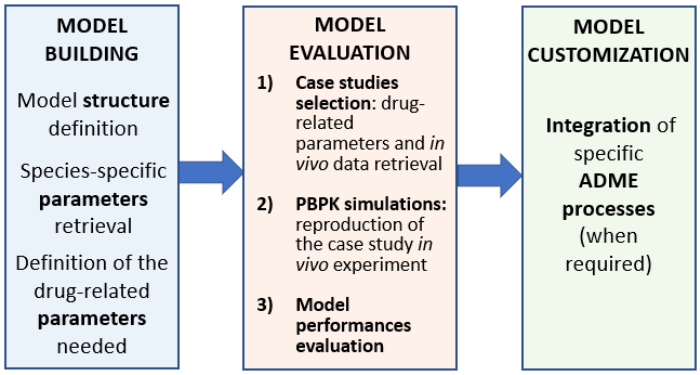

Figure 2-1 The workflow followed for the development of the generic PBPK model.

2.1. The PBPK model formulation

2.1.1. Model structure

PBPK models consist of a series of compartments representing the body organs and tissues. Among those typically included in a basic PBPK model there are the adipose tissue, the brain, the gut, the heart, kidneys, the lung, muscles, the skin and the spleen. Depending on the specific needs, other tissues can be included or lumped together, in Figure 2-2 the basic structure adopted in this work is shown. The time course of drug concentration in each tissue is described with a mass balance equation, that for a generic tissue T has the following expression [41]:

$$\frac{dC_T}{dt} = \left(\frac{1}{V_T}\right)\left(Q_T C_{in} - \frac{Q_T C_T}{P_{T:B}} - CL_T C_{in}\right) \quad (2.1)$$

where V_T and Q_T are the tissue volume and blood flux, respectively; C_{in} is the blood drug concentration in input to the tissue, that is the arterial blood concentration for all the tissues except for the lung

which receives the venous blood and for the venous compartment; $P_{T:B}$ is the tissue to blood partition coefficient, defined as the ratio between the total drug concentration of a compound in a tissue T and the total drug blood concentration at the steady state, it is a measure of the drug distribution into tissues. CL_T is the tissue clearance that can be present in some of the tissues.
The equation for the venous compartment, receiving as input the output of all the other tissues (except lung) has the following expression:

$$\frac{dC_{VEN}}{dt} = \frac{1}{V_{VEN}}\left(\frac{\sum Q_T C_T}{P_{T:B}} - Q_{VEN}C_{VEN} + D_{IV}\right) \quad (2.2)$$

where C_{VEN} , V_{VEN} and Q_{VEN} are the venous drug concentration, volume and flux, respectively, and D_{IV} represents the IV dose, if present. The mass balance equation for the arterial compartment can be analogously derived as:

$$\frac{dC_{ART}}{dt} = \frac{1}{V_{ART}}\left(\frac{Q_{LUNG}C_{LUNG}}{P_{LUNG:B}} - Q_{ART}C_{ART}\right) \quad (2.3)$$

where C_{ART} , V_{ART} and Q_{ART} are the arterial drug concentration, volume and flux, respectively. Fluxes Q_{VEN}, Q_{ART} and Q_{LUNG} are equal to the cardiac output, Q_{CO}.
Each tissue could be further modelled as perfusion-limited or permeability-limited. The first situation generally occurs for small lipophilic compounds for which the tissue perfusion is the step limiting the absorption, the second one for large hydrophilic compounds for which the permeation through the cell membrane is the limiting step.

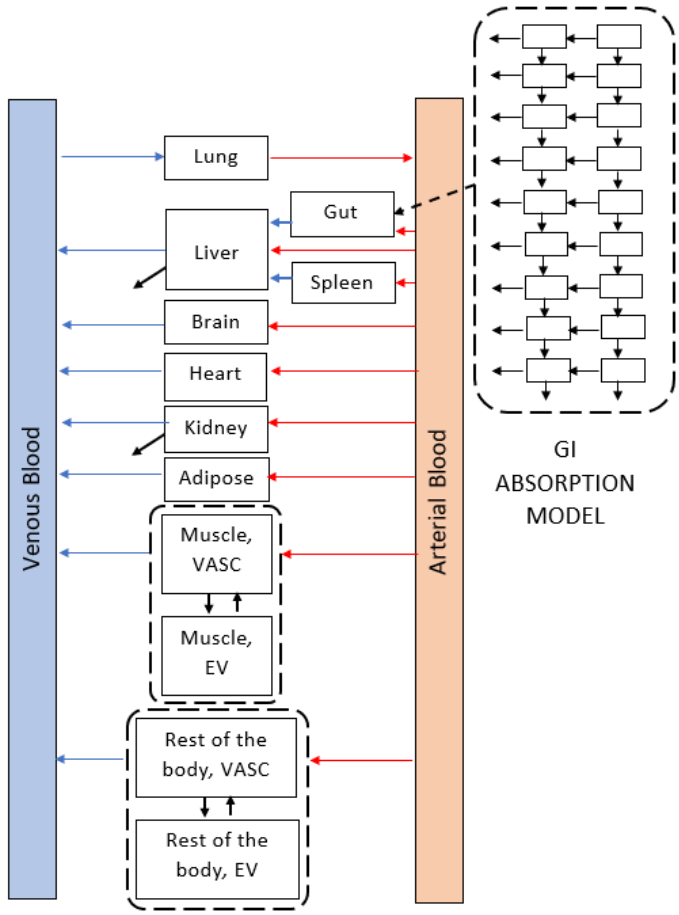

Figure 2-2 The structure of the developed PBPK model.

To model the latter, the tissue compartment can be divided in two parts: the extravascular (EV) space and the vascular (VASC) space, divided by a membrane which acts as a barrier [40], the representation of this modelling and of the classical perfusion limited modelling is represented in Figure 2-3.

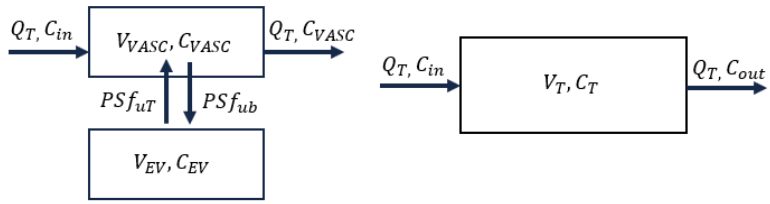

Figure 2-3 A representation of a permeability limited modelled tissue (on the left) and of a perfusion limited one, whose mass balance was described previously.

The typical equation for a permeability-limited tissue (without clearance) can be the following one:

$$\frac{dC_{T,VASC}}{dt} = \left(\frac{1}{V_{T,VASC}}\right)(Q_T C_{in} - Q_T C_{T,VASC} - PSC_{T,VASC} f_{ub} + PSC_{T,EV} f_{uT}) \quad (2.4)$$

$$\frac{dC_{T,EV}}{dt} = \left(\frac{1}{V_{T,EV}}\right)\left(PS\ C_{T,VASC} f_{ub} - PS\ C_{T,EV} f_{uT}\right) \quad (2.5)$$

where $C_{T,VASC}$ is the drug concentration in the VASC part of the tissue T and $V_{T,VASC}$ its volume; $C_{T,EV}$ and $V_{T,EV}$ are the corresponding quantities for the EV part of the tissue; PS is the permeability-surface product taking into account the limitation of the permeability that prevents the distribution of the drug into the tissue [57], f_{ub} is the fraction of unbound drug in blood and f_{uT} that in tissue.

In the developed model the organs/tissues included are those deemed to be relevant to study the kinetics of inhaled drugs. The "non-eliminating" tissues selected are spleen, brain, heart, muscle, fat, gut, lung. An additional compartment, called "rest of the body", is also considered to take into account the other tissues not explicitly considered, such as bone and skin. Conversely, liver and kidney are the only two eliminating tissues. A possible expression of the mass

balance for the liver is reported in [58], in which the elimination process is considered through a term of hepatic extraction, E_R:

$$\frac{dC_{LIVER}}{dt} = \frac{1}{V_{LIVER}}\left\{\left[(Q_{LIVER} - Q_{GUT} - Q_{SPLEEN})C_{ART} + Q_{GUT}\frac{C_{GUT}}{P_{GUT:B}} + Q_{SPLEEN}\frac{C_{SPLEEN}}{P_{SPLEEN:B}} - Q_{LIVER}\frac{C_{LIVER}}{P_{LIVER:B}}\right] - \left[(Q_{LIVER} - Q_{GUT} - Q_{SPLEEN})C_{ART} + Q_{GUT}\frac{C_{GUT}}{P_{GUT:B}} + Q_{SPLEEN}\frac{C_{SPLEEN}}{P_{SPLEEN:B}}\right]E_R\right\} \quad (2.6)$$

where V_{LIVER} is the liver volume, C_{LIVER}, Q_{LIVER}, $P_{LIVER:B}$ are the liver concentration, flux and tissue blood partition coefficient respectively. C_{GUT}, Q_{GUT}, $P_{GUT:B}$ are those of gut and C_{SPLEEN}, Q_{SPLEEN}, $P_{SPLEEN:B}$ those for spleen. The mass balance equation for kidney has been formulated in its simplest form considering the passive filtration mechanism governed by the glomerular filtration rate and neglecting processes of active tubular secretion and reabsorption [59]:

$$\frac{dC_{KIDNEY}}{dt} = \frac{1}{V_{KIDNEY}}\left(Q_{KIDNEY}\left(C_{ART} - \frac{C_{KIDNEY}}{P_{KIDNEY:B}}\right) - GFR\, f_{ub}\, C_{ART}\right) \quad (2.7)$$

where C_{KIDNEY} is the kidney concentration, V_{KIDNEY} and Q_{KIDNEY} the kidney volume and blood flux respectively, GFR is the glomerular filtration rate.

To describe the time course of drugs after PO administrations, a model of GI absorption has to be added to the basic structure just described, that is able to predict tissue drug concentrations only after IV administrations. In this work, a simplified version of the Advanced Compartmental Absorption and Transit (ACAT) model was adopted [60]. The GI system was

divided in 9 segments, the first, receiving the solid drug, is the stomach, the other ones represent the small intestine and the last segment is the colon. Each intestinal section is composed of a compartment in which the drug is in its undissolved form (from here it can dissolve or transit in the same form in the subsequent section) and by a compartment in which the drug is dissolved in the physiological fluids (from there drug can be absorbed or transit in the subsequent section), in colon the drug can also be excreted. A schematic representation of the model adopted is reported Figure 2-4.

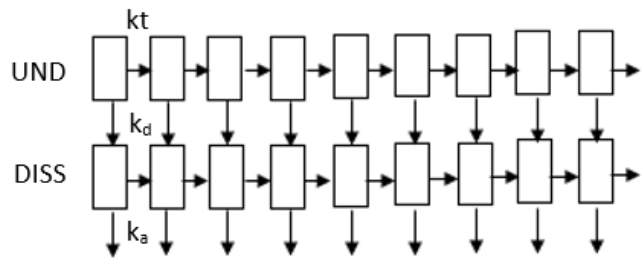

Figure 2-4 A schematic representation of the GI absorption model, UND indicates the undissolved amount of the compound, DISS the dissolved part.

The mass balance equations of the stomach undissolved and dissolved drug mass compartments are the following:

$$\frac{da_{st,und}}{dt} = D_{PO} - k_{t,st}a_{st,und} - k_d a_{st,und}, \quad (2.8)$$

$$\frac{da_{st,diss}}{dt} = +k_d a_{st,und} - k_a a_{st,diss} - k_{t,st}a_{st,diss} \quad (2.9)$$

where D_{PO} is the amount of the dose administered PO, $a_{st,und}$ is the stomach undissolved amount, $k_{t,st}$ the stomach transit constant, k_d the dissolution rate

constant and k_a is the absorption rate constant, for all this last three, details about their calculation will be explained hereinafter. The equations for the first small intestine segment are:

$$\frac{da_{1,und}}{dt} = +k_t a_{st,und} - k_t a_{1,und} - k_d a_{1,und}, \quad (2.10)$$

$$\frac{da_{1,diss}}{dt} = +k_t a_{st,diss} - k_t a_{1,diss} + k_d a_{1,und} - k_a a_{1,diss}. \quad (2.11)$$

where $a_{1,und}$ and $a_{1,diss}$ are the undissolved and dissolved amount in the first small intestine segment, respectively. k_t is the transit constant. The equations, for all the other small intestine segments are formulated as follows:

$$\frac{da_{i,und}}{dt} = +k_t a_{i-1,und} - k_t a_{i,und} - k_d a_{i,und}, \quad (2.12)$$

$$\frac{da_{i,diss}}{dt} = +k_t a_{i-1,diss} - k_t a_{i,diss} + k_d a_{i,und} - k_a a_{i,diss}, \quad for\ i = 2, \dots, 8. \quad (2.13)$$

where $a_{i,und}$ is the undissolved amount in the $i-th$ segment, $a_{i-1,und}$ that in the preceding compartment, $a_{i,diss}$ and $a_{i-1,diss}$ are those related to the dissolved amount compartments.
For the last segment, representing the colon the equations of the model are the following:

$$\frac{da_{co,und}}{dt} = +k_{t,8} a_{8,und} - k_{t,co} a_{co,und} - k_d a_{co,und} \quad (2.14)$$

$$\frac{da_{co,diss}}{dt} = +k_{t,8} a_{8,diss} - k_{t,co} a_{co,diss} + \quad (2.15)$$

$k_d a_{co,und} - k_a a_{co,diss}$

where $a_{co,und}$ and $a_{co,diss}$ are the undissolved and dissolved amounts related to colon. $k_{t,co}$ is the colon transit constant.
The GI absorption model is connected to the PBPK structure, the amount of dissolved drug is absorbed through the gut walls that are perfused by the blood circulation. Therefore, differently from generic tissues, whose mass balance equation has the expression reported in Eq. 2.1, the equation for the gut compartment has to consider the input of the drug from the GI absorption model. The mass balance equation for the gut tissue has been modelled as follows, [59]:

$$\frac{dC_{GUT}}{dt} = \frac{1}{V_{GUT}}\left(Q_{GUT}C_{ART} - Q_{GUT}\frac{C_{GUT}}{P_{GUT:B}} + F_{GUT}\left(\sum_{i=1}^{9} k_a\, a_{i,diss}\right)\right) \quad (2.16)$$

where C_{GUT} is the gut concentration, Q_{GUT} and V_{GUT} are its blood flux and volume, respectively. F_{GUT} is the fraction that considers a possible metabolism in the intestinal mucosa, limiting the bioavailability from the gut wall.

2.1.2. Model parameterization

As discussed in the Introduction, in PBPK models it is possible to distinguish between system-specific and drug-related parameters. In the next Subsections, it will be discussed how the systems-specific parameters were obtained and how the drug-related parameters were derived. The model was parameterized to be used for the *in vivo* PK prediction in two preclinical species of interest, rat and dog and in man.

2.1.3. Systems-specific parameters for the PBPK model

The physiological values of tissue blood fluxes and volumes were found in the literature, mainly in the work of Brown et. al [61], that reports the physiological parameter values to build PBPK models.

Physiological parameters for rat
In [61], the different organ weights are reported as a percentage of the total body weight (relative organ weight); to obtain organ volumes from these values for a typical subject with a body weight of 250 g was considered. Moreover, it was assumed that tissues have the same density of water. To estimate the percentage of adipose tissue in the total body weight, the following relationship reported in for Sprague-Dawley rats has been used:

$$\%\, Adipose\ Tissue = 0.199(BW) + 1.664, \qquad (2.17)$$

where BW is the body weight, in grams.
The volume of the rest of the body compartment was calculated assuming that the tissues included in the model represent the 85% of the total body weight (BW) [62]. Hence its weight has been calculated subtracting the sum of all the other weights from the 85% of BW. The volume of blood was taken from the work of Davies et. al., [63], in which the blood and plasma volumes for a rat of 250 g of body weight are reported, in the same work, the repartition between arterial and venous blood was reported, a 75% vs 25% split was suggested for arterial and venous blood, respectively and adopted in this model. The volumes of the EV and VASC compartments for the tissues with a permeability-limited kinetics can be calculated from the volume fractions of vascular and interstitial spaces, that

can be found for rats tissues in [64]. In the model here proposed, the VASC compartment includes also the interstitial space.
Concerning fluxes, in [61], the regional flow distribution in different organs as a percentage of the cardiac output is reported. Therefore, the cardiac output (Q_{CO}) expressed in L/h has been calculated for a standard rat of 250 g to obtain the values of blood flow in each organ, using the allometric equation reported in the same work:

$$Q_{CO} = 15(BW)^{0.74} \tag{2.18}$$

where BW is expressed in kg. The value of the liver flux was calculated as sum of the gut, spleen and hepatic artery fluxes.
The portion of blood flow in gut and spleen with respect to Q_{CO} was obtained from [65]. For gut it was calculated considering the reported gut flow of 14.9 ml/min referred to a Q_{CO} of 112.3 ml/min, for the spleen the reported flux value of 117/ml/min/100 g of tissue was considered.
Regarding the renal filtration, a value of GFR of 1.31 ml/min was obtained from [63].

Physiological parameters for dog
A typical dog of 10 kg has been considered, the organ and tissues volumes were calculated from the relative weights reported in [61], the values of blood volume were taken from [63] and the same repartition of the blood in arterial and venous used for rats has been considered. The fluxes were taken from [61] for all the organs except for the gut, for the liver and for the adipose tissue which are obtained from internal data. The value of the liver flux was obtained as the sum of the gut and spleen flux, plus the value of the hepatic artery flux, this last obtained from [61]. The Q_{CO} in

ml/min has been obtained with the equation reported in [61]:

$$Q_{CO} = 1.05BW^{0.75} \quad (2.19)$$

where BW is in grams. The repartition between VASC and EV tissue follows the same proportion adopted for rats because no specific information about that were found in the literature. The value of the GFR of 61.3 ml/min was obtained from [63].

Physiological parameters for humans
A typical subject of 70 kg with 35 years of age has been considered, organs and tissues volumes were calculated from the relative weights reported in [61], values of blood volume were taken from [63], and the same repartition of blood in arterial and venous used for rats has been considered. Blood fluxes were obtained from [61], except for gut and spleen (that were taken from internal studies), considering a Q_{CO} in L/min obtained with the equation reported in [61]:

$$Q_{CO} = -6.846 * \log(AGE) + 16.775 \quad (2.20)$$

where AGE is the age in years. The value of the liver flux was obtained as the sum of the gut and spleen flux, plus the value of the hepatic artery flux, this last obtained from [61]. The repartition between VASC and EV tissue follows the same proportion adopted for rats. The value of the GFR of 125 ml/min was obtained from [63].

Organ surfaces needed to compute the permeability-surface product (PS) for permeability limited organs (muscle and rest of the body in model of Figure 2-2) according to the authors' knowledge are not present in the literature, except for lung for which volumes and

surfaces for the tracheobronchial and alveolar regions are available [49]. Hence, in this work, surfaces for other organs or tissues were obtained by scaling the surface area of the tracheobronchial region through the following formula:

$$S_T = S_{TB}\left(\frac{V_{T,EV}}{V_{TB,EV}}\right)^{\frac{2}{3}} \quad (2.21)$$

where S_T and $V_{T,EV}$ are the surface and the EV volume of the tissue T of interest, respectively; analogously, S_{TB} and $V_{TB,EV}$ are the tracheobronchial surface and EV volume, respectively. The surface value S_{TB} for rat and human was taken from [49], for dog it was estimated by linear regression using the rat and man body weight-S_{TB} data. The values are 81.75 cm^2, 1176 cm^2 and 4800 cm^2 for rat, dog and man respectively.

2.1.4. Physiological parameters for the GI absorption model

The volumes of the different intestinal segments were obtained from [59] for rat, dog and human. The transit constants were calculated from the Mean Residence Time[3] (MRT) as $\frac{1}{MRT}$. MRTs of the small intestine segments were obtained dividing the total small intestine MRT reported in the literature by 7 (assuming, hence, that the transit time is the same for each of the segments). The values of MRT for the stomach, small intestine and colon obtained from the different sources for the different species are reported in Appendix A.

[3] MRT represents the average time a molecule stays in the body, [155].

The pH values in the different intestinal segments that are used to take into account the dependency of the solubility on the pH (how this was done will be explained in the subsequent Section related to drug-related parameters) are taken from [59].

2.1.5. Drug-related parameters

The PBPK model drug-related parameters can be obtained mainly by three sources: directly by *in vitro* tests, through *in silico* calculation or by *in vitro-in vivo* extrapolation (IVIVE) techniques [66]. In this Subsection will be presented how the drug related parameters were obtained for each component of the PK i.e., *absorption, distribution, metabolism, elimination.* A summary of parameters that have to be obtained to build the PBPK model presented here, with the related sources are reported in Table 2-2.
In case of PO drug delivery, before the drug is absorbed, it undergoes the dissolution process. The dissolution process depends mainly on the physico-chemical characteristics of the compound and on the dissolution medium. The dissolution rate k_d constant of the GI absorption model has been modelled considering the widely used Nernst-Brunner equation, here reported:

$$k_d = \frac{D*S_s}{T}(C_s - C), \tag{2.22}$$

in this equation, the dissolution rate depends on the diffusion coefficient D, on the specific surface area of the undissolved form Ss, on the solubility of the drug C_s, on the concentration in the dissolution medium C and on diffusional layer the thickness T. Supposing that particles are spherical, the specific surface area for this geometry can be expressed as:

$$S_s = \frac{4\pi r^2}{\rho V} = \frac{4\pi r^2}{\rho \frac{4}{3}\pi r^3} = \frac{3}{\rho r}, \tag{2.23}$$

where ρ is the density of the particles to be dissolved, r is their radius. Then, the Nernst-Brunner equation can hence be formulated as:

$$k_d = \frac{3D}{\rho r T}(C_s - C), \tag{2.24}$$

The value of D can be obtained through the Stokes-Einstein equation:

$$D = \frac{k_B T}{6\pi\eta Rs} \tag{2.25}$$

where k_B is the Boltzmann constant, T is the absolute temperature in Kelvin, η is the solute viscosity expressed in Pascal·second, Rs is the hydrodynamic radius of the diffusing solute, calculated (in meter), as [67]:

$$Rs = 3\sqrt{\frac{3MW \cdot 10^{-3}}{4\pi NA\rho}} \tag{2.26}$$

where MW is the molecular weight, NA is the Avogadro Number, ρ is the drug density (in kg·ml^{-1}). The diffusional layer thickness T can be computed following the approximation of Hintz and Johnson [68]:

$$T = r \; if \; r < 30\ \mu m$$
$$T = 30\ \mu m, \quad otherwise \tag{2.27}$$

The concentration C can be calculated as the ratio between the amount dissolved in a certain segment a_{diss} and volume of the intestinal compartment, [69]. The solubility C_s has been calculated for each of the intestinal segments, to take into account the changes in the pH along them, that affect the ionization of the molecule and finally the solubility. The dependency of the solubility on the pH can be described according to the Henderson-Hasselbalch equations, that are reported for the different molecular species, in Table 2-1.

Table 2-1 The Henderson-Hasselbalch equations.

Molecular species	**Equation**
Monoprotic acid	$Cs_{pH} = S_{int}\left(1 + 10^{(pH - p_{Ka1})}\right)$
Diprotic acid	$Cs_{pH} = S_{int}\left(1 + 10^{(-pH + pKa1)} + 10^{(2pH - pKa1 - pKa2)}\right)$
Monoprotic Base	$Cs_{pH} = S_{int}(1 + 10^{-pH + pKa1})$
Diprotic base	$Cs_{pH} = S_{int}(1 + 10^{-pH + pKa1} + 10^{-2pH + pKa1 + pKa2})$
Neutrals	Cs_{pH}=S_{int}
Zwitterions	$Cs_{pH} = S_{int}(1 + 10^{-pH + pKaA} + 10^{pH - pKaB})$

Cs_{pH} is the solubility calculated at a certain pH, S_{int} is the intrinsic solubility i.e. the solubility of the unionized form, p_{Ka1} is the acidic dissociation constant for monoprotic species, p_{Ka2} is the second acidic dissociation constant characterizing polyfunctional acids or basis; for zwitterions $pKaA$ is the acidic dissociation constant of the acidic group and $pKaB$ that of the basic group of the zwitterionic molecule, that have a net formal charge of zero, but negative and positive formal charges on individual atoms within its structure.

Absorption

The drug absorption consequent to PO administration has been modelled as a first order process with the absorption rate constants k_a, calculated starting from the measure of the apparent drug permeability to the gastrointestinal barrier that can be obtained *in vitro* from the Caco-2 cells. It is the most widely used cell line for developing human GI tract *in vitro* models, derived from a human colorectal adenocarcinoma. In particular,

$$k_a = P_{eff} * ASF \tag{2.28}$$

where P_{eff} is the effective permeability computed from the apparent permeability measured on the Caco-2 cells and ASF is the absorption scaling factor, assumed to be equal to $\frac{2}{r}$, with r the mean intestinal radius. The absorption rate constant k_a in stomach was fixed to 0, since in the stomach the absorption is usually negligible; for similar reasons it has been assumed k_a equal to 0 also in colon [70]. The value of human effective permeability, $P_{eff,human}$, has been calculated using the relation reported in [71] for the Caco-2 obtained apparent permeability P_{app}:

$$\log\left(P_{eff,human}\right) = 0.4926 \log\left(P_{app,pH7.4}\right) - 0.1454 \tag{2.29}$$

whereas the effective permeability in rats, $P_{eff,rat}$, was obtained by the following relationship [71]:

$$P_{eff,human} = 3.6P_{eff,rat} + 0.03 \tag{2.30}$$

For dog has been assumed that $P_{eff,dog} = P_{eff,rat}$.

Distribution

Drug distribution in tissues was taken into account through tissue to blood partition coefficients $P_{T:B}$, as reported in Eq. 2.1. These values, in the past, originated from expensive and time-consuming experiments, however, nowadays, they can be calculated by *in silico* models accounting for the tissue composition in terms of water, lipids, and proteins. The two most widely used methods are the one developed by Poulin and co-workers [72], [58] and the one proposed by Rodgers and co-workers [73], [74], which extends the first one to take into account the nature of the compound (e.g., acid, base, neutral, zwitterion) and ionization phenomenon during the interactions with tissues. In this work, the second one has been applied, it allows to calculate the tissue to plasma unbound partition coefficient $P_{T:P,u}$ defined as the ratio between the tissue and the plasma unbound concentration at the steady state. The values of $P_{T:B}$ can be finally obtained as:

$$P_{T:B}=\frac{P_{T:P,u}}{BP} f_{up} \tag{2.31}$$

where f_{up} is the fraction of drug unbound in plasma and BP is the blood to plasma ratio, i.e., a measure of drug binding and distribution to erythrocytes relative to plasma, compounds having similar degree of binding to erythrocytes and plasma have BP equal to 1 [59]. Both are additional measures giving information about drug distribution and are generally obtained through *in vitro* tests.

Metabolism and Elimination

Organs that generally constitute the major routes of elimination in the organism are the liver and the gut, responsible for the FPE, and the kidneys. Hepatic metabolic clearance values can be obtained starting from *in vivo* data or from *in vitro* experiments. In the

latter, the quantification of the *in vivo* clearance can be obtained applying the IVIVE method, it consists of three main steps [43]:

- determination of *in vitro* intrinsic clearance CL_{int} (that can be obtained from hepatocytes, microsomes or recombinant enzymes);
- scaling of CL_{int} to an *in vivo* value, here indicated as $CL_{int,vivo}$, by using appropriate scaling factor, to obtain the value for the whole liver; in case of test with microsomes, the scaling factor is the milligram of proteins per gram of liver (MPPGL) and, in case of hepatocytes, is the millions of hepatocytes per gram of liver (HPGL). Of course, these factors have to be multiplied for the liver weight to obtain the final value for the whole liver. The scaling factors for all the species considered in this work are summarized in Appendix A.
- conversion of $CL_{int,vivo}$ to a net value of hepatic clearance CL_H. One of the widely used models to compute this CL_H is the well-stirred liver model [75], here reported:

$$CL_H = \frac{(CL_{int,vivo})\left(\frac{f_{ub}}{f_{uH}}\right)Q_{LIVER}}{CL_{int,vivo}\left(\frac{f_{ub}}{f_{uH}}\right)+Q_{LIVER}} \tag{2.32}$$

where f_{uH} is the fraction unbound in microsomes or hepatocytes, [76], [41]. In this work it has been assumed that the liver binding is equivalent to blood binding. From CL_H the hepatic extraction ratio was calculated as:

$$E_R = \frac{CL_H}{Q_{LIVER}} \tag{2.33}$$

2.2. The PBPK model evaluation study

In recent years, the number of PBPK model publications and regulatory submissions have grown rapidly and regulatory agencies are working to define the best practice on development, qualification, application and reporting of PBPK modelling activities [77]. In 2018, EMA published the guideline about that [78] and FDA provided guidelines about PBPK analysis formats and contents of applications [79]. In this view, the evaluation of a PBPK model platform is an important and critical step of the model development, as also mentioned in both the EMA and FDA guidance [11,12]. In particular, the EMA guidance affirms that if a PBPK model is intended to support a regulatory decision, it has to be qualified for the intended use. The evaluation of the model predictive performances and the level of qualification depend on the impact that the modelling exercise has on the decision making and on the patient's risk associated with wrong regulatory decisions based on modelling predictions. Even if most of the regulatory submissions including PBPK models deal with the use of commercially available specialized (and validated) software tools [11], the use of in-house built platforms is not discouraged by the regulatory agencies. In fact, FDA guideline does not prescribe the use of particular software for PBPK modelling and the EMA guideline applies also to in-house built PBPK platforms. However, it is clearly reported that if an in-house built platform is used for high regulatory impact simulations (e.g., as an alternative to clinical studies) the applicant is strongly encouraged to seek the Committee for Medicinal Product for Human Use (CHMP) Scientific Advice for further guidance [11].

In this Section the evaluation study performed to assess the predictive performance of the developed PBPK model prior its extension with the physiologically based pulmonary absorption model is reported. The model was implemented with the general-purpose computing software MATLAB (The MathWorks Inc.), and the ordinary differential equations solved with the stiff problem solver *ode23s*. The assessment was carried out on plasma concentration profiles generated after IV and PO administrations studies, coming from the literature or in-house experiments, involving different drugs/compounds, administered in single dose or multiple doses, in three different species (i.e., rat, dog and man). Studies were selected to explore drugs with different physico-chemical properties and based on the availability of all the drug parameters required to perform the simulations, summarized in Table 2-2.

Table 2-2 The compound-related properties needed to parameterize the PBPK model presented here.

Parameter	Notes
Nature of the compound	e.g. acid, base, neutral, zwitterion
Acidic dissociation constants, pKa	generally obtained by *in silico* predictions
Molecular weight, MW	generally, *in silico* obtained
Particle Density, ρ	rarely available, a value frequently present in the literature and used as a default in the GastroPlus™ software, i.e. 1 *g/ml* [69], [80], [81].
Particle radius, r	if not available, a value suggested in the literature is that used as default in the GastroPlus™ software [69], i.e. 25 μm.

Intrinsic solubility, Cs	if not available, but the solubility is known to a certain pH, Cs can be calculated with the Henderson-Hasselbalch equations.
In vitro apparent permeability, $Papp$	typically obtained from Caco-2 test
In vitro intrinsic clearance, Cl_{int}	generally, *in vitro* obtained from microsomes or hepatocytes
Blood to plasma ratio, BP	typically obtained from *in vitro* test
Fraction unbound in plasma, f_{up}	generally obtained from *in vitro* test
Log of n-octanol: water partition coefficient, $logP$	usually obtained from *in vitro* test or *in silico* calculated

The final list of selected compounds with the references in which experimental data and drug parameters were found is reported in Table 2-3.

Note that, as a general rule, all the PBPK model compound-related parameter values were computed, starting from the compound properties reported in Table 2-2, by applying the mathematical relationships reported in the previous Sections. However, if the *in vitro* intrinsic clearance, required to characterize the hepatic metabolism, was not available, or the *in vivo* data of the plasma clearance CL_p was available, the hepatic extraction ratio E_R was directly calculated using the *in vivo* data as:

$$E_R = \frac{CL_{b,nr}}{Q_{LIVER}} \tag{2.34}$$

where $CL_{b,nr}$ is the non-renal blood clearance obtained dividing the non-renal plasma clearance $CL_{p,nr}$, obtained after IV administration, for BP. If information about non-renal clearance were not available, the total plasma clearance CL_p was used.

Table 2-3 The drug included in the study with the respective data and parameter values sources.

Drug/Compound	Drug Parameters References	Study References
Amitriptyline	[82], [83], [84]	[82]
R-Carvedilol	[85]	[85]
Chlorpromazine	[76], [86], [87], [88]	[89]
Ciprofloxacin	[81], [90]	[91]
Clozapine	[76], [86]	[92]
Compound A	Internal data	Internal data
Compound B	Internal data	Internal data
Compound C	Internal data	Internal data
Compound X	[40]	[40]
Digoxin	[93]	[94]
Diltiazem	[76], [86], [95]	[96]
Ibuprofen	[76], [86], [95]	[97]
Levothyroxine	[80], ChEMBL	[80]
Metoprolol	[98]	[98]
Midazolam	[99]	[100], [101]
Nifedipine	[102], [103]	[104], [105]
NVS732	[106]	[106]
Paracetamol	[107]	[107]
PF-02413873	[108]	[108]
Pracinostat	[109]	[109]
Repaglinide	[110], [111]	[112]
TPN729MA	[113]	[113]
Sotalol	[107]	[107]
UK-453,061	[114]	[114]
Verapamil	[76], [86], [95]	[115]

F_{GUT} values in man were fixed to values reported in the literature, if available, or calculated using the "Q_{GUT}" model where possible; for the other species F_{GUT} was fixed to 1. Equations of the "Qgut" model [71], with the related scaling factors to obtain F_{GUT} in human from measurement of *in vitro* intrinsic clearance from human liver microsomes (HLM), for CYP3A metabolizers are here reported. The fraction of drug escaping the first pass metabolism can be calculated as follows:

$$F_{GUT} = \frac{Q_{villi}}{Q_{villi} + f_{uGUT} CL_{uint,GUT} \left(1 + \frac{Q_{villi}}{CL_{perm}}\right)} \tag{2.35}$$

where Q_{villi} is the intestinal villi blood flow that for humans is 300 ml/min; f_{uGUT} is the unbound drug fraction in gut, if not available can be supposed equal to 1; $CL_{uint,GUT}$ is the net metabolic intrinsic clearance based on the unbound drug concentration, this last term can be obtained from the HLM as follows:

$$Cl_{uint,GUT} = \left(\frac{Cl_{uint}}{PEMP}\right) NEWI \tag{2.36}$$

where Cl_{uint} is the unbound hepatic intrinsic clearance obtained from HLM and expressed in microliter/minute/milligram of protein, PEMP is the pmol of CYP3A Enzymes for Milligram of Protein that is 155 pmol/milligram of protein, NEWI is the value of nmol of Enzyme for the Whole Intestine that is 70.5 nmol.

The value of CL_{perm}, can be obtained as the product between the human effective permeability and the area of the intestine that for human is 6600 cm2 obtained supposing a radius of 1.75 cm and a length of 6 m [71].

2.3. Evaluation results

Model performances were examined by visual inspection, comparing the plasma concentration simulated profiles with the experimental data, and quantifying the deviation between the PK metrics generated from the predicted profiles and those computed on the experimental data. The comparison was made in terms of fold error (FE):

$$FE = \frac{P_{pred}}{P_{obs}} \tag{2.37}$$

where P_{pred} is the PK metric computed on the PBPK model predicted profile while P_{obs} refers to those obtained from in *vivo* data.
The selected metrics were the Area Under Curve (AUC), the maximum concentration (C_{max}) and the time to reach the maximum concentration (T_{max}). In particular, the AUC was considered for both the IV and PO experiments, whereas C_{max} and T_{max} were considered only for PO administrations and for IV infusions.
In Figure 2-5 are reported, as an example, simulations related to an IV infusion of a single dose of Paracetamol and to a repeated PO administration of the drug Clozapine.
When for the same drug both IV and PO data were available, PO predictions were obtained after having adjusted, if needed, model parameters on the IV data, as suggested in [69]. In particular, the drug distribution was adjusted multiplying all the partition coefficients for the same factor and tuning the PS parameters of the permeability limited tissues.
In general, this procedure improved predictions of PO administrations. An example of the benefit of tuning the parameters on IV profile is reported in Figure 2-6 for

drug Nifedipine. The choice of adjusting the distribution on the *in vivo* data and of using the *in vivo* clearance to calculate the hepatic extraction ratio wants to simulate the incremental model building process mentioned previously, in which the knowledge is progressively added as soon as it is made available during the development process to refine the model.

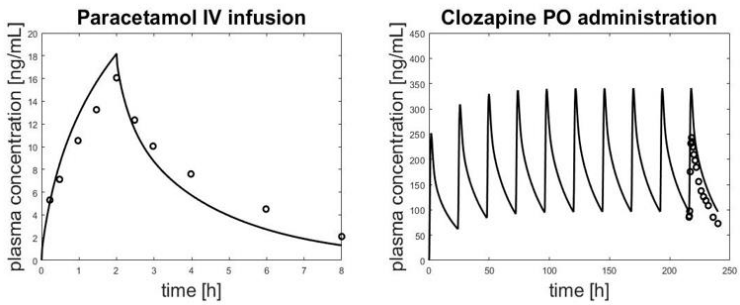

Figure 2-5 two examples of comparison between experimental data and PBPK model prediction related to two drugs included in the study.

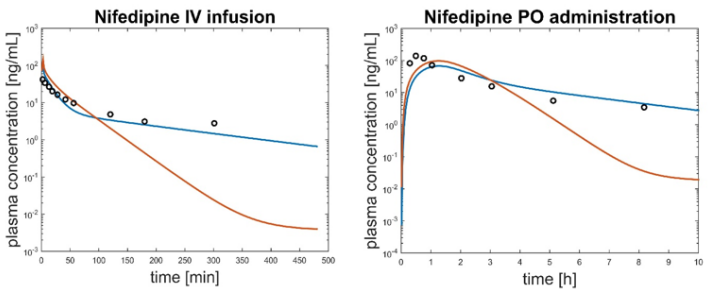

Figure 2-6 in the left panel, simulation of an IV infusion of Nifedipine with (blue line) and without (red line) adjustments. In the right panel the profiles generated for a PO administration, fixed the adjustment on IV data (blue line) or without adjustments (red line).

For highly lipophilic compounds, PS values were adjusted directly on PO simulations when the IV data were not available, in particular, PS values were

increased with the same factor for both permeability-limited tissues, to reach perfusion limited kinetics[4], this improved predictions when compared with real data.
The results of the fold error analysis are summarized in Figure 2-7. It can be observed that for a large number of cases the predicted PK parameters are inside the two-fold error limit.

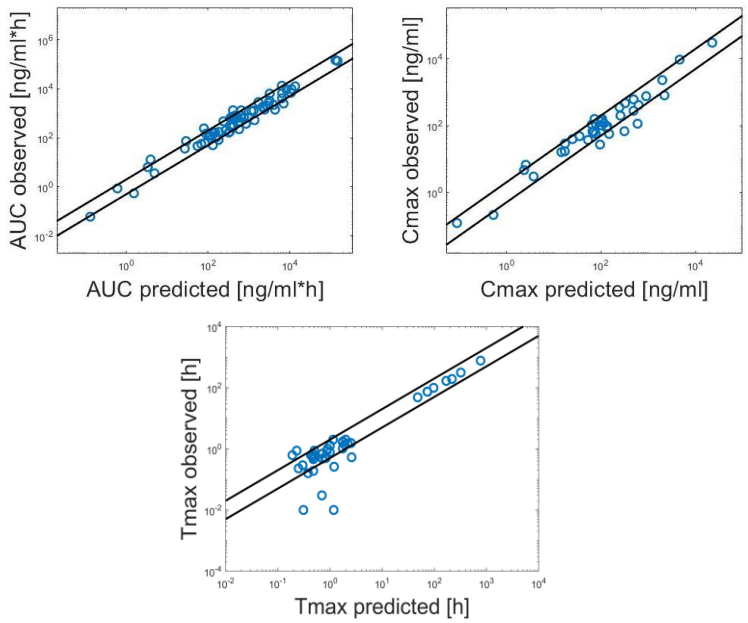

Figure 2-7 The fold error analysis results, black lines represent the two-fold line deviation, blue circles represent the couples formed by the P_{pred} and P_{obs} value generated for each experiment considered.

As a metric of the overall performance the average fold error (AFE) was calculated for the three PK parameters as:

$$AFE = 10^{\frac{\sum \log FE}{N}} \tag{2.38}$$

[4] Amitryptiline, logP 4.85, PS correction coefficient 10^4; Chlorpromazine, logP 5.18, correction coefficient 10^4; Clozapine, logP 3.42, correction coefficient 10^3; Verapamil, logP 4.05, correction coefficient 10^4.

where N is the number of experiments for which FE was calculated. The AFE for the AUC is 0.98, for the C_{max} is 1.1 and for the T_{max} is 1.37. The model showed good prediction performances since the AFE is for all the parameters under the two-fold limit. However, it should be considered that the use of the *in vivo* clearance data (where available) contributed to improve the predictive performances of the model, since is known that *in vitro* clearance measurements are often under predictive of the *in vivo* clearance [69]. The PBPK model presented here does not consider possible kinetics caused by the action of specific enzymes and transporters that could play an important role in some cases. For example, their integration in the model could allow it to capture non-linearities in the PK due to some saturation effects. This behavior can occur for mechanisms associated with absorption, first pass metabolism, binding, excretion and biotransformation; an example is the partial saturation of presystemic metabolism, one of the most important sources of non-linearity [116]. The modelling of specific kinetics could also be necessary to improve the model prediction capabilities in case of complex BCS[5] class IV drugs, characterized by low solubility and low permeability for which the action of absorptive and efflux transporters could play an important role in their disposition [117].

The study here reported demonstrates that it is possible to create simplified in-house PBPK tools, from literature information and collecting basic drug-specific information, that can constitute a basis for subsequent studies of specific ADME mechanisms such as those associated with special routes of administration. In this

[5] The Biopharmaceutical Classification System (BCS) is a scientific framework for classifying drug substances based on their aqueous solubility and intestinal permeability [156].

work, the aim is to inform and support the drug development process of inhaled drugs, by using the proposed PBPK model, extended with a mechanistic pulmonary model that will be presented in the subsequent Chapter.

Chapter 3

Development of a pulmonary absorption model to study the inhaled drugs PK in rats[6]

As explained in the Introduction, PBPK models, due to their mechanistic nature, represent an interesting approach to study inhaled drugs PK and have the potential for being used during the entire development process. In these last years, several attempts were made to develop mechanistic mathematical models to address some questions related to the development of inhaled drugs. The trend that can be observed in the literature is an increase in the model complexity in attempt to represent the lungs in more detail, from considering

[6] This chapter is taken from, Grandoni S., Cesari N., Melillo N., Brogin G., Puccini P. and Magni P., *Development and evaluation of a PBPK modelling framework for inhaled drugs PK studies from the early stages of drug development* (2019), manuscript ready to submit for publication.

regional heterogeneity [48], [49] and later the respiratory generations [118], up to describe the whole organ as a continuum with a partial differential equation approach [52]. However, an increase of complexity in the model typically means an increased number of parameters to characterize the lung and the related PK processes that, as explained in the Section 1.6, are strongly dependent on the lung anatomy and physiology, these parameters, are nowadays still uncertain or scarcely known and in some cases need to be estimated from the *in vivo* data. Furthermore, the major part of the available publications up to now seem to be focused on a single specific drug with its peculiar features, and mostly have not been evaluated in the perspective of predicting lung concentration-time profiles in absence of experimental *in vivo* data. A recent paper by a group of AstraZeneca, reports an elegant effort to evaluate through a compartmental PK approach the lung disposition for different classes of compounds administered by inhalation [47]. In the author's framework, however, animal experiments are requested to fit and evaluate several model parameters, as the main focus of the work was the translation of the PK of orally inhaled compounds from preclinical species to human.

For all these reasons, efforts in this work were made to build a PBPK modelling framework to support inhaled drugs development from the early phases of drug development. A mechanistic pulmonary absorption model was developed [119], [120] to predict the lung and plasma disposition of inhaled compounds in rats from *in silico* and *in vitro* information routinely collected during the discovery phases of the development process and evaluated using lung and plasma concentration preclinical data of compounds with different physico-chemical properties.

At the beginning of this Chapter, the description of

inhaled compounds *in vitro* characterization to assess their pulmonary ADME is reported, since such information was used to structure and parameterize the model. The preclinical experimental setting that generated the data used for the model validation is also reported. Finally, the physiologically based pulmonary model structure and its evaluation will be presented.
To better characterize the model, following the suggestion of the regulatory agencies, a Global Sensitivity Analysis (GSA) of this model was also performed [121] in order to understand how the uncertainty and variability in the model input impact on the uncertainty in the model output, this analysis is reported in Appendix C.

3.1. *In vitro* characterization of compounds used in the study

The *in vitro* properties related to the pulmonary PK collected in this study comprise the powder particle size distribution (PSD), the pulmonary solubility measured in Simulated Lung Fluid (SLF), the lung tissue permeability, the pulmonary fluid and tissue binding. The *in vitro* characteristics related to the systemic PK collected are the *BP*, the plasma protein binding and the Caco-2 GI permeability. How this characterization was done will be described hereinafter. The experiments described were performed by Chiesi S.p.A Laboratories. The physicochemical properties of compounds such as pKa and logP values have been obtained *in silico* using the Percepta Software (Advanced Chemistry Development, Inc.).

Particle size distribution analysis
Cascade impactors are the most widely used instruments to characterize the PSD of compounds for

medical inhalation. A typical cascade impactor is composed of several stages, each of which allow to separate by size the aerosol particles entering the instrument and moving through a gas stream (usually air) at constant velocity (flow rate). Each stage comprises a nozzle and a collection plate located at a fixed distance, that deflects the flow, as reported in Figure 3-1.
The stages classify particles based on their differing inertia, the magnitude of which reflects the resistance to a change in direction of the laminar flow streamlines, particles with a size greater than a critical value impact on the surface, while smaller particles continue to be transported by the gas flow and eventually impact in one of the subsequent stages of the filter. The size at which a given impactor stage collect the 50% of the entering mass is called effective cutoff diameter [122].

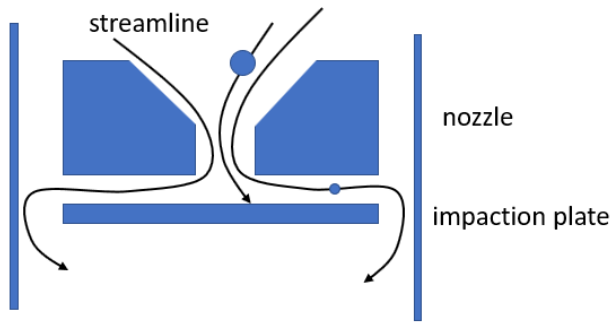

Figure 3-1 The representation of a cascade impactor stage.

Cascade impactor determine particle aerodynamic mass-weighted size distribution, from this, other parameters can be derived, the most important is the Mass Median Aerodynamic Diameter (MMAD), defined as the central tendency of this distribution. The distribution can often be approximated to a log-normal function whose spread is defined by the geometric standard deviation (GSD).

The PSD of the compounds used in this study and the related MMAD and GSD were measured with the PreciseInhale™ (Inhalation Sciences Sweden AB, Stockholm, Sweden) 9-stage Marple cascade impactor (MSP Corp., Shoreview, MN) at a final flow rate of 2 L/min.

Solubility in simulated lung fluid

In the R&D experimental setup considered, to have a measure indicative of solubility in ELF, an *in vitro* solubility test in SLF was applied [123]. This solubility will be used to model the dissolution process in the PBPK model.

The experimental protocol will be described hereinafter.

The SFL was prepared dissolving PBS tablets in Milli-Q water to obtain a final concentration of 10mM and the pH was adjusted to 6.9 by adding few drops of 1M HCl. The surfactant Curosurf® (Chiesi Farmaceutici S.p.A., Parma, Italy) was added to obtain final concentration of 0.02% w/v, [123]. A measure of "apparent solubility" (S_{app}) was determined by the evaluation of the diffusion rate of the analytes from a drug-saturated solution through a membrane and by the diffusion rate of the analytes in a solid-state form, as reported by Stefani et al. [123]. Briefly, a glass container filled with 300 mL of SLF was put at 37°C under slow stirring. During the diffusion with solution experiment, the cassette with the membrane (Slide-A-Lyzer™ G2 Dialysis Cassettes, 10K MWCO, 15 mL, Fisher Scientific Italia) was filled with 10 mL of test compound SLF solution at 5 µg/mL, while in the diffusion with powder experiment, 5 mg of test compound powder were added to 10 mL of SLF already inside the cassette. In both cases, the cassette was closed and put into the glass container. Aliquots for analysis were withdrawn from the outside compartment

before the immersion of the cassette and at a series of time points up to 2h after the immersion. The advantage of this test was the possibility to avoid any issues due to separation of the solution from the undissolved powder and the biological matrix of the test, which was SLF at pH 6.9.

Binding measurements

Plasma protein binding (PPB), lung tissue binding (LTB) and simulated lung fluid binding (SLFB) determination were carried out by equilibrium dialysis. While PPB will be used to calculate f_{up}, SLFB and LTB will be used to calculate the free drug concentration in fluid and in lung as will be explained in Section 3.3.2.

Stock solutions of compounds were prepared and added to the matrix of interest: plasma for rats and man to measure their respective PPB, rat lung homogenate to obtain LTB and simulated lung fluid to obtain SLFB. The addition was done to give a final concentration of 5 µM and then dialyzed for 4 h at 37°C, in accordance with established literature methods. Compounds concentrations in plasma, lung homogenate, lung fluid and in their corresponding buffers, were analysed by high-performance liquid chromatography with mass spectrometric detection (HPLC-MS/MS) on a API 2000 tripe quadrupole mass spectrometer (AB Sciex LLC, Framingham, MA) with an electrospray ionization (ESI) source, coupled to a Water Aquity UPLC I class.

Permeability assays

In the experimental setting of this work, the drug permeability to the GI barrier was assessed through Caco-2 cells, while permeability through the lung barrier was evaluated using Calu-3 cells. Calu-3 cells derive from a bronchial adenocarcinoma of the human airway and form confluent mixed cultures of ciliated

and secretory cells [124]. Commonly used due to the capability of reaching high trans epithelial electric resistance (TEER) [7] values and for their transporter expression similar to those of the respiratory cells [125], this type of cells is robust and easy to culture so can be used for routine screening purposes. They are often used to characterize inhaled drugs, good correlation between the permeability values and the *in vivo* drug absorption in lung has been shown, [126], [127]. Permeability values derived from Calu-3 cells have been integrated in the PBPK model as will be explained in the subsequent Section.

The experimental protocol used is described hereinafter. Gastrointestinal permeability was evaluated using Caco-2 cells lines seeded onto Transwell assay plates, the incubation medium used was Hanks' balanced salt solution buffered at pH 7.4 at 37°C. Compound solutions were made by diluting stock solutions prepared in DMSO with Hanks' balanced salt solution to give a final concentration of 5 µM (final DMSO concentration <1%).

The compound was placed in the apical side to assess permeability in the A-B (apical to basolateral) direction and in the basolateral side to assess permeability in the B-A (basolateral to apical) direction, a schema of the assay is reported in Figure 3-2.

Both the apical and basolateral sides were maintained at pH 7.4. After incubation for 2 h, the apical and basolateral sides were sampled for analysis and compounds concentrations were determined by HPLC-MS/MS using calibration curves normalized with an appropriate internal standard.

[7] The transepithelial electrical resistance (TEER) is a test for the continuous monitoring of tissue viability and integrity through the measurement of potential difference and the current flow across the tissue due to flow of inorganic ions across the epithelium, [59]. High TEER values indicates tight cells junction [157].

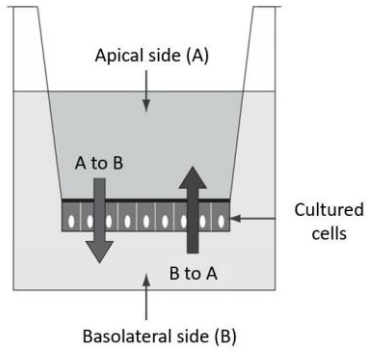

Figure 3-2 The representation of the permeability test used in the *in vitro* compound characterization.

From the test the apparent permeability P_{app} can be calculated for both side test as reported:

$$P_{app} = \frac{dq}{dt}\frac{1}{AC_0} \tag{3.1}$$

where $\frac{dq}{dt}$ is the amount of compound received in the receiver compartment in the time interval dt, A is the exposed surface area and C_0 is the initial concentration in the donor compartment.

Calu-3 permeability assay was performed by a similar protocol as those just described and typically used to study the permeability across the GI barrier.

Efflux transporter Analysis

The analysis of permeability assay results can be used to identify compounds that are efflux transporters substrates. The gold standard for Caco-2 cells, is the calculation of the efflux ratio, i.e. the ratio of the permeability from A to B on those from B to A. If for a compound the value is greater than 2 to or 3 it is typically considered as an efflux substrate, [59]. The same can be applied also to study the efflux in cells derived from respiratory system, [128]. To analyze if a

compound is subject to a certain efflux transporter, the same experiment is generally repeated in presence of an inhibitor of the transporter of interest. For example, if the apparent permeability from B to A decreases in presence of the inhibitor, it means that the transporter has a certain role in moving the compound toward the apical direction.
From the in-house Calu-3 assay data obtained, appears that some of the compounds used in this study are subject to the action efflux transporters.

3.2. Preclinical experimental setting

Nowadays, administration by inhalation to rodents is still an important step in preclinical development of new drugs designed for the inhalation route [38]. Experiments performed in an animal model can provide information on the drug PK as well as on drug and formulation tolerability [12]. Small rodents (mice, rats and guinea-pigs) are commonly used for the earlier *in vivo* evaluations because they can be used in large number, ethical issues and costs limits the use of non-human primates even if they have very similar physiology to human, therefore, they are used only in advanced research.
Several methods exist to deliver compounds by inhalation to rodents, they can be administered by passive inhalation or they can be delivered directly to the lung, in powder or liquid form. With passive inhalation animals are allowed to breath normally, the aerosolized compounds are delivered in an aerosolization chamber with different exposure such as whole body, head only or nose only exposure. Even if with this setup animals can breathe normally, it leads to a poor control of the dose delivered and to a very small percentage of the dose actually delivered to the lungs

(<0.01%), that can be estimated using information about the aerosol chamber concentration, the respiratory frequency, the exposure time and the body weight. IT administration of compounds, indeed, allows a precise control of the dose that reaches the lung as with this technique the compound is delivered directly in the trachea avoiding nasal and oropharyngeal deposition. It allows also to minimize the drug loss in the instrumentation. This method is not representative of the natural inhalation process as the compound is forced into the airways and the animal is under anesthesia [12], however, due to the great advantage of requiring small amounts of the test compound but allowing accurate dosing, it is the principal method used to study lung PK of candidates in small rodents. It is the method used for the *in vivo* preclinical PK studies whose data were used in this work for the model assessment. A particular technology that allow a very precise delivery of the dose through the respiratory system was used as explained hereinafter.

3.2.1. *In vivo* compounds characterization

In the preclinical setting of this work Male Sprague Dawley (CD) rats (Charles River France), weighting 275–330 g at day of the experiments, were used for the intravenous (IV), oral (PO) and IT (IT) administration experiments. The animals were housed under a 12 h light/dark cycle and had free access to pellets and water. The animals were allowed to acclimatize for at least 7 days after arrival at the preclinical laboratory at Chiesi Farmaceutici S.p.A., Parma, Italy, prior to the experiments.

Intravenous administration

For intravenous administration, compounds were administered as a bolus to male CD rats with double

Vascular Access Harness (VAH) catheterization to jugulars and femoral veins (three rats per compound). All compounds were administered using the jugular catheter in 1 mL/kg volume and serial blood samples were taken from femoral vein catheter over a 24 h period. Plasma samples were obtained by refrigerated centrifugation of blood at 2400 g for 10 min and stored at -80°C until analysis.

IT administration

IT dosing was conducted using the PreciseInhale™ aerosol generator (Inhalation Sciences Sweden AB, Stockholm, Sweden) which is capable of delivery powders to the lung with high accuracy and reproducibility (reported typical CV: 15%). To simultaneously evaluate compounds plasma and lung concentration-time profiles, a composite design was used for these experiments which consisted in the administration of compounds to three CD rats /time point in a range 24-96 h period, depending on compound characteristics, and in a range of lung deposited dose of 10 -20 µg/rat. After administration, at each time-points, animals were anesthetized with sevoflurane and sacrificed by total bleeding from abdominal aorta. 5 mL of blood were withdrawn and placed in heparin coated vial. Then the lung was excised, washed with cold saline, accurately weighted and placed in suitable homogenization vials, to obtain the total lung concentration data. Plasma samples were obtained by refrigerated centrifugation of blood at 2400 g for 10 min. and stored at -80°C until analysis.

Plasma samples were prepared at the moment of analysis by protein precipitation with acetonitrile and subsequent dilution with buffered water. Lung samples were added with saline/acetonitrile mixture (50/50) at ratio of 3 mL per gram of tissue and homogenized using Precellys Evolution® homogenator coupled to Precellys

Cryolys temperature controller. The resulting homogenized was purified by protein precipitation with acetonitrile and diluted with buffered water.
Plasma and tissue samples were analysed by HPLC-MS/MS system, using an API 5500 tripe quadrupole mass spectrometer (AB Sciex LLC, Framingham, MA) with an electrospray ionization (ESI) source, coupled to a Water Aquity UPLC I class. Analyte separation was obtained by reversed phase chromatography optimized for each compound and the quantitation was performed by interpolation to a calibration curve using the area ratio between the analyte and an internal standard.
The aerodynamic PSD of the aerosol was determined by cascade impaction analysis using the PreciseInhale™ system with a Marple cascade impactor (MSP Corp., Shoreview, MN, USA) attached to the exposure outlet by gravimetric measurement. The fractions available for bronchial, alveolar and total lung deposition were calculated using Multiple-Path Particle Dosimetry Model (MPPD) software (Applied Research Associates, Inc.) and a breathing simulation model for the rat at default settings (tidal volume 2.1 mL and 102 breaths/min).

In vivo PK quantification
The *in vivo* PK was analyzed through non compartmental analysis (NCA). NCA does not require the assumption of a specific compartmental model for the compound under study. It is essentially based on the application of the trapezoidal rule for measurements of the AUC of the concentration–time curve, on which other parameters can be derived. This methodology is generally applied to determine the degree of exposure following the drug administration.
The lung PK profiles after IT administration were characterized in terms of AUC of the concentration-time curve, of mean residence time (MRT) and of

terminal half-life (THL [8]). For plasma also the maximum concentration (C_{max}) and the time to reach the maximum concentration (T_{max}) were included. AUC and MRT were calculated from the first up to the last sample time point. The NCA analysis were performed with Phoenix WinNonlin 8.1 (Certara L.P.), the golden standard tool for this kind of analysis.

3.3. Model formulation and parameterization

In this Section the physiologically-based pulmonary model is presented. The pulmonary model structure consists of two main regions, the central (C) and the peripheral one (P), as previously proposed by [48] and [52], to reflect the respiratory system division in airways and pulmonary regions. Each region is characterized by a different volume, surface and perfusion (the C region is connected with the systemic circulation, the P region with the pulmonary one). The model includes the main processes occurring when a drug is inhaled: deposition, dissolution, mucociliary clearance removal and the absorption in the blood circulation [32]. Hence, in each model region, the drug deposits following a certain deposition pattern, exists in the undissolved form, can dissolve in the ELF and be absorbed through the tissue. The non-absorptive clearance due to the mucociliary clearance action is included and acts on the undissolved drug in the C region since in the pulmonary region this mechanism is negligible [32]. The drug is absorbed through the lung via passive bidirectional transport, the contribution of a

[8] THL is defined as the time in which the drug concentration decreases of one-half in the terminal phase (the terminal region of the PK curve where drug concentration follows a first-order elimination kinetics) [158], [159].

monodirectional transport from the tissue to the fluid is included in the model to reproduce the possible action of efflux transporters. The lung tissue is divided in two parts, one representing the EV part of the tissue and one representing the VASC part, for both the regions. The representation of the pulmonary model is reported in Figure 3-3. The whole model structure is depicted in Figure 3-5.

3.3.1. Model formulation

Deposition

The deposition of drug in the lung is modelled introducing deposition fractions. The fraction F_{INH}, represents the portion of the delivered drug that actually reaches the respiratory system (the remaining is exhaled). Of the net amount inhaled, a fraction F_{LUNG} actually reaches the lung and the remaining (F_{SWA}=1-F_{LUNG}), those deposited in the oropharyngeal region, is swallowed and reaches the stomach compartment of the GI absorption model. The inhaled drug partitioning between the C and the P regions is modelled and with the fractions F_C and F_P=1-F_C. The central deposition F_C has been calculated as:

$$F_C = \sum_{i=1}^{9} f_i F_{C,i} \tag{3.2}$$

where f_i is the fraction of the total mass filtered by the $i-th$ stage of the filter, obtained from the PSD analysis, $F_{C,i}$ is the central deposition for particles with diameter equal to the mean diameter d_i, calculated considering the range of filtration of the $i-th$ impactor stage.

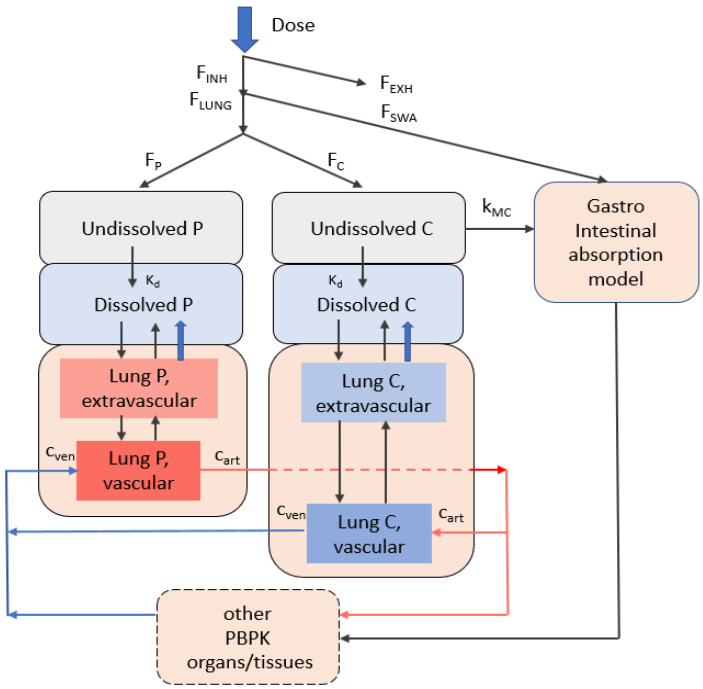

Figure 3-3 The pulmonary model developed to study IT administration of compounds in rats.

Dissolution and clearance

The dissolution of solid drug in the ELF is modelled by the Nernst-Brunner equation, the dissolution rate k_d it is supposed to depends on particle properties such as radius r, solubility of the drug in the ELF, S_{ELF}, and on the free drug concentration in the fluid, here calculated as the product of the dissolved concentration $c_{diss}$with the fraction of the free drug in the ELF f_{ufluid}.

$$k_d = \frac{3D}{\rho r T}\left(S_{ELF} - c_{diss} f_{ufluid}\right) \tag{3.3}$$

Since the drug concentration in the fluid differs between the two regions for the heterogeneity of the

lung, two distinct dissolution rates, $k_{d,C}$ and $k_{d,P}$, govern the dissolution.
The mucociliary clearance is modelled as a first order process characterized by a constant k_{MC}.
The resulting equations describing the time change of the undissolved mass in the undissolved drug compartments, the first for the C region and the second for the P region are reported below:

$$\frac{da_{und,C}}{dt} = -k_{d,C}a_{und,C} - k_{MC}a_{und,C} \quad (3.4)$$

$$\frac{da_{und,P}}{dt} = -k_{d,P}a_{und,P} \quad (3.5)$$

whose initial conditions for an IT administration are:

$$a_{und,C}(0) = F_{INH}F_{LUNG}F_C D_{INH} \quad (3.6)$$

$$a_{und,P}(0) = F_{INH}F_{LUNG}F_P D_{INH} \quad (3.7)$$

The dissolved compartments represent the amount of drug dissolved in the ELF, from here, the free dissolved drug can enter the EV tissue compartment and return via passive transport. The free drug in tissue can also move upward toward the dissolved compartment by a monodirectional transport, included to mimic the possible action of efflux transporters. As explained in Section 1.6 the passive transport depends on the drug properties (e.g. tissue permeability) and on the tissue properties such as the surface area (this has been included in the model as also proposed in [49]) and the thickness. Since permeability measures derive from Calu-3 cells that are representative of the bronchial tissue, a correction factor α has been included in the model to take into account the different tissue thickness in the P region. It is assumed that the passive transport

is faster in the P region for the lower tissue thickness. The monodirectional efflux it is supposed to be governed by the drug permeability and on the surface area, supposing that transporters presence is proportional to the surface considered. Details regarding the permeability components will be explained hereinafter. The equations describing the mass changes during time in the C and P dissolved compartments are reported below:

$$\frac{da_{diss,C}}{dt} = k_d a_{und,C} - P_p S_C \left(\frac{a_{diss,C}}{V_{ELF,C}}\right) f_{ufluid} + P_p S_C c_{C,EV} f_{ulung} + P_a S_C c_{C,EV} f_{ulung} \quad (3.8)$$

$$\frac{da_{diss,P}}{dt} = k_d a_{und,P} - \alpha P_p S_P \left(\frac{a_{diss,P}}{V_{ELF,P}}\right) f_{ufluid} + \alpha \cdot P_p S_P c_{P,EV} f_{ulung} + P_a S_P c_{P,EV} f_{ulung} \quad (3.9)$$

where $a_{diss,C}$ and $a_{diss,P}$ are the dissolved mass in the C and P compartments, $c_{C,EV}$ and $c_{P,EV}$ are the C and P lung EV concentrations, f_{ulung} the fraction unbound in lung, S_C and S_P the C and P surface areas, $V_{ELF,C}$ and $V_{ELF,P}$ the respective ELF volumes, P_p is the passive component of the permeability, P_a is the active one.
The free drug in EV tissue compartments is subject to passive transport toward the VASC compartment, the free drug in blood can move from it back to the EV compartments.
The equations describing the changes during time of drug concentration in the C and P EV compartments are reported below:

$$\frac{dc_{C,EV}}{dt} = \frac{1}{V_{C,EV}} (P_p S_C \left(\frac{a_{fluid,C}}{V_{ELF,C}}\right) f_{ufluid} - 2P_p S_C c_{C,EV} f_{ulung} - P_a S_C c_{C,EV} f_{ulung} + P_p S_C c_{C,VASC} f_{ub}) \quad (3.10)$$

$$\frac{dc_{P,EV}}{dt} = \frac{1}{V_{P,EV}}(\alpha P_p S_P \left(\frac{a_{fluid,P}}{V_{ELF,P}}\right) f_{ufluid} - 2\alpha P_p S_P c_{P,EV} f_{ulung} - P_a S_P c_{P,EV} f_{ulung} + \alpha P_p S_P c_{P,VASC} f_{ub}) \quad (3.11)$$

where $c_{C,EV}$ and $c_{P,EV}$ are the EV concentration in the C and P region, f_{ub} is the fraction unbound in blood, $V_{C,EV}$ and $V_{P,EV}$ are the EV C and P volumes.
The resulting equations for the VASC compartments are reported hereinafter:

$$\frac{dc_{C,VASC}}{dt} = \frac{1}{V_{C,VASC}}\left(Q_C\left(c_{art} - c_{C,VASC}\right) - \alpha P_p S_C c_{C,VASC} f_{ub} + \alpha P_p S_C c_{C,EV} f_{ulung}\right) \quad (3.12)$$

$$\frac{dc_{P,VASC}}{dt} = \frac{1}{V_{P,VASC}}\left(Q_P\left(c_{ven} - c_{P,VASC}\right) - \alpha P_p S_P c_{P,VASC} f_{ub} + \alpha P_p S_P c_{P,EV} f_{ulung}\right) \quad (3.13)$$

the terms $c_{C.VASC}$ and $c_{P,VASC}$ are the VASC concentration in the C and P region, Q_C and Q_P are the C and P region blood fluxes, $V_{C,VASC}$ and $V_{P,VASC}$ are the C and P region VASC volumes, c_{art} and c_{ven} are the arterial and venous concentration. The VASC C compartment is connected with the systemic circulation, while the P one is connected with the pulmonary circulation, hence, Q_P represents the cardiac output.

3.3.2. Model parameterization

Systems specific pulmonary parameters
The values of system-related pulmonary parameters such as surfaces, volumes and blood fluxes were obtained from [49], the repartition of the lung volume in EV and VASC part was done as explained in Section 2.1.3 for the muscle and the rest of the body tissues and was assumed to be the same for both the regions. The

mucociliary clearance rate for rats was calculated from the average particles half-life in the rat respiratory system, $T_{1/2}$, reported in [129]. It has been assumed that the process of particle transport is governed by a linear kinetics and the final value of k_{MC} has been computed as $\ln(2)/T_{1/2}$. The permeability correction factor α was derived as the ratio between the bronchial and the pulmonary tissue thickness in rats, averaging the values extracted from different sources [49], [130], [26].
The values of the parameters used are summarized in Table 3-1.

Table 3-1 Values of the physiological pulmonary parameters for rat.

Rat parameter	**Central**	**Peripheral**
Blood Flow (as fraction of Q_{CO})	0.021	1
Surface Area [cm^2]	81.75	6910
ELF volume [ml]	0.0409	0.048375
Volume (as fraction of the total lung volume)	0.195	0.805
Vascular volume (as fraction of the region volume)	0.45	0.45
k_{MC} [s^{-1}]	$1.54*10^{-4}$	
Alveolar permeability adjustment constant, α		15.58

Drug-specific parameters
Since the drug in the experimental setup considered is delivered by IT administration, the deposition parameters F_{INH} was set to 1 and it is supposed that a small fraction can be swallowed by rats, hence F_{LUNG} was set to 0.9. The fraction of drug repartition in the two regions, F_C and F_P, were obtained with the deposition modelling tool Multiple Path Particle Deposition (MPPD) tool v.2.1 (Applied Research Associates, Inc.), widely used in pharmaceutical

research [131]. The tool contains a deposition model implemented in it to predict the particle deposition in different species that comprises those of interest in this work, i.e. rat and man. The tool allows the user to insert the main particles size descriptor used in inhalation studies such as the MMAD and the GSD. Furthermore, different experimental setup such as IT administration and nose-only exposure can be selected. To calculate F_C, each repartition fraction $F_{C,i}$ was obtained calculating, for each mean stage diameter d_i, the deposition with the tool.
In the *Particle properties* menu, d_i was set as the MMAD for each simulation and a GSD of 1 was imposed (a value <1.05 indicates that particles are monodispersed). In the *Exposure Scenario* menu, the *body orientation* was set as *on back*, while the breathing scenario was set as *endotracheal*. All the other parameters were set as default. The *deposition only* mode was selected in the *Deposition/Clearance* section, for the final computation. The repartition fraction $F_{C,i}$ was calculated from the *Central/Peripheral* output. The final deposition for the C compartment was then calculated using the mass fractions $f_i$obtained from the PSD distribution characterization, as explained in the Section 3.3.1.
The parameters related to dissolution such as D, T and ρ were computed as reported in Section 2.1.2 for the GI absorption model. The viscosity to calculate the diffusion coefficient D was fixed to those of the surfactant Curosurf® used to obtain the SLF, that is of 10 cP. The particle radius used was calculated from the geometrical diameter d_g assuming that it is equal to the aerodynamic one. As explained in the Section 1.6 the aerodynamic diameter d_{ae} is a measure that takes into account the particle density and shape and can be derived from the geometric radius as:

$$d_{ae} = d_g \sqrt{\frac{\rho/\rho_0}{X}} \tag{3.14}$$

where ρ_0 is the unit density (i.e., 1 g/cm^3), X is the shape factor, whose value is 1 if the particle is perfectly spherical, a value larger than one indicates that the particle is not spherical. In this work we supposed that particles are perfectly spherical and hence X was fixed to 1, with density of 1 g/cm^3. This makes possible to equal the d_g to d_{ae} and hence r was calculated as d_{ae} /2, as d_{ae} the MMAD obtained from the PSD characterization was used. The solubility in the ELF was fixed to those obtained in the SLF, that was used as a proxy of the real solubility in the ELF both in the C and in the P region, in absence of further information and as proposed also in the work of Boger et. al, where however, the solubility parameters is derived by fitting *in vivo* data [49]. Instead here, in the perspective of using the model in the drug discovery setting, was fixed to the value obtained from *in vitro* test, as explained in the previous Section.

The permeability values governing the absorption to input in the PBPK model were derived modelling the passive transcellular exchanges and the efflux of the compounds during the Calu-3 permeability *in vitro* test as proposed in [132], with a modelling approach similar to those reported in [133] and in [134], this was done in order to discriminate the passive and active transport components. The model consists of three compartments, one representing Calu-3 cells, two representing the apical and the basolateral fluid present in the experimental setup. A representation of the model is reported below:

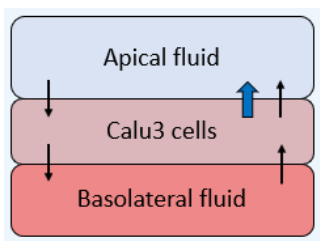

Figure 3-4 The model of the *in vitro* Calu-3 permeability system.

The compound flux due to the passive transcellular exchanges it is supposed to be dependent on the available free drug, on the available surface, and on the drug permeability as in the pulmonary model. The active efflux depends also on the free drug and on the surface as it is supposed that the presence of transporters is proportional to the available surface. The binding to the cells was considered, no binding to the media of the apical and basolateral side was included. As Calu-3 cells in culture produce mucus [135] to evaluate the presence of mucus in the apical side fluid and hence the possible inclusion of a binding to the ELF in the apical side, the percentage of mucus in the total apical medium volume was calculated as the product of the culture surface with the thickness of mucus produced in the human bronchial tissue reported in [136], this percentage was negligible.
The equations describing the variation during time of the compound concentration in the different compartments are reported hereinafter:

$$\frac{dc_{AF}}{dt} = \frac{1}{V_{AF}}(-P_p A c_{AF} + P_p A c_C f_{ulung} + P_a A c_C f_{ulung}), \quad (3.15)$$

$$\frac{dc_C}{dt} = \frac{1}{V_C}(-2P_p A c_C f_{ulung} - P_a A c_C f_{ulung} + P_p A c_{AF} + P_p A c_{BF}), \quad (3.16)$$

$$\frac{dc_{BF}}{dt} = \frac{1}{V_{BF}}(-P_p A c_{BF} + P_p A c_C f_{ulung}) \quad (3.17)$$

where c_{AF} and c_{BF} are the apical and basolateral fluid concentration respectively, c_C is the cell concentration, V_{AF} and V_{BF} are the apical and basolateral fluid volumes respectively, V_C is the cell volume. A is the area of the cell culture P_p and P_a are permeabilities governing the passive bidirectional exchange and the monodirectional efflux.
The area A, the volumes of the media and of the cells were obtained from the experimental setup, the value of the binding to the cells derive from the *in vitro* binding

measurements for rats. Fixed all these parameters, P_p and P_a were estimated simultaneously fitting the experimental apical and basolateral cell concentration obtained from the assay.
Concerning the model parameters related to the compound binding to fluid, to the lung, to plasma and to blood, they were calculated using those experimentally obtained by equilibrium dialysis as explained in Section 3.1. In particular $f_{ufluid} =$ 1-SLFB, $f_{ulung} =$ 1-LTB, $f_{up} =$1-PPB and $f_{ub} = f_{up}/BP$.

All the drug specific parameters for the compounds used in the evaluation study, that will be presented in the subsequent Section, are reported in Table 3-2.

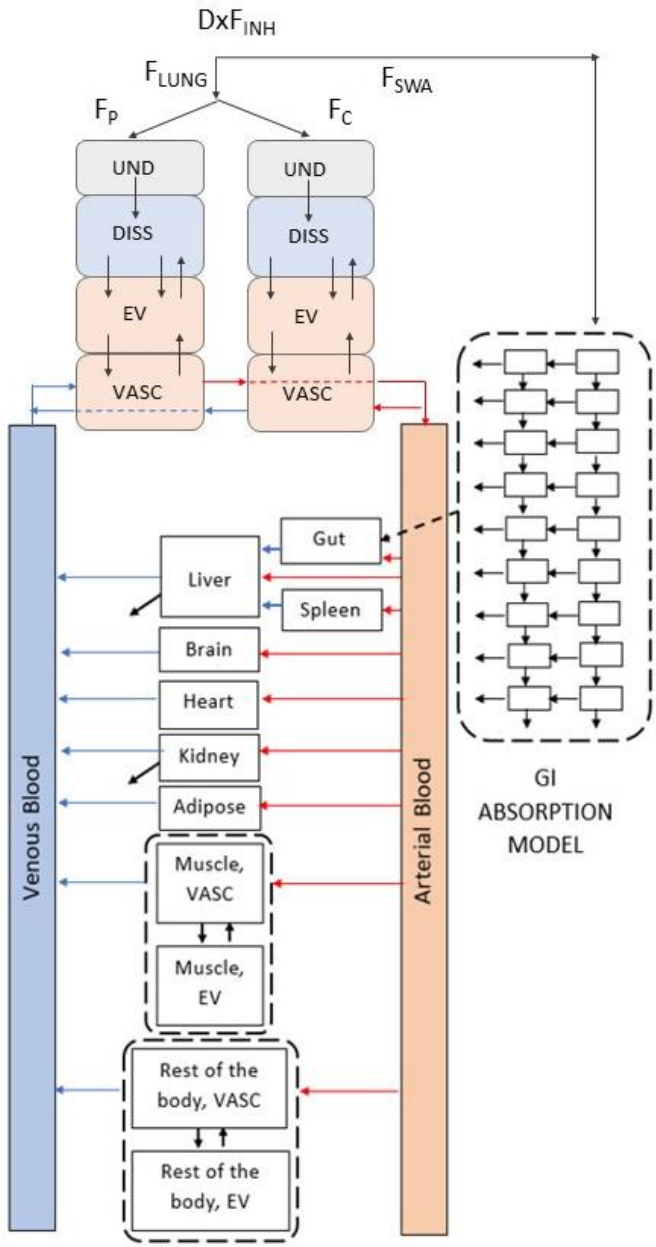

Figure 3-5 The whole model structure.

Table 3-2 Summary of the compound specific parameters. N=neutral, B=base, DB=diprotic base.

	Compounds									
	A	**B**	**C**	**D**	**E**	**F**	**G**	**H**	**I**	**L**
Species	N	N	DB	B	DB	B	DB	N	B	B
pKas			3.43, 7.59	9.81	7.4, 8.8	7.9	3.28, 8.7	8.7	8.5	8
logP	1.32	-1.34	2.38	1.99	2.83	3.23	5.4	3.87	5.4	5
logD	1.32	-0.89								
PPB [%]	94.61	74.4	80.67	17.84	98.6	96.42	98.57	96.8	99.85	99.4
BP	0.6	0.55	0.78	1.6	0.7	0.99	1.47	0.8	1	1
Er	0.523	0.95	0.82	0.95	0.95	0.83	0.953	0.8	0.95	0.95
MMAD [µm]	2.86	2.9	3.52	3.2	2.57	3.27	3.92	2.59	1.71	3.51
GSD	1.69	1.66	1.86	1.67	1.93	1.75	1.67	2.1	2.33	1.68
D [cm^2/s]	3.51e-07	3.79e-07	3.69e-07	4.41e-07	3.52e-07	4.07e-07	3.37e-07	3.51e-07	3.58e-07	3.48e-07
ρ [ng/ml]	1.00e+9	1.00e+9	1.00e+9	1.00e+9	1.00e+9	1.00e+9	1.00e+9	1.00e+9	1.00e+9	1.00e+9
T [µm]	1.43	1.45	1.76	1.6	1.285	1.635	1.96	1.295	0.855	1.755
S_{SLF} [ng/ml]	291000	2.50e+06	377000	360000	43600	6600	15800	696	14300	600
F_{LUNG}	0.9	0.9	0.9	0.9	0.9	0.9	0.9	0.9	0.9	0.9

F TB	0.47	0.57	0.54	0.51	0.54	0.46	0.56	0.43	0.36	0.51
LTB [%]	99.5	96.1	96.5	73.6	99.5	98.52	99.4	99.85	99.9	99.8
SLFB [%]	30	4	3	0	59	0	49	84	90	86
Calu-3 AB permeability [nm/s]	0.28	1.10	1.36	1.61	0.90	29.9	0.48	0.99	0.080	30
Calu-3 AB permeability [nm/s]	6.84	1.83	37.90	0.10	32.00	56.60	167.00	0.83	2.360	25
Pp [nm/s]	19.47	12.85	42.22	13.06	47.38	149.66	174.7	55.86	20.54	154
Pa [nm/s]	454.00	8.5	1134	68.82	1658.2	134	60600	4.00e-06	598.74	63

3.4. Model evaluation

The model was tested using the plasma and total lung concentration data obtained after IT administration with the PreciseInhale™ Technology as explained in the Section 3.2.1, of the 10 compounds in rats. Even if the primary endpoint was the prediction of the lung PK, the plasma PK after IT administration was also considered since it is often evaluated in preclinical trials to monitor toxicity and to compare the lung and systemic exposure through the lung to plasma AUC split ratio calculation, an high value of this ratio is often considered as positive for inhaled drug candidates. Furthermore, plasma concentration represents the endpoint monitored in clinical trials, as explained previously, for the challenges in sampling lung.

To evaluate the ability of the model to prospectively predict the lung PK of inhaled compounds in the *in vivo* data free phases, all the pulmonary drug-related parameters of the model were fixed at those derived by *in vitro* or *in silico* experiments as explained in the Section 3.1 (e.g. solubility, lung tissue binding, lung membrane permeability) and summarized in Table 3-2. However, as we want also to evaluate the ability of the model to predict the plasma profiles due to pulmonary absorption, when necessary, the IV simulations were adjusted to fit the observed data and the hepatic extraction ratio was derived from *in vivo* IV experiments as explained in Section 2.1.5, as generally IV experiments are performed to characterize the PK before IT *in vivo* administrations. This procedure improved the ability of the model to predict plasma PK after IT administration. The simulated profiles after IT administration were obtained without any parameter fitting on IT data. It should be noted also that compounds used in this study have high hepatic extraction ratios and hence the systemic contribution of a possible GI absorption (e.g. due to the mucociliary clearance

action) is minimized, hence, plasma profiles represent mainly the pulmonary absorption.

3.4.1. Evaluation plan and results

The selected compounds have different characteristics in terms of solubility and *in vivo* lung retention, hence, to evaluate the model predictive ability in different scenarios, compounds were classified on the basis of their degree of solubility and of lung retention. The compounds used in this study were divided in two classes, highly soluble (HS) and poorly soluble (PS), following the publication of Hastedt et. al [137], in which the possibility to define a pulmonary biopharmaceutical classification is discussed. The application of the dose number as in the BCS for orally administered drug is proposed. In this work the dose number D_0, was calculated as:

$$D_0 = \frac{D_{IT}/V_{ELF}}{S_{SLF}} \tag{3.18}$$

where D_{IT} is the dose that actually reaches the lung, as stated above, in this study it has been assumed that the 90% of the drug reaches the lung and that 10% can be swallowed by rats, V_{ELF} is the total volume of the ELF for rats and S_{SLF} is the solubility measured in simulated lung fluid. Compounds with D_0 equal or greater than 1 were classified as PS, the others as HS. The model was evaluated at first on HS compounds, for which the dissolution was not a limiting step for entering the systemic circulation. This simplified the hypothesis on the absorption dynamics and restricted the lung disposition mainly to the interplay of two parameters: the permeability across the lung barrier and the lung tissue binding. Then, the analysis was extended to PS compounds to evaluate the ability of the model to capture a more complex absorption dynamics in which the

dissolution process contributes to control the absorption rate.

Compounds were further classified in poorly lung retained (PR), when their THL and MRT are below 12 h, and in highly lung retained (HR) when they are above 12 h. The complete classification of compounds is reported in Table 3-3. To quantitatively evaluate the prediction capabilities of the model, in addition to the visual inspection comparing the total lung (obtained as the sum of the drug concentration in all the lung compartments) and the plasma concentration predicted profiles with the *in vivo* data, a FE analysis was performed. The PK metrics obtained from the *in vivo* data were compared with those obtained from the simulated profiles. The metrics selected are those reported in Section 3.2.1.

The comparison between the *in vivo* data and the predicted profiles for the different compounds is reported in Figure 3-6 and in Figure 3-7.

Table 3-3 The compounds classification in terms of solubility and lung retention (SC= solubility classification, RC= retention classification).

Compound	D_0	SC	MRT	THL	RC
A	0.04	HS	9.62	29.25	PR
B	0.34	HS	21.75	33.77	HR
C	0.41	HS	6.44	7.48	PR
D	0.42	HS	2.57	3.4	PR
E	2.31	PS	14.26	13.16	HR
F	15.3	PS	1.87	2.18	PR
G	6.39	PS	5.4	7.32	PR
H	144	PS	18.84	25.68	HR
I	16.2	PS	13.97	49.94	HR
L	168	PS	12.65	-	HR

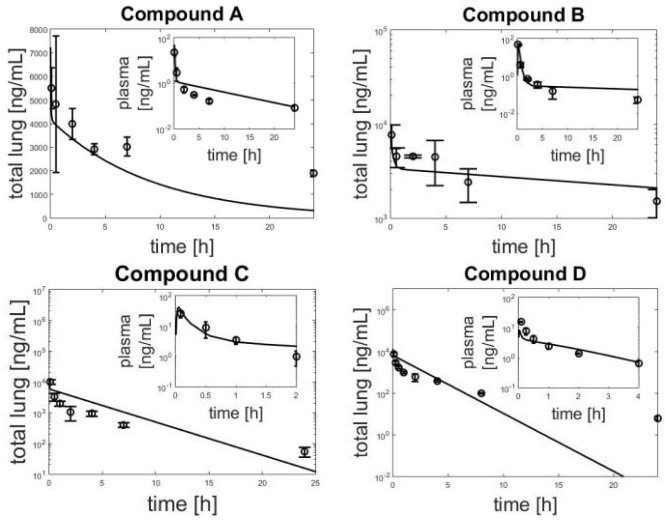

Figure 3-6 The results of the comparison for the HS compounds.

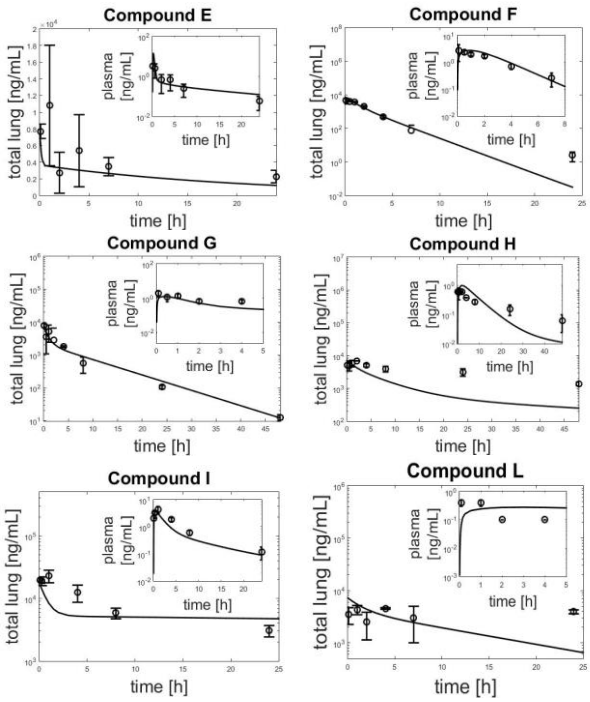

Figure 3-7 The results of the comparison for the PS compounds.

The FE analysis was performed as for the PBPK model evaluation presented in Section 2.2. The results related to the lung PK prediction are reported graphically in Figure 3-8. The compounds are distinguished by the category to which they belong, to understand if for a certain group a specific trend can be observed.

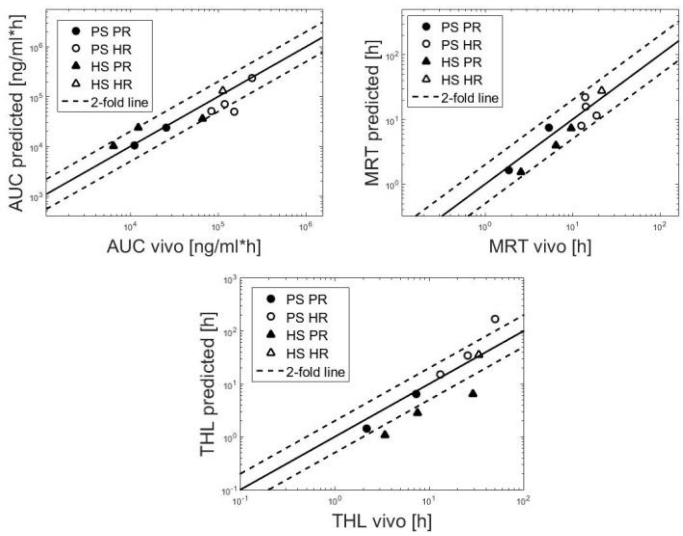

Figure 3-8 The lung PK FE analysis is reported considering for each compound its group. In the first panel is reported that for the AUC, in the second for the MRT, in the last for the THL, calculated up to the last observation time.

The results show that the model is able to correctly predict the selected PK metrics for the lung, that are inside the two fold limit in almost all cases for the AUC and MRT, with less accuracy the model predicts the THL, in particular for the HS and PR compounds, where it is underestimated, this can be probably explained with an overestimation of the passive permeability.
Concerning the PK metrics related to plasma profiles, the results are reported in Figure 3-9.

Results show that plasma profiles overall exposure metrics such as the AUC and the MRT are correctly predicted, as well as the C_{max} and the THL, while the model fails in some cases in reproducing the correct T_{max}, where deviations from the two-fold line occur.

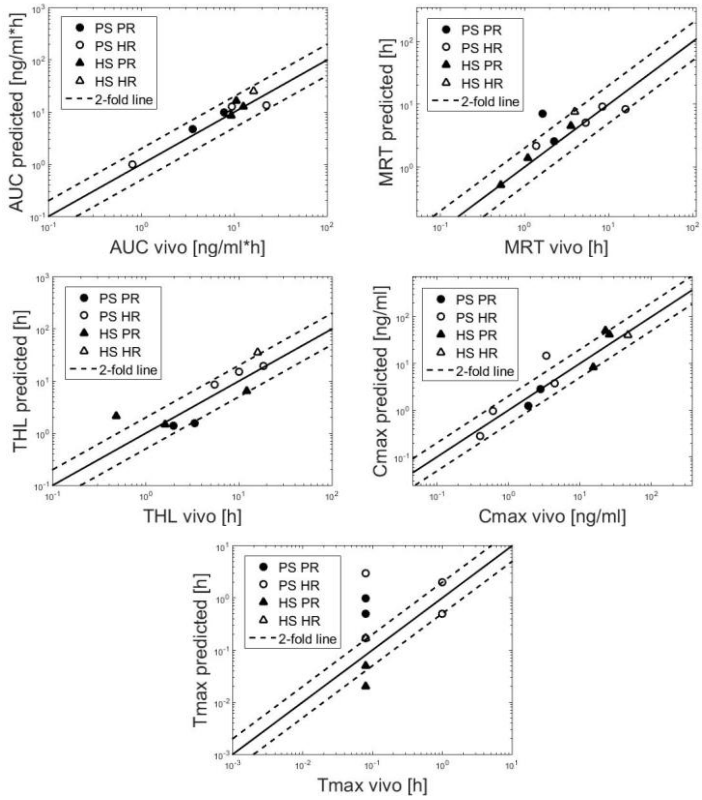

Figure 3-9 The FE analysis related to the selected plasma PK metrics. AUC in the first panel, MRT in the second, THL in the third, C_{max} and T_{max} in the fourth and fifth respectively.

3.5. Analysis of the inclusion of the particle size distribution in the dissolution model

Since in the model presented here the PSD was considered only in the calculation of the deposition fractions, simulation studies were performed to evaluate if, with the level of details in the lung structure of this model, its inclusion in the dissolution modelling leads to substantial changes in the considered model outcomes (i.e. the total lung and plasma profiles). Furthermore, this analysis allows a better characterization of the model.

To perform this evaluation, we extended the dissolution model previously formulated. The solid drug compartment was hence discretized in 9 sub-compartments, the choice of this number is due to number of sections in the filter used in the PSD analysis as explained in Section 3.1. The resulting fraction of mass inside each filter stage, f_i , was used to calculate the mass in input to each sub-compartment, the particles inside each of them were supposed to be monodispersed and with an MMAD equal to d_i. Hence, due to their different size, in each sub-compartment particles dissolves with different dissolution rates according to the Nernst-Brunner equation.

According with this hypothesis, the equations for the undissolved compartments are the following:

$$\frac{da_{und,C,i}}{dt} = -k_{d,i}a_{und,C,i} - k_{MC}a_{und,C,i} \qquad (3.19)$$

$$\frac{da_{und,P,i}}{dt} = -k_{d,P,i}a_{und,P,i} \quad (3.20)$$

$i = 1, \dots, 9$

where, the dissolution rate for each compartment was calculated as:

$$k_{d,C,i} = \frac{3D}{\rho r_i T}\left(S_{ELF} - \frac{a_{diss,C}}{V_{ELF,C}}\right), \quad (3.21)$$

$$k_{d,P,i} = \frac{3D}{\rho r_i T}\left(S_{ELF} - \frac{a_{diss,P}}{V_{ELF,P}}\right) \quad (3.22)$$

$i = 1, \dots, 9$

where r_i are obtained as $d_i/2$, where d_i is the mean diameter given the filtration range of the $i-th$ stage of the impactor.
All the other compartments equations are the same as previously formulated in Section 3.3.1.
The initial conditions for an IT administration are:

$$a_{und,C,i}(0) = D_{INH}F_{INH}F_{LUNG}F_{C,i}f_i \quad (3.23)$$

$$a_{und,P,i}(0) = D_{INH}F_{INH}F_{LUNG}(1 - F_{C,i})f_i \quad (3.24)$$

$i = 1, \dots, 9$

For the different compounds, several IT experiments were simulated with different PSDs, maintaining the same MMAD fixed in the scenario of Section 3.4.1, in which particles were monodispersed. The PSD selected ranged from the classical bell-shaped profiles to completely different scenarios in which the PSD is U-shaped**.** An example of the distributions used in this analysis is shown in Figure 3-10.
For each compound, the differences Δ_p in the PK metrics computed on the profiles simulated with the

current version of the model (P_{PSD}) respect to those obtained with the previous version of the model (P_{MMAD}), were considered, for each PSD scenario. These deviations were hence calculated as:

$$\Delta_p = \left(\frac{P_{MMAD} - P_{PSD}}{P_{MMAD}}\right) * 100 \quad (3.25)$$

Hence, a negative change indicates an increase in the parameter of interest.

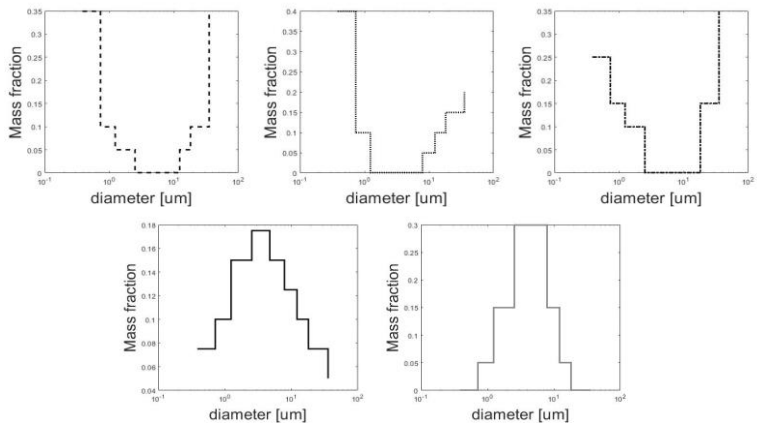

Figure 3-10 Examples of PSD used in this study (in semi-log scale). Three different U-shaped distributions: symmetric U distribution (first panel), a U left skewed distribution (second panel), a U right skewed distribution (third panel). Two bell shaped distributions: one large (fourth panel) and one narrow around the MMAD value (fifth panel).

3.5.1. Results

The first analysis was carried out on HS compounds in order to verify if, as expected for this class, outputs are substantially insensitive to the introduction and changes in

the PSD. The results confirm this hypothesis as shown in Figure 3-11 for the compound C.

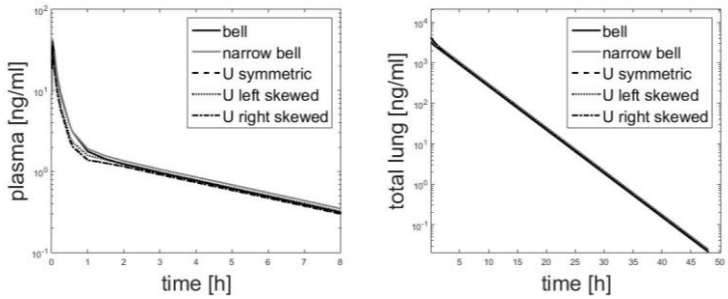

Figure 3-11 The different profiles generated by the different PSDs (previously shown) for the compound C.

For this reason, results presented hereinafter are focused on PS compounds. In the next graphs are reported the changes Δ_p related to total lung concentration profiles.

In Figure 3-12, results of the analysis for the AUC are reported. They show a limited sensitivity of the overall exposure metric AUC, under the 40% for the bell-shaped distribution and greater, but under the 60%, for the U-shaped distributions.

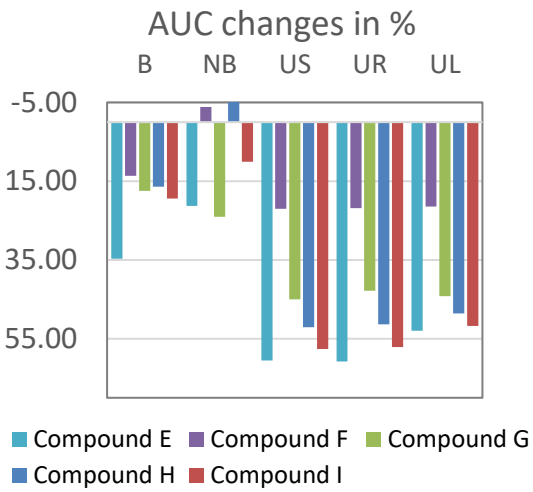

Figure 3-12 The total lung AUC sensitivity to the PSD.

A systematic decrease of the AUC is observed for almost all the compounds and distributions, especially in case of U-shaped distributions. Understand the reason of this behavior is not an easy task, since the total lung profile is the sum of the dissolved, undissolved and lung tissue concentration, an explanation, could be the introduction of fast dissolution components that leads to a faster emptying of the lung and hence a reduced exposure.
Smaller changes are observed for the lung MRT (Δ_p between ±30%), Figure 3-13, where a particular trend referred to compounds and distributions cannot be observed.

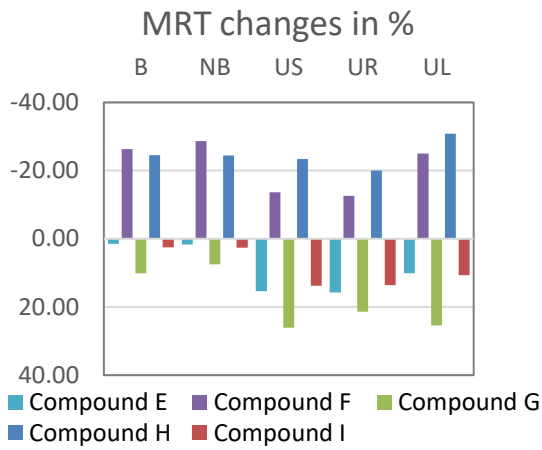

Figure 3-13 total lung MRT sensitivity to the PSD.

Concerning the THL, variations are very limited (less the 10%) for all the compounds except for one compound G whose variations are for the bell-shaped profiles around the 200% and double in case of U-shaped profiles, the differences are shown in Figure 3-14.
Concerning the second endpoint analyzed (plasma concentration), simulations on AUC and MRT reveal similar results to those previously obtained on total lung, with variation around the 40% for the first metric and about ±60% for the second (the graphs are shown in Appendix B).

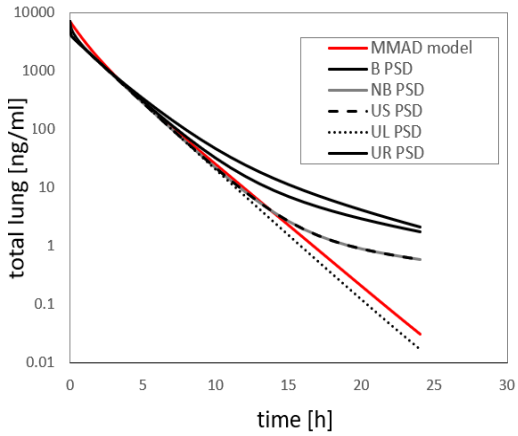

Figure 3-14 A comparison between the total lung profiles simulated with the test distributions and with the previous version of the model in which the particles are monodispersed and characterized by the MMAD (red line), for compound G.

The PSD has greater impact on C_{max}, T_{max} and THL. In Figure 3-15 results for the plasma C_{max} are shown. From them, appears that the C_{max} is sensitive to the PSD. In case of bell-shaped distributions, the changes range from 20% to 100%, while reach higher values in case of U-shaped distributions. Considering that almost all these compounds have high extraction ratio values and hence plasma profiles are mainly due to pulmonary absorption, this result can be explained by the fact that introducing the PSD means to introduce fractions of particles with diameters smaller than the MMAD, that, in accordance with the Nernst-Brunner equation dissolve faster, can escape the mucociliary clearance (process in competition with dissolution) and consequently being rapidly absorbed in plasma leading to higher plasma peaks. This amount dramatically increases in case of U-shaped distributions when, compared to the realistic bell-shaped ones smaller particles are overrepresented.

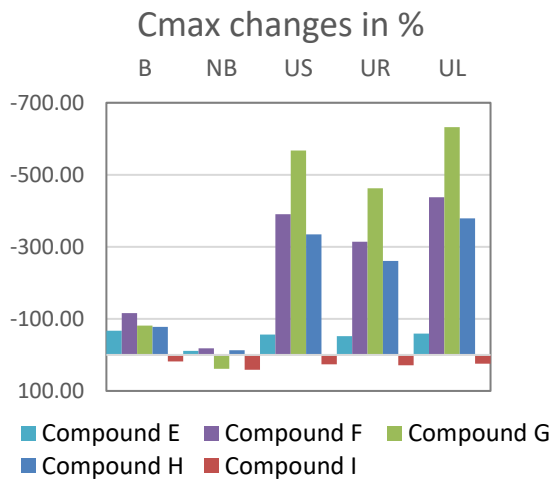

Figure 3-15 The plasma C_{max} sensitivity to the PSD.

The T_{max} observed changes are for all cases under the 100% and can be observed that, with few exceptions, the T_{max} is always reduced introducing the PSD, this can be explained, as for the C_{max}, with the fact that fast dissolving components have been introduced in the model.

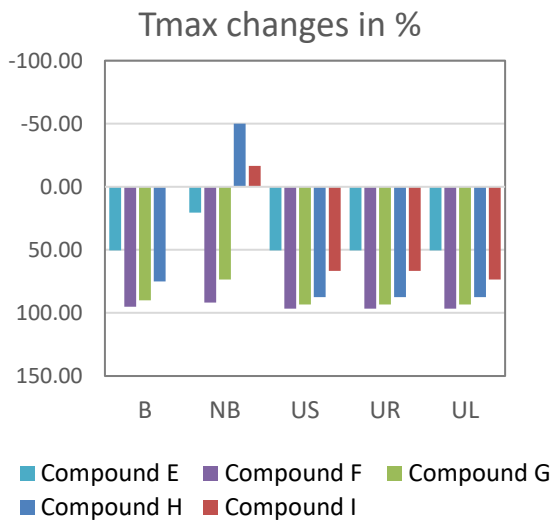

Figure 3-16 The plasma T_{max} changes.

Regarding the THL variations, instead, a trend among the distributions cannot be observed, furthermore, the THL seems to be substantially insensitive to the changes in the PSD but very different between compounds as can be seen in Figure 3-17.

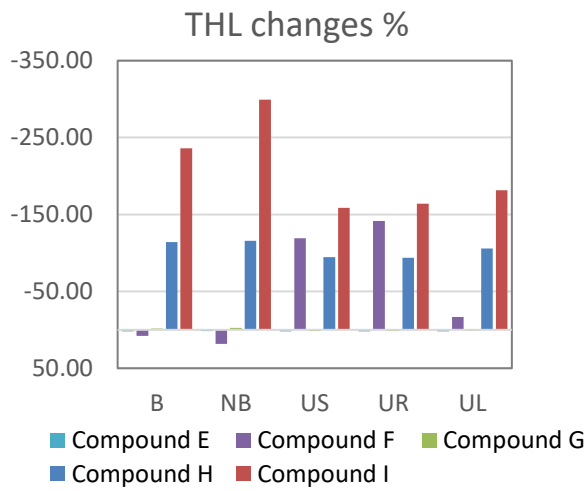

Figure 3-17 The plasma THL sensitivity to the PSD.

3.6. Analysis of the introduction of particle radius variation during dissolution

A further analysis was performed in order to evaluate if the impact of the PSD on simulations changes introducing in the model the variation during time of the particle radius, that was previously neglected. For this reason, the model presented in Section 3.5 was modified according to the work of Boger et. al [49], the new equations consider the compound mass as composed of N spherical particles with their own volume, mass and density. It is supposed that during dissolution the volume of particles decreases due to the change in their radius. Following this assumption, the variation of the undissolved amount in the

in the C region ($a_{und,C}$) and in the P region ($a_{und,P}$) can be modelled as follows:

$$a_{und,C} = N(t)\frac{4}{3}\pi r(t)_C^3\rho\,, \tag{3.26}$$

$$a_{und,P} = N_{0P}\frac{4}{3}\pi r(t)_P^3\rho, \tag{3.27}$$

where ρ is the particle density, the term $\frac{4}{3}\pi r(t)^3$ represents the volume of a particle, in particular $r(t)$ is the time-varying radius whose equation will be described afterwards, N_{0P} is the number of particles in the P region, that is constant during the dissolution process, $N(t)$ is the number of particles in the C region, that decreases during time due to the mucociliary clearance action, supposing that only particles that are not dissolved are removed.
This clearance, it is supposed to be a first order process, hence, the resulting equation is:

$$N(t) = N_{0C}e^{-k_{MC}t} \tag{3.28}$$

where N_{0C} is the initial number of particles in the C region, k_{MC} is the mucociliary clearance rate constant.
To obtain equations of the radius variation, two expressions representing the dissolved mass were equaled. The first describes the dissolving mass with the Nernst-Brunner equation previously shown, here, the term T representing the diffusional layer has been parameterized with the radius, that here varies during time, according to the Hintz and Johnson approximation, the resulting equation is:

$$\frac{da_{diss}}{dt} = \frac{3D}{\rho r(t)^2}(S_{ELF} - c_{u,fluid})a_{und} \tag{3.29}$$

Where $C_{u,fluid}$is the concentration of the unbound drug in the ELF, the a_{und} term can be calculated as shown previously.
The second describes the dissolving mass, composed of N spherical particles, as the product between the time-varying volume and the density.

$$\frac{da_{diss}}{dt} = -N\rho 4\pi r(t)^2 \frac{dr}{dt} \tag{3.30}$$

Equaling the two expressions, the resulting equation describing the variation of the radius during time is:

$$\frac{dr}{dt} = -\frac{D}{\rho r(t)}\left(S_{ELF} - c_{u,fluid}\right) \tag{3.31}$$

In the two lung regions the radius will change differently depending on the concentration of the unbounded drug in their fluid.
These equations were adapted, following the structure presented in Section 3.5, to consider the PSD: in this case a different amount with a different radius is present in each of the 9 sub-compartments, for the C and P regions. Hence, there resulting equations are, for each undissolved amount sub-compartment i:

$$a_{und,C,i} = N(t)_i \frac{4}{3}\pi r(t)_i^{\,3}\,\rho \tag{3.32}$$

$$a_{und,P,i} = N_{0P,i} \frac{4}{3}\pi r(t)_i^{\,3}\,\rho \tag{3.33}$$

where $N(t)_i = N_{0C_i} e^{-kMCt}$.
For the radius:

$$\frac{dr_{C,i}}{dt} = -\frac{D}{\rho r(t)_{C,i}}\left(S - \frac{a_{diss,C}}{V_{ELF,C}} f_{ufluid}\right) \tag{3.34}$$

$$\frac{dr_{P,i}}{dt} = -\frac{D}{\rho r(t)_{P,i}}\left(S - \frac{a_{diss,P}}{V_{ELF,P}} f_{ufluid}\right) \tag{3.35}$$

$i = 1, \dots, 9$

Since the radius $r(t)_i$ decreases during dissolution and tends to zero, the term $\frac{1}{r(t)_i}$ can lead to numerical instability. For this reason, the radius decreasing function has been further modified following a function proposed by Boger et. al [49], which overcomes this issue.
The equations of the dissolved mass for the C and P region respectively are the following:

$$\frac{da_{diss,C}}{dt} = -\sum_{i=1}^{9} N(t)_i \rho 4\pi r(t)_{C,i}{}^2 \frac{dr_{C,i}}{dt} - P_p S_C \left(\frac{a_{diss,C}}{V_{ELF,C}}\right) f_{ufluid} + P_p S_C c_{C,EV} f_{ulung} + P_a S_C c_{C,EV} f_{ulung} \quad (3.36)$$

$$\frac{da_{diss,P}}{dt} = -\sum_{i=1}^{9} N_{0P} \rho 4\pi r(t)_{P,i}{}^2 \frac{dr_{P,i}}{dt} - \alpha P_p S_P \left(\frac{a_{diss,P}}{V_{ELF,P}}\right) f_{ufluid} + \alpha P_p S_P c_{P,EV} f_{ulung} + P_a S_P c_{P,EV} f_{ulung} \quad (3.37)$$

The same equations for the EV and VASC part of the lung, presented in Section 3.3.1, apply.

3.6.1. Results

The same procedure used in the previous Section has been used also with this model formulation.
Results, very similar to the previously ones were obtained, both in terms of lung and plasma profiles, where a highest variation in terms of plasma MRT is observed. Results are reported in Appendix B.

Chapter 4

Prediction of the PK in man through *in vitro* and minimal animal information

PBPK models, as explained in Chapter 2, represent an example of incremental building strategy. As reported in the paper of Miller et. al [138], they can act as a "growing repository of knowledge" on the PK of a compound, that evolves during drug development to include new information. This aspect is particularly interesting in the perspective of applying PBPK models for the prediction of the clinical PK prior to first in human (FIH) studies. The use of this modelling approach has been deemed useful for *in silico* FIH studies by FDA [139], for informing the right dose in healthy volunteers by EMA [140]. In addition, many companies use mechanistic models for FIH studies in their developmental strategy [138].

As proposed by Jones et. al, with an iterative "learn, confirm, and refine" paradigm [40], PBPK models can support the entire drug development process. In drug

discovery, with *in vitro* data from tests on animal tissues and compound physicochemical properties, the model can be used to predict *in vivo* animal PK. In preclinical phase animal simulations can be compared with the *in vivo* data and the model can be refined in order to improve the predictive performances. Then, simulations of healthy volunteers PK can be performed using the model parameterized with healthy volunteer physiology and *in vitro* data from ADME tests on human tissues, where possible. These simulations can be checked, and the model further refined once human in *in vivo* data are generated after FIH studies. If the predictions are reasonable, simulations can then be extended to various special patient populations with appropriate changes in ADME and physiology.

The procedure just described for the preclinical to clinical translation of the PK provides for the incremental integration of the knowledge about ADME processes as it becomes available from the discovery to the preclinical phase, however, the need to predict human PK as early as possible with no animal or minimal animal data, in order to optimize the drug development process, is growing [55]. An accurate prediction of the human PK from the first stages of drug development has the potential to reduce future failures in clinic related to poor ADME properties, allowing the early selection of the best candidates and the rejection of those with a low chance of success [55].

With this aim, in the following, it is proposed the use of the developed PBPK framework for the prediction of the human PK by using the information collected during the early phases of drug development. The modelling strategy will be presented at first and then the model evaluation on healthy volunteers plasma concentration data after inhalation will be reported.

4.1. Modelling strategy

The works of Caniga et. al [48] and of Boger et. al [49], propose the use of their PBPK framework for a rational translation of the PK from rat to man, the possibility of updating PBPK species-specific parameters with those of human constitutes the core of their translational strategy. In 2018, Boger et. al applied their PBPK approach for the prediction of the inhaled bronchodilator salbutamol efficacy in human. This work is interesting since it allows an indirect evaluation of the free drug concentration prediction in the lung. The first step toward the translation proposed by the authors provides for the set-up of the model for salbutamol in rats, using the physico-chemical and *in vitro* properties of salbutamol and the preclinical *in vivo* data. *In vivo* plasma and lung concentration data after IV administration were used to calculate the lung-plasma partition coefficient while the same data after IT administration were used to adjust the drug permeability to the lung tissue. These parameters have been conserved across species.
Subsequently, the translation of the PK from rat to man has been made using the same model structure developed for rats, using physiological and ADME parameters (e.g. blood to plasma ratio, fraction unbound in plasma, lung deposition) of human.
The modelling strategy adopted in this work is also based on the use of the same model structure proposed for rats, in which the *physiological parameters* are those of man (and reported in Table 4-1), those related to lung physiology were derived from the work of Boger et. al [49]. The correction to obtain the alveolar permeability α was calculated as for rats, but using human tissue thickness values, obtained from the same literature sources. All the other physiological

parameters were fixed at those reported in Appendix A, calculated as explained in Chapter 2.
Concerning the *pulmonary drug-specific* parameters, the solubility was fixed to those measured in SLF, the values related to ELF and lung tissue binding (i.e., SLFB and LTB) it has been assumed to be conserved across species and were hence fixed to those used for rats. The permeability values were fixed to those obtained from Calu-3 *in vitro* tests as for rats, this choice, is driven by the fact that Calu-3 cells are of human origin. Concerning deposition, to determine human deposition fractions, information related to in house *in vitro* or *in vivo* studies were used as well as the MPPD tool.

Table 4-1 Values of the human physiological pulmonary parameters.

Human Parameter	**Central**	**Peripheral**
Blood Flow (fraction of Q_{CO})	0.025	1
Surface Area [cm^2]	4800	841000
ELF volume [ml]	3.84	5.89
Volume (as fraction of the total lung volume)	0.27	0.73
k_{MC} [s^{-1}]	2.2E-5	
Alveolar permeability adjustment constant, α		10.26

The *systemic drug-specific* parameters such as BP ratio and the plasma protein binding PPB, were set to those *in vitro* obtained for human. Concerning clearance, for the compounds used in this study, the hepatic extraction ratio was calculated, if available, from *in vitro* intrinsic clearance in hepatocytes, through IVIVE as explained

in Section 2.1.5, or taken from literature.
Since no IV data were available, the partition coefficients were not adjusted to fit plasma profiles, only the PS correction term has been maintained fixed to those obtained analyzing *in vivo* preclinical data after IV administration, considering that it is related to a possible well-stirred kinetics, due to drug characteristics, lipophilicity in particular, rather than on the species. Simulations using the same correction of partition coefficients as in rats or without any adjustment were also performed. In all these cases very limited changes in simulations can be observed. No *in vivo* preclinical information about the PK after IT experiments were used for the translation.

4.2. Predictive performance evaluation

The capability of the model of predicting human PK was evaluated on plasma concentration data obtained after inhalation of the HS and PR compound D and of the PS and HR compound H. This allowed to assess the model in two different scenarios in which the compounds have opposite characteristics in terms of solubility and pulmonary retention.

Compound D

The *in vivo* data used in this study refer to two different experiments:

- *Experiment A*: administration of compound D with charcoal block to inhibit the GI absorption.
- *Experiment B*: administration of compound D without charcoal block.

The PK data of experiment A are particularly interesting since the charcoal block technique avoids

the possible contribution of the amount swallowed and absorbed via the GI route, on the plasma profile generation, that proves to be generated from the pulmonary absorption only.
Furthermore, since compound D is HS, the same observation related to the simplification of the absorption dynamics drivers that allows to evaluate the model in a more favorable condition as in Section 3.4.1 applies.

Experiment A

In vivo PK study
The experiment provides for the administration of 100 µg to 25 healthy volunteers of compound D with an inhaler, with charcoal co-administration.

Model Parameterization
The formulation delivered was characterized in terms of PSD, MMAD, GSD and fine particle fraction (FPF), i.e. the fraction of particles ≤ 5 µm, that is considered the respirable fraction [141], has been calculated.
The fraction of the dose F_{INH} that effectively reaches the lung, was fixed to the FPF. The F_C and F_P fractions were calculated through MPPD™, using the obtained MMAD and GSD as input. The other parameters were set as explained in the Section 4.1. The human drug-specific parameters used were summarized in Table 4-2.

Experiment B

In vivo PK study
In this experiment, 24 µm of compound D was administered to 6 healthy volunteers with an MDI.

Model Parameterization

In house studies on healthy volunteers with the radioactively labelled compound, allow to determine the drug deposition after inhalation with the device used. The average fraction of compound retained in the device is the 11% per shot, the extra thoracic deposition was 55%. The repartition between the C and the P lung regions was expressed as C to P ratio, the value obtained was of 1.41. These deposition data were used to fix deposition fractions in the PBPK model. The particles MMAD used in the simulations is that of the unlabeled compound, that however is very similar to that of the labelled compound used to study the deposition. The hepatic extraction ratio was calculated from a systemic clearance value published in the literature [142], as explained in Section 2.2. The drug parameters used are summarized in Table 4-2.

Table 4-2 Drug-specific parameters related to the administration of compound D to human.

Parameter	**Value**
BP ratio	1.4
PPB	51.03%
E_r	0.73
Experiment A	
MMAD [µm]	1.58
GSD [µm]	1.61
F_{INH}	1
F_{LUNG}	0.66
F_C	0.24
Experiment B	
MMAD [µm]	0.72
F_{INH}	0.96
F_{LUNG}	0.45
F_C	0.59

Compound H

In vivo PK study

The data used refers to a single ascending dose administration study of compound H to healthy volunteers using a single-dose dry powder inhaler (SDDPI) as device. The doses administered were 20, 100, 400, 800, 1600 and 2000 µg.

Model Parameterization

The deposition fractions were fixed to values obtained from internal experimental knowledge. The hepatic extraction ratio was calculated using *in vitro* hepatic intrinsic clearance value obtained from human hepatocytes applying IVIVE. The other parameters were set as explained in the Section 4.1 and the overall parameter set is reported in Table 4-3.

Table 4-3 Drug-specific parameters related to the administration of compound H to human.

Parameter	**Value**
BP ratio	0.55
PPB	99.2%
E_r	0.66
MMAD [µm]	3
F_{INH}	0.9
F_{LUNG}	0.4
F_C	0.5

Results

Compound D

In Figure 4-1, results of plasma profiles prediction for Compound D are shown.

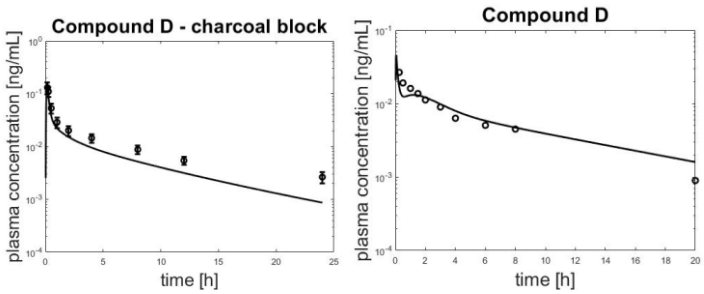

Figure 4-1 Simulated plasma profiles after compound D inhalation, experiment A (left panel) and B (right panel) and the experimental data (black circles), in the experiment A the related standard deviation is shown.

The model seems to be able to correctly predict the plasma profiles generated after pulmonary absorption of compound D. In case of experiment B, without charcoal co-administration a deviation from the *in vivo* data can be observed in the first hours after the administration. This could be related to some parameters to model GI absorption, since in the previous case for the same compound the pulmonary absorption is correctly captured.

Compound H

The single ascending dose experiment data allowed to assess if the *in vivo* PK linearity of compound H is correctly captured by the model as the dose increases, or some saturation effect occur due to the drug accumulation in the lung, limiting the absorption in the blood circulation. In Figure 4-2, the predicted AUC and the *in vivo* AUC for the different doses are reported. As the dose increases the deviation between the predicted and the observed exposure to the drug does not increase, this suggests that some saturation effects that prevent the drug passage in the blood circulation do not occur in the model.

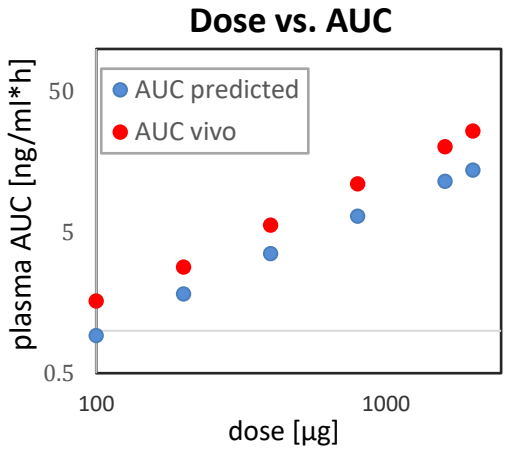

Figure 4-2 The dose-AUC relationship reported for the *in vivo* data and for the simulated profiles.

In Figure 4-3 the simulated profiles and the related experimental data are reported.

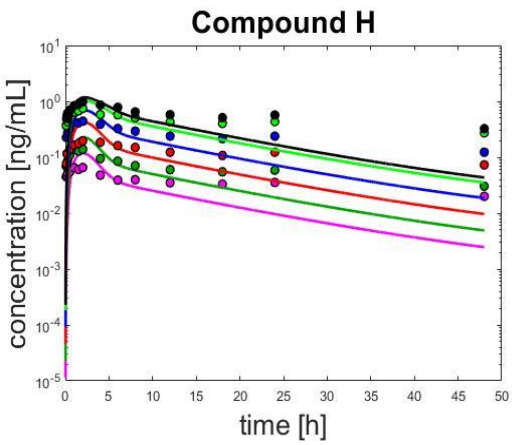

Figure 4-3 Simulated plasma profiles (lines) and *in vivo* data (circles) obtained after single dose administrations of compound H in healthy volunteers, in semi-logarithmic scale. Each color refers to different doses, purple line: 100 µg, dark green: 200 µg, red line: 400 µg, blue line: 800 µg, light green: 1600 µg, black line: 2000 µg.

The model is able to capture the time course of the drug plasma concentration in the first phases after the administration but does not capture the concentration increase after 24 h due to the possible presence of a drug sequestration mechanism with the subsequent release not modelled.
However, the overall exposure is predicted with an acceptable accuracy in terms of the PK metrics of interest, as can be seen in the FE analysis reported in Table 4-4.

Table 4-4 The FE analysis related to the simulated plasma profiles generated after compound H inhalation in man.

	100 µg	**200 µg**	**400 µg**	**800 µg**	**1600 µg**	**2000 µg**
AUC pred [ng/ml*h]	0.92	1.82	3.53	6.48	11.46	13.79
AUC vivo [ng/ml*h]	1.62	2.82	5.63	11.01	20.18	26.11
AUC FE	**0.51**	**0.58**	**0.57**	**0.54**	**0.52**	**0.49**
C_{max} pred [ng/ml]	0.13	0.25	0.46	0.76	1.14	1.29
C_{max} vivo [ng/ml]	0.07	0.14	0.20	0.44	0.75	0.98
C_{max} FE	**1.73**	**1.59**	**2.08**	**1.53**	**1.37**	**1.20**
MRT pred [h]	8.68	8.75	8.94	9.39	10.06	10.28
MRT vivo [h]	19.76	18.50	20.12	19.09	20.32	19.81
MRT FE	**0.45**	**0.49**	**0.46**	**0.51**	**0.51**	**0.53**

Discussion

The model, exploiting information from *in vitro* tests carried out in the first phases of the drug development,

seems to be able to describe, in a satisfactory manner, the plasma PK after inhalation in man in two different scenarios, without asking to use preclinical lung and plasma PK data after IT administration to calibrate the model or to gain mechanistic insight on the compounds PK. The two compounds used in this study differs in solubility and lung retention, this, allowed to have a preliminary assessment on the ability of the model to capture the human plasma PK for compounds with different properties.

The evaluation results on compound D data shows a good capability of the model to describe the pulmonary absorption in human. Compound D is HS and this enables to exclude the possible contribution of the dissolution process on the absorption dynamics control. This could be useful especially for the evaluation of the model in clinical context, where the lung concentration data are not available for a more complete evaluation of the model dynamics. Furthermore, the data obtained with charcoal co-administration are particularly interesting since in human the amount of drug that can be swallowed for extra-thoracic deposition can be relevant, given that inhalation is carried out by devices. If the FPE is not high, the amount absorbed via the GI route can contribute in generating the plasma concentration profile and preventing to distinguish the absorption dynamics. Hence, the scenario of experiment A, makes possible a finer evaluation of the ability of the model to describe this process.

In the more complex scenario of compound H, that is PS, the model seems to give a first description of the human PK after inhalation with an acceptable degree of accuracy, considering that it has been simulated in a context in which only early ADME information can be exploited to predict the PK and no other knowledge is available to have more in-depth information on its PK.

Given the overall satisfactory performances of the model, questions may arise on what could have contributed in generating these promising results. Apart from the

similarity in the respiratory anatomy and physiology among the species, that allowed to use the same model structure already validated in rats [48], [49], [50], understanding which ADME modelling choices, more than other, could contribute to a good description of the human PK is not an easy task because of the model complexity and for the limited number of clinical data available. However, it is possible to focus on ADME pulmonary parameters that, from the GSA reported in Appendix C, seem to most impact on the prediction of plasma profiles: the passive permeability and the fraction of drug unbound in lung tissue. Concerning the passive permeability obtained from Calu-3 cells, a correlation between the apparent permeability from this assay and the *in vivo* pulmonary absorption in rats has been reported in the literature [126]. From our simulations it seems adequate to predict also the compounds permeability in man. Of course, this is not surprising since Calu-3 are human cells. Furthermore, the correction to obtain the alveolar permeability, based on epithelium thickness, seems to provide a reasonable estimate also in man. This is probably due to the fact that the major barriers to the transport in the alveolar region are the alveolar epithelial cells and not the underlying endothelial cells [143]. Concerning the lung tissue binding, the value obtained *in vitro* from rat tissue seems, at least in our study, to be an adequate proxy for the binding in man.

Chapter 5

Overall conclusions

As a preliminary step, a generic PBPK model was built and implemented from scratch, to simulate IV and PO experiments, starting from literature information and using some *in vitro* drug-specific properties that are typically routinely collected during the drug development process. The model structure definition and implementation from scratch required a deep understanding of the model assumptions, interdisciplinary skills ranging from physiology to programming and enough modelling expertise. Model parameters had to be found somewhere directly by the modeler. This is not an easy task and necessarily has led to build a simplified model, but with satisfactory performances to be suited as a base for an extension to describe the PK of inhaled drugs. As an alternative strategy to the model building from scratch there are tools specifically designed for PBPK modelling. These tools are validated and have a lot of knowledge already contained in them. However, models are often pre-encoded and the assumptions are generally hidden to the user. These elements, clash with the need to define a structure and a parameterization of the model that

integrate the drug-specific information of interest and to explore if the hypothesis made on the underlying ADME dynamics are reasonable. In-house platform, instead, allowed to have the needed flexibility.

The physiologically based pulmonary model was developed using as a base the few publications available in the field. It was designed to incorporate the drug-related information collected during the early *in vitro* characterization of locally acting inhaled compounds ADME. Understanding how this *in vitro* characterization is performed has been of great importance in order to understand how such information could be exploited for the mechanistic modelling of the PK.

The study presented in this work represents the first attempt to evaluate PBPK models as a tool for the perspective prediction of *in vivo* preclinical and clinical lung and plasma PK of inhaled drugs primarily starting from the discovery phase *in vitro* tests information.

The implementation of the proposed modelling framework in the R&D context, thus, requires the retrieval of several *physicochemical properties* of compounds and the acquisition of information from *in vitro* tests to characterize their *pulmonary* and *systemic ADME*.

For what concern the *physicochemical properties* of compounds, information on MW, species (e.g. acid, base, neutral), pKas and logP should be known. Such information can be easily obtained also *in silico*. Regarding the formulation-dependent information, if the complete data of PSD analysis are not available, at least the MMAD and GSD should be known to characterize the deposition in the respiratory system and the particle radius that influences the dissolution process.

Regarding the *pulmonary ADME*, the quantification of the solubility in the ELF, the binding to ELF, the

binding to lung tissue and the permeability to the lung tissue is needed. Such information, in the typical R&D context considered this work, is obtained through the specific *in vitro* tests previously described in Chapter 3. However, several other *in vitro* tests have been proposed to retrieve the abovementioned *pulmonary ADME* information, some of them are also well established, but a standard does not exist. For instance, to quantify the solubility in pulmonary fluids, several methods are reported in the literature. They comprise *in vitro* measurements (in order of physiological relevance) in water or physiological salt solutions, in surfactant or dilutions of surfactant-based products, however, a consensus regarding the methodology that should be applied has not been achieved [39]. Regarding permeability measures, Calu3 and 16HBE14 cell lines are well established model of human lung tissue, but methods have not been validated and standardized [39]. Furthermore, how to take into account the lung regional heterogeneity in a single assay is still an open issue [39].

Hence, it should be considered, for a possible application of this framework in an R&D context, that the results here reported are related to a specific experimental setup and how the model performances change in relation to the application of other possible *in vitro* test to obtain information regarding the *pulmonary ADME* it is not known.

For what concern the *systemic ADME* characterization, some other *in vitro* tests are needed such as the quantification of the plasma protein binding, the blood to plasma ratio and the permeability to the Caco-2 cells to the assess the GI absorption. However, minimal *in vivo* animal data, such as plasma concentration obtained after IV experiments, could be useful to obtain information about the *in vivo* clearance, whose determination from *in vitro* experiments it is known to

be a critical step [55] and to calibrate the distribution in the model, especially when a more precise prediction of the plasma PK is needed.
The evaluation of the pulmonary model using preclinical data is a precious step for the possibility of using *in vivo* lung tissue concentration data, that however present the limitation of being a global measure without the possibility of distinguishing, for example, between the drug in ELF and those in tissue or between the different lung regions. This prevents a more in-depth evaluation of the dynamics included in the model. For the same reason, a too fine modelling of the ADME processes could be tricky for the difficulties in its evaluation, with the risk of introducing additional uncertainty in the model. An example of that can be found in the analysis of the PSD introduced in the dissolution model and discussed in Chapter 3.
Considering that the ADME information included in the model derives mainly from the early characterization of compounds, without model calibration on *in vivo* lung PK data, the model predictive performances were surprisingly good for the several scenarios considered. These results are positive since the selected compounds have different characteristics of solubility and lung retention, two key aspects on which companies focus their attention for the PK optimization. It suggests that the model can constitute the first step toward a general rather than drug-specific tool that could support the industrial practice in addressing some questions rising during the first phases of drug development. Examples of these are the prioritization of candidates before performing *in vivo* animal experiments, the reduction of their number or to gain mechanistic insights of which compound properties can be optimized to obtain a desired PK profile. With this purpose, the use of this tool has been introduced for modelling activities in Chiesi Farmaceutici.

It is worthwhile to notice that the model could be used also during the preclinical phase. Following the "learn, confirm and refine" paradigm proposed by Jones et. al [40], the model could be refined using the preclinical information as it becomes available once animal *in vivo* experiments are performed for aims such as informing the PK optimization and guide the preclinical experiments planning.

The developed PBPK model has proved to be able to predict also the PK in healthy volunteers in a satisfactory manner, mainly from the *in vitro* characterization of compounds and minimal animal data. This study, as for rats, represents the first assessment of a PBPK model for predicting inhaled drugs human PK from *in vitro* ADME data. Given the very encouraging results in the future will be worth to extend the evaluation on further clinical data.

On the basis of the abovementioned "learn, confirm and refine" paradigm, the model could be also used for translational purposes, for example, to inform FIH studies. This can be done once preclinical *in vivo* information is available and can be translated in terms of parameters to input in the model or in terms of mechanistic insights that can be added to refine the model.

In conclusion, given the good performances of the model in the prediction of the inhaled drugs PK in an *in vivo* data poor context, the framework has the potential of being used also to inform the *in vivo* phases, covering the different stages of the drug development process.

Appendix A

Generic PBPK model development and evaluation

System-specific parameters values

Values of the physiological parameters used in the PBPK model described, are here summarized. These values refer to a typical subject of 250 g for rats, 10 kg for dogs and 70 kg for man.

Rat parameters

Table A-1 Fluxes and volumes values for a 250 g rat.

Fluxes [ml/min]		**Volumes [ml]**	
Q_{brain}	1.79	V_{brain}	1.43
Q_{gut}	11.92	V_{gut}	6.75
Q_{spleen}	0.8	V_{spleen}	0.5
Q_{liver}	14.6	V_{liver}	9.15
Q_{muscle}	24.91	V_{muscle}	101.8
$Q_{adipose}$	6.27	$V_{adipose}$	16.6
Q_{heart}	4.39	V_{heart}	0.83

Q_{kidney}	12.64	V_{kidney}	1.83
$Q_{Restofthebody}$	23.1	$V_{Restofthebody}$	72.36
Cardiac Output	89.6	V_{lung}	1.25
		V_{ven}	10.12
		V_{art}	3.38

Hematocrit to compute the distribution: 0.46 [63].

Conversion factor to calculate the hepatic extraction ratio:

- MPPGL: 45 mg/g [59],
- HPGL: 125*10^6 cells/g [59],
- Liver Weight: 9.15 g [61].

Table A-2 Rat gastrointestinal absorption model parameters.

Gastrointestinal absorption model parameters	
Volumes of intestinal segments [ml]	
$V_{stomach}$	3
V_1	0.6
V_2	0.66
V_3	0.66
V_4	0.41
V_5	0.41
V_6	0.41
V_7	0.41
V_{colon}	3
pH of intestinal segments	
$pH_{stomach}$	3
pH_1	7.1
pH_2	7.3
pH_3	7.5
pH_4	7.7
pH_5	7.9
pH_6	8
pH_7	7.4
pH_{colon}	7.6
MRT values [min]	

Stomach	10
Small intestine	88
Colon	228

Dog parameters

Table A-3 Fluxes and volumes for a dog of 10 kg.

Fluxes [ml/min]		**Volumes [ml]**	
Q_{brain}	21	V_{brain}	78
Q_{gut}	216	V_{gut}	368
Q_{spleen}	24	V_{spleen}	27
Q_{liver}	288	V_{liver}	329
Q_{muscle}	227.9	V_{muscle}	456.5
$Q_{adipose}$	34	$V_{adipose}$	1380
Q_{heart}	48.3	V_{heart}	78
Q_{kidney}	181.65	V_{kidney}	55
$Q_{Restofthebody}$	246.8	$V_{Restofthebody}$	1538
Cardiac Output	21	V_{lung}	82
		V_{ven}	675
		V_{art}	225

Table A-4 Dog gastrointestinal absorption model parameters.

Gastrointestinal absorption model parameters	
Volumes of intestinal segments [ml]	
$V_{stomach}$	14.54
V_1	30.54
V_2	32
V_3	32
V_4	20.1
V_5	20.1
V_6	20.1
V_7	20.1
V_{colon}	290.9
pH of intestinal segments	

$pH_{stomach}$	1.5
pH_1	6
pH_2	6
pH_3	6
pH_4	6.2
pH_5	6.2
pH_6	6.2
pH_7	7.4
pH_{colon}	6.5
MRT values [min]	
Stomach	30
Small intestine	109
Colon	564

Hematocrit to compute the distribution: 0.42 [63].

Conversion factor to calculate the hepatic extraction ratio:

- MPPGL: 43 mg/g [59],
- HPGL: 120*10^6 cells/g [59],
- Liver Weight: 329 g [61].

Human parameters

Table A-5 Fluxes and volumes for a man of 70 kg.

Fluxes [ml/min]		**Volumes [ml]**	
Q_{brain}	745	V_{brain}	1400
Q_{gut}	1046	V_{gut}	1155
Q_{spleen}	160	V_{spleen}	182
Q_{liver}	1578	V_{liver}	1799
Q_{muscle}	1055	V_{muscle}	28000
$Q_{adipose}$	310	$V_{adipose}$	14994
Q_{heart}	248	V_{heart}	329
Q_{kidney}	1179	V_{kidney}	308
$Q_{Restofthebody}$	1308	$V_{Restofthebody}$	10801
Cardiac Output	6204	V_{lung}	532
		V_{ven}	3900
		V_{art}	1300

Hematocrit to compute the distribution: 0.44 [63].

Conversion factor to calculate the hepatic extraction ratio:

- MGPPGL: 32 mg/g [144],
- HPGL: 99*10^6 cells/g [144],
- Liver Weight: 1799 g [61].

Table A-6 Human gastrointestinal absorption model parameters.

Gastrointestinal absorption model parameters	
Volumes of intestinal segments [ml]	
$V_{stomach}$	50
V_1	105
V_2	110
V_3	110
V_4	69
V_5	69
V_6	69
V_7	69
V_{colon}	1000
pH of intestinal segments	
$pH_{stomach}$	2
pH_1	6
pH_2	6.2
pH_3	6.6
pH_4	6.8
pH_5	7
pH_6	7.2
pH_7	7.4
pH_{colon}	7
MRT values [min]	
Stomach	30
Small intestine	199.2
Colon	660

Physico-chemical properties of compounds used in the assessment study

Table A-7 Drug-specific properties of the compounds used in the evaluation study. A=Acid, B=Base, N=neutral, Z=zwitterion. * Value for men, ° value for rats, § value for dogs.

Drug/ Compound	**MW [g/mol]**	**Sint [ng/ml]**	**Chemical behavior**	**pKa**	**logP**	**BP ratio**	**f_{up}**	**Papp [nm/s]**	**E_R**	**F_{GUT}**
Amitriptyline	277.00	$2*10^3$	B	9.4	4.85	0.86*	0.056*	210	0.6*	0.68*
R-Carvedilol	406.47	$55.7*10^3$	B	7.97	4.19	0.67*	0.005*	312	0.75*	0.58*
Ciprofloxacin Hydrochloride	385.50	$65*10^4$	Z	6.16, 8.82	1.32	0.75*	0.8*	12.6	0.27*	0.98*
Chlorpromazine	318.86	$2.6*10^3$	B	9.2	5.18	0.78*	0.05*	199.5	0.57*	1*
Clozapine	326.80	$12*10^3$	B	7.7	3.42	0.87*	0.05*	309	0.15*	0.55*
Compound X	520.00	$5.6*10^4$	B	6.6	2	0.9°, 1.1§, 0.9*	0.1°, 0.6§, 0.6*	150	0.51°, 0.41§, 0.75*	1*
Diltiazem	414.51	$4.6*10^5$	B	7.7	2.67	1*	0.22*	295	0.45*	0.5*
Ibuprofen	206.29	$2.1*10^4$	A	4.7	4.06	0.55*	0.1*	263	0.08*	1*
Levothyroxine Sodium	798.60	$5*10^4$	Z	2.2, 10.1	2.93	1*	0.1*	35.7	0.04*	1*
Metoprolol	267.37	$1.1* 10^5$	B	9.7	2.39	1.13*	0.89*	37	0.34*	0.84*

Midazolam	325.77	$2.1*10^4$	B	6	3.15	0.55*	0.037*	324	0.59*	0.55*
Nifedipine	346.30	$17.1*10^3$	N	-	2	0.69*	0.03*	320	0.46*	0.73*
NVS372	300.00	$3*10^7$	B	7.4	0.83	0.97*	0.9*	15	0.10*	1*
Paracetamol	151.20	$1*10^7$	A	9.46	0.51	1.6*	0.88*	3100	0.15*	1*
PF-02413873	359.50	$39*10^3$	N	-	3.14	0.93°, 0.82§, 0.61*	0.047°, 0.036§, 0.031*	410	0.95°, 0.16§, 0.19*	0.89*
Pracinostat	358.00	$2.6*10^8$	B	7.45, 4.13	2.39	1°, 1*	0.07°, 0.082*	70	0.95°, 0.5*	0.97*
Repaglinide	452.60	$6.8*10^4$	Z	4.01, 6.17	3.98	0.62*	0.023*	281	0.64*	0.99*
Sotalol	272.36	10^3	B	8.28, 9.72	0.37	1*	0.62*	29	0*	1*
TPN729MA	516.00	$1.1*10^5$	A	4.56	3.74	1.38°, 1.14§, 1.06*	0.158°, 0.14§, 0.099*	70.6	0.86°, 0.80§, 0.54*	0.8*
Verapamil	454.60	$4.5*10^3$	B	8.5	3.79	0.84*	0.082*	155	0.98*	0.74*
UK-453,061	310.00	$2.7*10^6$	B	2.9	2.1	0.98°, 0.95§, 0.77*	0.27°, 0.53§, 0.42*	301	0.45°, 0.37§, 0.56*	0.96*

Results of the evaluation

Table A-8 Fold error values calculated for all the experiments considered in the study (*infusion, **multiple administrations, single administration - bolus- in the other cases) are reported below; in bold, values out of 2-fold range.

Drug	AUC Fold Error	Cmax Fold Error	Tmax Fold Error
Amitriptyline Human PO	**0.25**	0.71	0.99
Carvedilol Human IV	1.67		
Carvedilol Human PO	0.85	0.66	1.31
Chlorpromazine Human PO **	**2.20**	**3.70**	1.00
Ciprofloxacin Human IV *	1.05	1.26	1.26
Ciprofloxacin Human PO	0.77	0.87	1.17
Ciprofloxacin Human PO	0.64	0.75	0.99
Clozapine Human PO **	1.30	1.40	1.00
Compound A Rat IV	1.10		
Compound A Rat PO	1.00	**2.45**	**0.32**
Compound A Dog IV	1.77		
Compound B Rat IV	1.20		
Compound B Rat PO	0.60	0.75	1.80
Compound B Human IV *	1.40	1.88	1.00
Compound B Human PO	**2.28**	1.63	**4.20**
Compound C Rat IV	1.28		
Compound C Rat PO	1.24	**2.66**	1.03
Compound C Dog IV	1.94		
Compound C Human IV	1.71		
Compound C Human PO	**4.55**	**2.20**	**6.00**
Compound X Rat IV	1.25		
Compound X Rat PO	0.86	1.66	0.53
Compound X Dog IV	0.78		
Compound X Dog PO	0.83	0.87	1.32

Compound X Human PO	0.81	1.14	1.19
Digoxin Human IV	1.07		
Diltiazem Human PO **	0.56	0.68	0.98
Ibuprofen Human IV **	0.19		
Ibuprofen Human PO **	0.61	0.90	0.99
Levothyroxine Human PO	**0.47**	**0.42**	2.08
Metoprolol Human IV	2.00		
Metoprolol Human PO	0.82	0.88	1.97
Metoprolol Human PO	1.10	0.99	1.29
Midazolam Human IV	0.99		
Midazolam Human PO	0.90	1.32	0.94
Nifedipine Human IV	1.08		
Nifedipine Human PO	0.84	0.72	**2.11**
NVS732 Human PO	1.39	1.28	**2.39**
Paracetamol Human IV *	0.92	1.13	1.00
Paracetamol Human PO	0.70	0.96	1.00
TPN729MA Rat IV	2.00		
TPN729MA Rat PO	**0.38**	1.04	**2.27**
TPN729MA Dog IV	1.35		
TPN729MA Dog PO	**0.38**	0.71	**2.18**
TPN729MA Human PO	0.58	1.28	0.69
PF-02413873 Rat IV	**2.33**		
PF-02413873 Dog IV	1.09		
PF-02413873 Dog PO	**0.34**	**0.34**	0.58
PF-02413873 Human PO	0.81	1.51	**2.17**
Repaglinide Human IV *	0.64	1.04	0.91
Repaglinide Human PO	0.67	0.65	1.40
Pracinostat Rat IV	**2.39**		
Pracinostat Rat PO	1.67	1.00	**5.16**
Pracinostat Human PO	**0.48**	0.63	1.54
Sotalol Human IV	1.45		
Sotalol Human PO	1.51	0.78	**2.76**
Verapamil Human PO **	**0.30**	1.02	0.99
UK-453,061 Rat IV	1.17		
UK-453,061 Rat PO	**2.84**	**3.84**	**2.23**
UK-453,061 Dog IV *	0.68	**2.35**	0.62

UK-453,061 Dog PO	0.62	0.53	**2.56**
UK-453,061 Human PO	1.30	1.78	1.94

Appendix B

Analysis of the particle size distribution impact on the simulated profiles

Results of simulations with constant radius during dissolution

The figures here reported represent the plasma AUC and MRT variations.

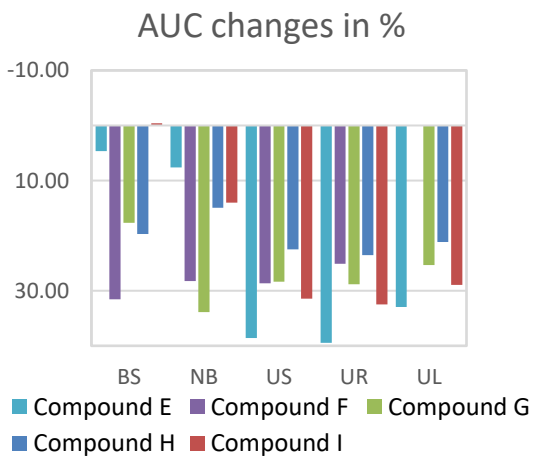

Figure B-1 AUC variations related to plasma, constant radius.

The AUC variation is under the 40% while the plasma MRT ranges from -60% to +60%, a trend among compounds and distributions cannot be observed.

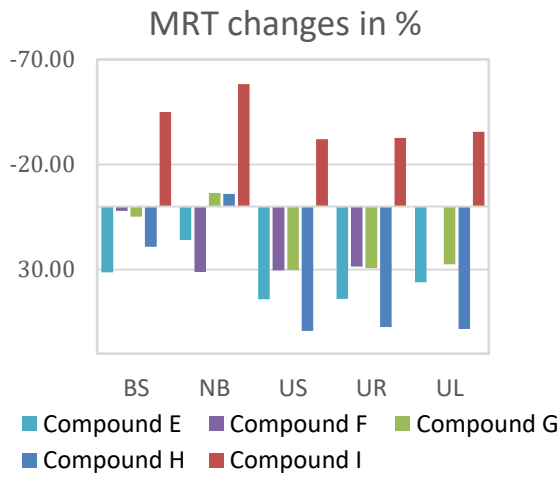

Figure B-2 MRT variation related to plasma, constant radius.

Results of simulations with radius varying during dissolution

The figures hereinafter report the variation on lung PK. The obtained AUC deviations are not so different from those resulting from the analysis of the model with constant radius, both in terms of variation range, that was under the 60%, and of behavior changing the PSD. Similarities to the scenario with constant radius can be seen also for the MRT changes both in terms of span (that was between -30% and + 30%) and in terms of trend among the distributions (except for compound E that in this case has an increase in the MRT).

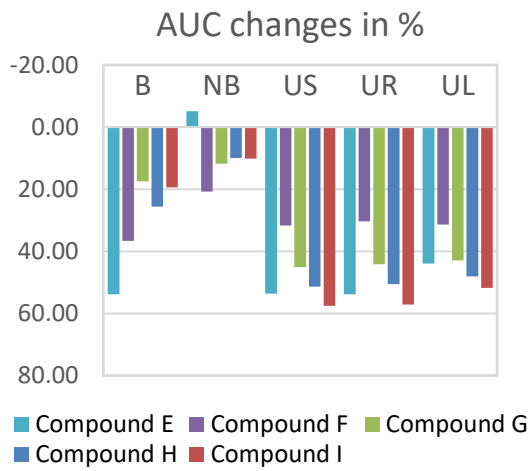

Figure B-3 Lung AUC variation, radius non constant.

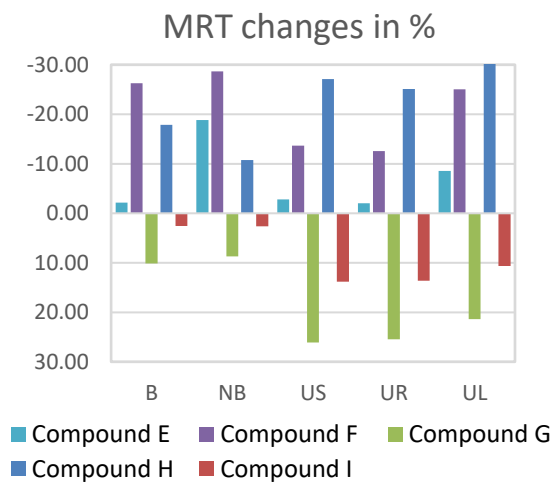

Figure B-4 Lung MRT variation, radius non constant.

Concerning the THL variation, as in the previous scenario with constant radius, changes are very limited for some compounds. Here, compound F has a relevant variation and also compound E has a significant change.

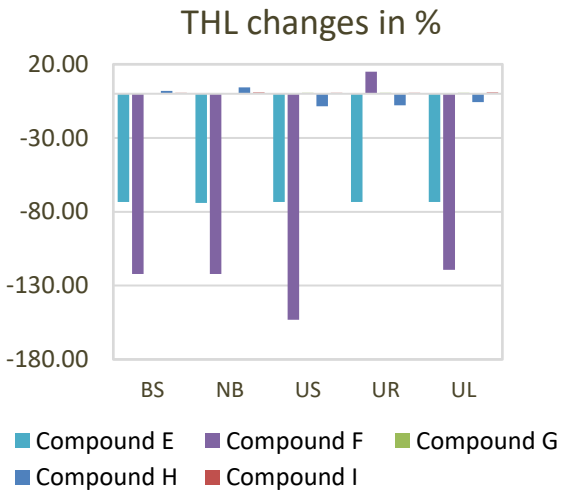

Figure B-5 Lung THL variation, radius non constant

The figures reported hereinafter show changes in plasma PK. The behavior of changes in C_{max}, with this version of the model, is very similar to the constant radius case, both in terms of span and of trend among PSDs.

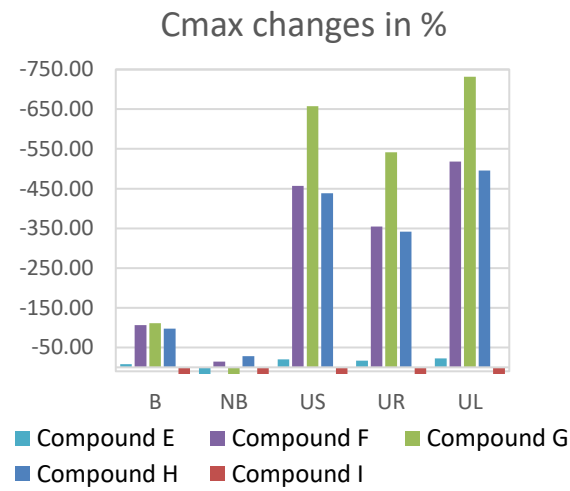

Figure B-6 Plasma C_{max} variation, radius non constant.

Also for T_{max} and AUC the results are very similar to those obtained with constant radius, both in terms of variation ranges and of trend among the different PSDs.

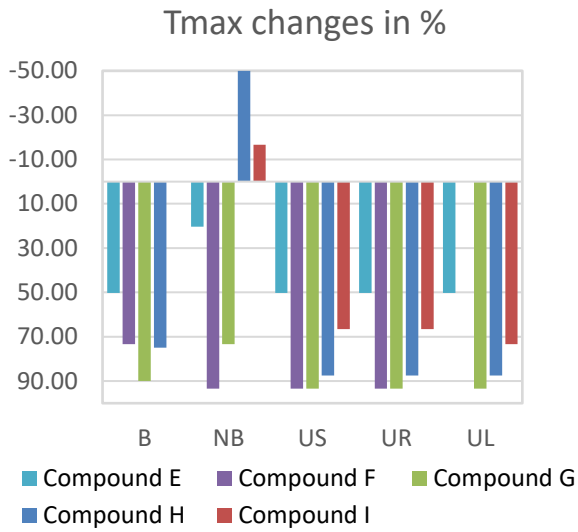

Figure B-7 Plasma Tmax variation, radius non constant.

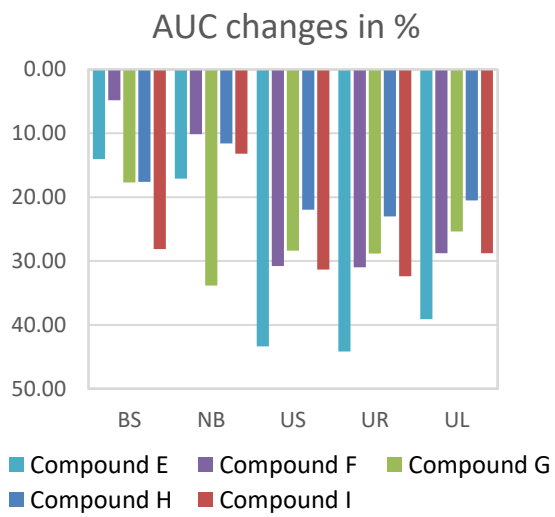

Figure B-8 Plasma AUC variation, radius non constant.

As for the model with constant radius, a trend among the distributions cannot be observed, neither for MRT nor for THL, however, for the first metric, in some cases the changes are more pronounced.

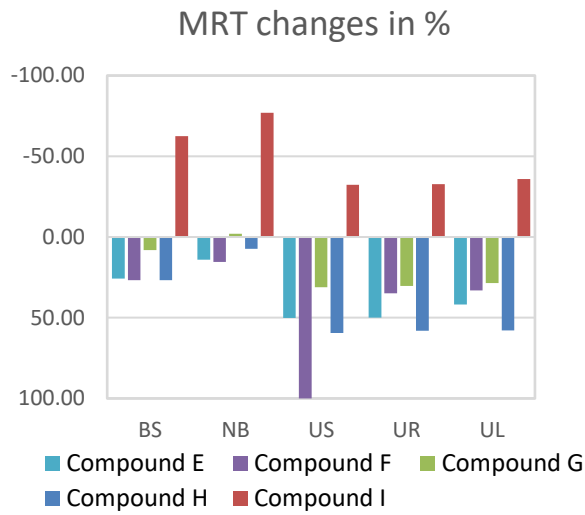

Figure B-9 Plasma MRT variation, radius non constant.

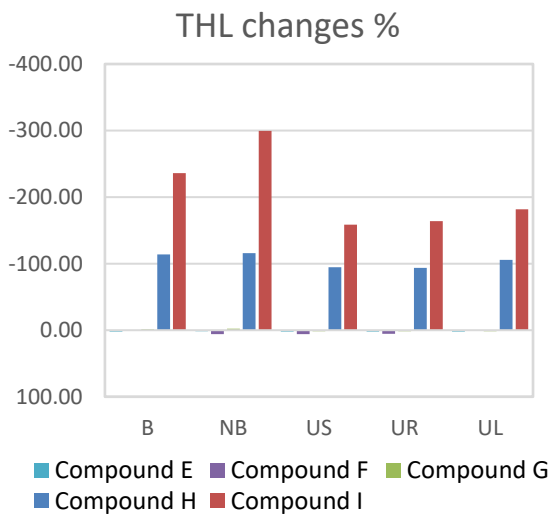

Figure B-10 Plasma THL variation, radius non constant.

Appendix C

Global sensitivity analysis of the pulmonary absorption model[9]

Regulatory agencies highlighted that a sensitivity analysis should be performed during the process of development and refinement of physiological models [78], [145]. Sensitivity analysis could be defined as "The study of how uncertainty in the output of a model (numerical or otherwise) can be apportioned to different sources of uncertainty in the model input" [146]. Like all the mechanistical models, physiological models have both uncertainty and variability in the input parameters. *Uncertainty* refers to an incomplete understanding of the system, lack of data or error in the measurement of certain parameters. *Variability,* instead, refers to the inherent heterogeneity of the system properties or parameters, for example among subjects or experiments. Typically, it is possible to reduce the

[9] This chapter is taken from Melillo N., Grandoni S., Cesari N., Brogin G., Puccini P. and Magni P., *Global Sensitivity Analysis of a physiological model for pulmonary absorption of inhaled compounds* (2019), manuscript ready to submit for publication.

uncertainty by performing better experiments and collecting more data. Instead, it is impossible to reduce the variability (given a certain population), however, it could be better characterized [147]. Given this uncertainty (or variability), it follows that also the predicted output metrics are uncertain (or variable) too, [148]. In our case, for example, the rat weight could be seen as a variable input parameter, while the values of the active and passive permeability across lung tissues as uncertain parameters. Pulmonary and plasma AUC are examples of predicted output metrics, whose uncertainties are driven by those of the model parameters. Sensitivity analysis helps to get insights into the model behavior as a function of parameters variation. By performing this type of analysis it is in fact possible to assess how much each parameter, with its variation, impacts on the variation of some model outputs of interest [148]. Consequently, sensitivity analysis could be a valuable instrument to help in understanding if the model behaves as expected or which are the parameters that need to be more precisely known to allow reliable model predictions.

In this context, a global sensitivity analysis (GSA) was performed to adequately characterize the pulmonary absorption model, by understanding how much uncertainties and variabilities in the input parameters drive predictions uncertainties and variabilities. GSA, with respect to local sensitivity analysis, performs a multivariate variation of all the considered input parameters in their whole range of variation [148]. Among all GSA methods, the variance-based method was chosen [149], [148], [150].

Variance-based GSA

Let us consider the generic model

$$Y = f(\boldsymbol{X}) \tag{C.1}$$

with Y a scalar model output (e.g., plasma drug AUC), f the input-output relationship and $\boldsymbol{X}$ the vector of the k uncorrelated input parameters (e.g., the parameters of the model considered in the GSA). GSA methods consider each X_i, $i = 1 \dots k$, as a random variable, with associated a certain probability distribution, [149], [148]. Thus, Y is a random variable, obtained through model evaluation after sampling from the joint probability distribution of $\boldsymbol{X}$. For each X_i, variance based GSA derives two sensitivity indices from the decomposition of the variance (V) of Y, the so called main (or first order) effect (S_i) and total effect ($S_{T,i}$), in Equations (C.2) and (C.3), respectively.

$$S_i = \frac{V_{X_i}\left(E_{\boldsymbol{X}_{\sim i}}(Y|X_i)\right)}{V(Y)} \tag{C.2}$$

$$S_{T,i} = \frac{E_{\boldsymbol{X}_{\sim i}}\left(V_{X_i}(Y|\boldsymbol{X}_{\sim i})\right)}{V(Y)} \tag{C.3}$$

E is the expectation operator and $\boldsymbol{X}_{\sim i}$ is the vector containing all the parameters, except X_i. Both S_i and $S_{T,i}$ are always included in [0,1]. S_i is related with the part of $V(Y)$ explained by the variation of X_i taken singularly and $S_{T,i}$ is the sum of S_i with the interaction effects of X_i with all the other inputs. Interaction effects could arise when more than one parameter can vary at the same time. The relationship $S_i \leq S_{T,i}$ is always valid. The higher S_i and $S_{T,i}$ are, the more the variation of X_i explains $V(Y)$ and so, the more X_i is considered important. Instead, $S_{T,i} = 0$ means that X_i is not influent on $V(Y)$. The difference $S_{T,i} - S_i$ gives information about the extent of interaction effect involving the i-th parameter.

In this work, two types of GSA have been performed, that differ in the considered parameters variability and thus, in the aim: *inter-compound* and *intra-compound*. The aim of *inter-compound* GSA is to understand which are the parameters that mostly influence the variability of the model predictions between different drugs [151]. Instead, the aim of the *intra-compound* GSA is to understand how much the uncertainty associated with parameters of a given drug impacts the model output uncertainty. Figure C-1, didactically shows the difference between the two version of GSA performed.

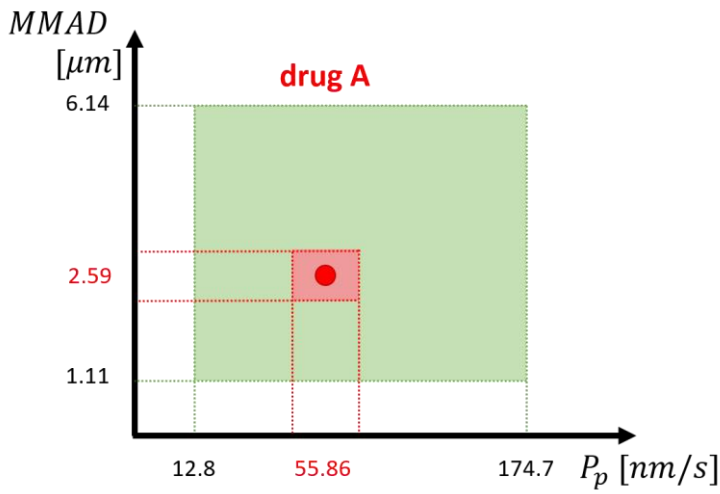

Figure C-1 A representation of the parameter space considered in performing the GSA (inter-compound in green, intra-compound in red).

It has been performed the *inter-compounds* GSA on the physiological pulmonary absorption model decoupled from the distribution PBPK and the intestinal absorption models. This was done to characterize the absorption process, simplifying the model and the results understanding. To decouple the model, blood inflow and outflow values of both C and P lung VASC compartments were set equal to zero. Moreover, fluxes due to passive permeability from the VASC to the EV

compartments were set equal to zero too, in both the lung regions. Thus, lung VASC compartments behave like wells (integrators). The outputs considered in this analysis are: the fraction absorbed (f_a), the AUC and MRT of the drug concentration in the whole lung. Whole lung concentration was obtained as sum of the solid and dissolved amounts with the ones in the C and P EV compartments, divided by the total lung volume. f_a was obtained as $f_a=1-f_{CL}$, where f_{CL} is the fraction of the drug eliminated by the mucociliary clearance at the steady state.

In the *inter-compounds* GSA, it has been considered each of the drug-related parameters varying in a range given by the minimum and the maximum values of the set of compounds presented in Section 3.1 (except compound L, whose data at the time of the analysis were not available). Their distributions were considered uniform in these ranges.

Compounds were classified in terms of solubility as HS and PS as done in Section 3.4.1. During GSA, at first the values of D_0 were extracted and then S_{SLF} was computed using Equation (3.18).

The *intra-compound* GSA was performed on the whole body PBPK model for three representative compounds, characterized by different properties (H, D, I). The outputs considered are the drug whole lung and plasma concentration AUC and MRT. Here, whole lung concentration was calculated as the sum of the drug amount in all the pulmonary absorption model compartments, divided by the lung total volume. All the drug-specific model parameters were considered uniformly distributed between the ranges reported in Table C-1, in Table C-2 and in Table C-3, except for the dose, that was considered normally distributed with a CV equal to 15% [152].

Table C-1 Ranges related to compound H, for intra-compound GSA.

Parameters	**Baseline**	**Min value[a]**	**Max value[a]**
$Dose\ [\mu g]$ [b]	10		
$logP$ [b]	3.87	3.715 (-30%)	3.983 (+30%)
pKa	8.7	8.6	8.8
$P_p\ [nm/s]$	55.86	16.76 (-70%)	94.962 (+70%)
$P_a\ [nm/s]$	$4 \cdot 10^{-6}$	$1.2 \cdot 10^{-6}$ (-70%)	$6.8 \cdot 10^{-6}$ (+70%)
$CACO2_{AB}$ permeability $[nm/s]$	4.7	1.41 (-70%)	7.99 (+70%)
BP	0.8	0.72 (-10%)	0.88 (+10%)
E_R	0.8	0.56 (-30%)	1
S_{SLF} $[ng/ml]$	696	487.2 (-30%)	904.8 (+30%)
$MMAD$ $[\mu m]$ [d]	2.59	2.205 (-30%)	4.901 (+30%)
$GSD\ [\mu m]$ [d]	2.1	1.12 (-30%)	2.509 (+30%)
F_{INH}	0.9	0.9	1
f_{ufluid}	0.16	0.112 (-30%)	0.208 (+30%)
f_{ulung}	0.0015	0.001 (-30%)	0.002 (+30%)
fup	0.032	0.0224 (-30%)	0.0416 (+30%)

[a] Minimum or maximum range limit (difference with respect to the baseline value, in percentage).
[b] The dose was considered normally distributed with a CV equal to 15%, [152].
[c] The ranges were calculated as +-30% of the natural value.
[d] Ranges were set equal to -30% the minimum and +30% the maximum of multiple measurements.

Table C-2 Ranges related to compound D, for intra-compound GSA.

Parameters	**Baseline**	**Min value[a]**	**Max value[a]**
$Dose\ [\mu g]$ [b]	15		
$logP$ [c]	1.99	1.8351 (-30% natural)	2.1039 (+30% natural)
pKa	9.81	9.71	9.91
$P_p\ [nm/s]$	16.06	4.818 (-70%)	27.302 (+70%)
$P_a\ [nm/s]$	68.82	20.646 (-70%)	116.994 (+70%)
$CACO2_{AB}$ permeability $[nm/s]$	49.2	14.76 (-70%)	83.64 (+70%)
BP	1.6	1.44 (-10%)	1.76 (+10%)
E_R	0.95	0.665 (-30%)	1
S_{SLF}	360000	252000 (-30%)	468000 (+30%)
$MMAD\ [\mu m]$ [d]	3.2	2.177 (-30%)	4.342 (+30%)
$GSD\ [\mu m]$ [d]	1.67	1.078 (-30%)	2.301 (+30%)
F_{INH}	0.9	0.9	1
f_{ufluid}	1	0.7	1
f_{ulung}	0.2640	0.1848	0.3432
fup	0.8216	0.5751	1

[a] Minimum or maximum range limit (difference with respect to the baseline value, in percentage).
[b] The dose was considered normally distributed with a CV equal to 15%, [152].
[c] The ranges were calculated as +-30% of the natural value.
[d] Ranges were set equal to -30% the minimum and +30% the maximum of multiple measurements.

Table C-3 Ranges related to compound I, for intra-compound GSA.

Parameters	**Baseline**	**Min value[a]**	**Max value[a]**
$Dose\ [\mu g]$ [b]	23		
$logP$ [c]	5.4	5.2451 (-30% natural)	5.5139 (+30% natural)
pKa	8.5	8.4	8.6
$P_p\ [nm/s]$	20.54	6.162 (-70%)	34.918 (+70%)
$P_a\ [nm/s]$	598.74	179.622 (-70%)	1017.9 (+70%)
$CACO2_{AB}$ permeability $[nm/s]$	0.3	0.09 (-70%)	0.51 (+70%)
BP	1	0.9 (-10%)	1.1 (+10%)
E_R	0.95	0.665 (-30%)	1
S_{SLF}	14300	10010 (-30%)	18590 (+30%)
$MMAD\ [\mu m]$ [d]	1.71	1.106 (-30%)	2.535 (+30%)
$GSD\ [\mu m]$ [d]	2.33	1.512 (-30%)	3.393 (+30%)
F_{INH}	0.9	0.9	1
f_{ufluid}	0.1	0.07	0.13
f_{ulung}	0.001	0.0007 (-30%)	0.0013 (+30%)
fup	0.0015	0.001 (-30%)	0.002 (+30%)

[a] Minimum or maximum range limit (difference with respect to the baseline value, in percentage).
[b] The dose was considered normally distributed with a CV equal to 15%, [152].
[c] The ranges were calculated as +-30% of the natural value.
[d] Ranges were set equal to -30% the minimum and +30% the maximum of multiple measurements.

When no experimental data supporting the variability range definition were available, arbitrary ranges reflecting the perceived parameter uncertainties were used.
To account for the population variability of rat weight, all the volumes and blood flows were multiplied for (w_{subj}/w_{mean}) and $(w_{subj}/w_{mean})^{0.75}$, respectively. w_{subj} is the extracted value of rat weight and w_{mean} is the mean rat weight equal to 250 g, as used in [45].
All the analyses were performed using MATLAB R2019a, on a 64-bit computer configured with Intel® Core™ i7-7700 @ 3.60 GHz x8 processors, running Ubuntu 16.04 LTS. The systems of differential equations were solved by using the *ode15s* MATLAB solver, for a time span ranging from 0 to 400 h. A program to perform variance based GSA was developed. To perform the GSA in both inter and intra-compound cases, a number of samples (n) equal to 20000 were used. These samples were extracted from a unit hypercube with the Latin hypercube sampling method and then reconducted to each parameter distribution by using a simple linear transformation. A number of n samples corresponds to n(k+2) number of model evaluation needed to compute the sensitivity indices, with k the number of parameters [149]. Uncertainty on the calculation of the sensitivity indices was estimated by using 1000 bootstrap samples [153].

Results

Inter-compound GSA

Here, the results of the inter-compound GSA on the pulmonary absorption model decoupled from the whole-body PBPK, for both HS and PS compounds are reported. In Figure C-2, the distributions of the selected model outputs are reported. In Figure C-3, the sensitivity indices for fa and for the logarithms of AUC and MRT of the drug concentration in the lungs are showed. The log scale for AUC and MRT was chosen

to avoid possible instabilities in the variance based sensitivity indices estimation due to the skewness of AUC and MRT distributions in natural scale [154].

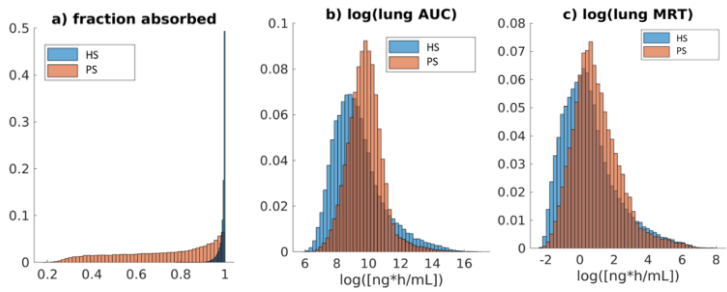

Figure C-2 Distributions of the selected model outputs are reported for HS (in light blue) and PS (in orange) compounds.

For HS compounds, the parameters that mostly explain the f_a variability are D_0 and MMAD. Concerning D_0, it is probably important because it controls the solubility, and so the dissolution rate. The higher the dissolution rate is, the faster the drug is removed from the solid compartment in the C region, in which the drug could be eliminated via mucociliary clearance. However, the f_a variability is quite low, as shown in Figure C-3. So, D_0 and MMAD are the most important parameters, but actually the variation of the model output is quite limited. For PS compounds, both MMAD and D_0, even if with a minor contribution of GSD and P_a, still impact the f_a variability. Concerning D_0, the reasons of its importance are probably the same of HS compounds. MMAD could be important in determining f_a variability mainly for two reasons. First, the MMAD value could impact the dissolution rate when the solubility is low. Second, it determines F_C and, mainly for poorly soluble compounds, f_a could be sensitive to the repartition between C and P regions. In fact, in the P region the mucociliary clearance does not occur.

The main difference with respect to the HS case is that f_a variability is quite high. Thus, MMAD and D_0 are responsible for a great variation of the model output.
Concerning lung AUC, the parameters that mostly explain its variability for HS compounds are f_{ulung}, P_p and P_a. This probably happens because f_{ulung} and the permeabilities are parameters that determine the drug retention into the lungs and thus they control the AUC. For PS compounds, in addition to parameters that control the drug retention into the lungs, D_0 and MMAD are also important. This happens because, as explained before, they could impact the f_a and, thus, the lung AUC.
Concerning lung MRT, the parameters that mostly explain the variability for HS compounds are still f_{ulung} and both passive and active permeabilities. The reasons of their importance are probably similar to the one for the AUC: these are the parameters responsible of the drug retention into the lungs. For PS compounds, the most important parameters are similar to the ones for HS compounds, with the addition of D_0 and MMAD.

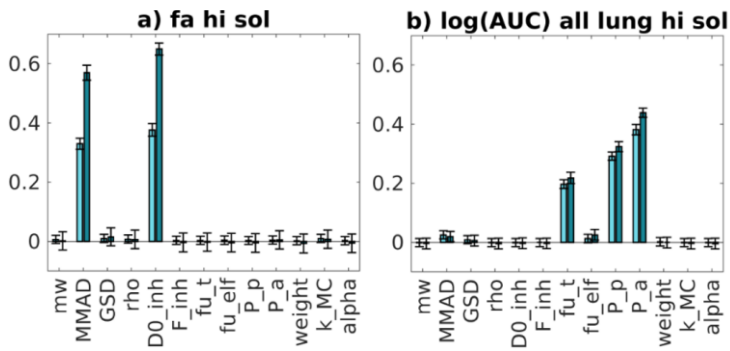

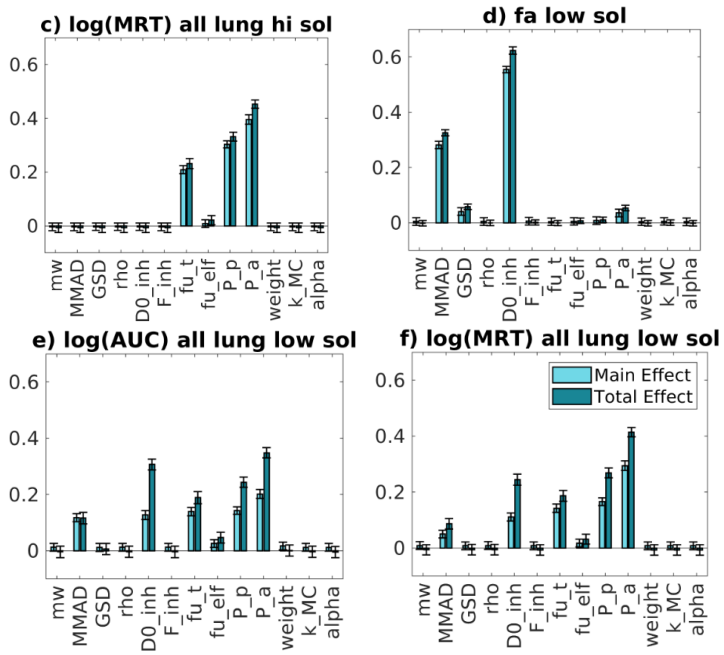

Figure C-3 the sensitivity indices for the selected outputs, hi sol=HS, low sol=PS.

Intra-compound GSA

Here the results of the intra-compound GSA for three representative compounds chosen. With respect to all the other Chiesi compounds, compound H is characterized by a lower solubility, a higher permeability and a low f_{ulung}. Compound D has a higher solubility, a lower permeability and a higher f_{ulung}. Finally, compound I has an intermediate solubility and permeability and a low f_{ulung}. The parameters values and the associated uncertainty or variability are reported in Table C-1, Table C-2, Table C-3.

Compound H

The distribution of drug whole lung and plasma AUC and MRT and the sensitivity indices are reported in Figure C-4 and Figure C-5, respectively.

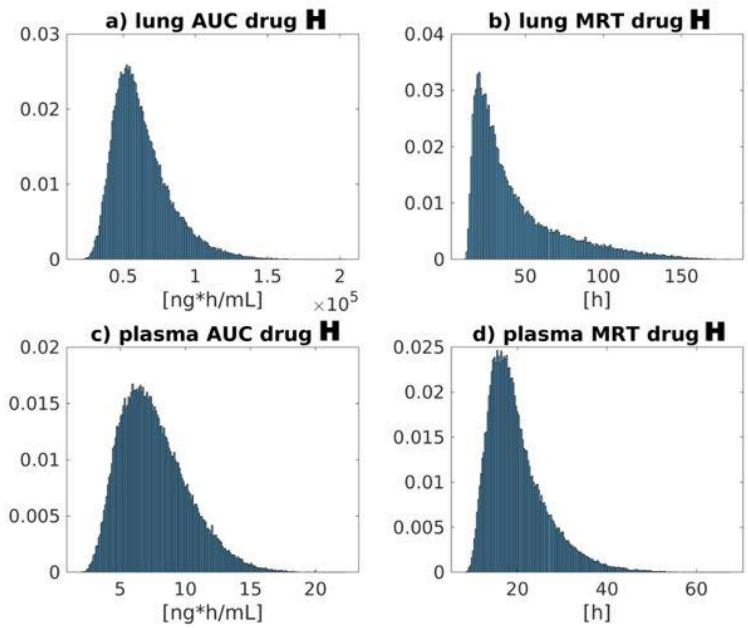

Figure C-4 The distribution of drug whole lung and plasma AUC and MRT for compound H.

Whole lung AUC variance is mainly explained by the passive permeability variation, together with a minor contribution of the dose, f_{ulung}, rat weight and k_{MC} variabilities. Even if the drug has a low solubility and solubility should control the absorption, it seems that the highest impact on the AUC can be attributed to the passive permeability.

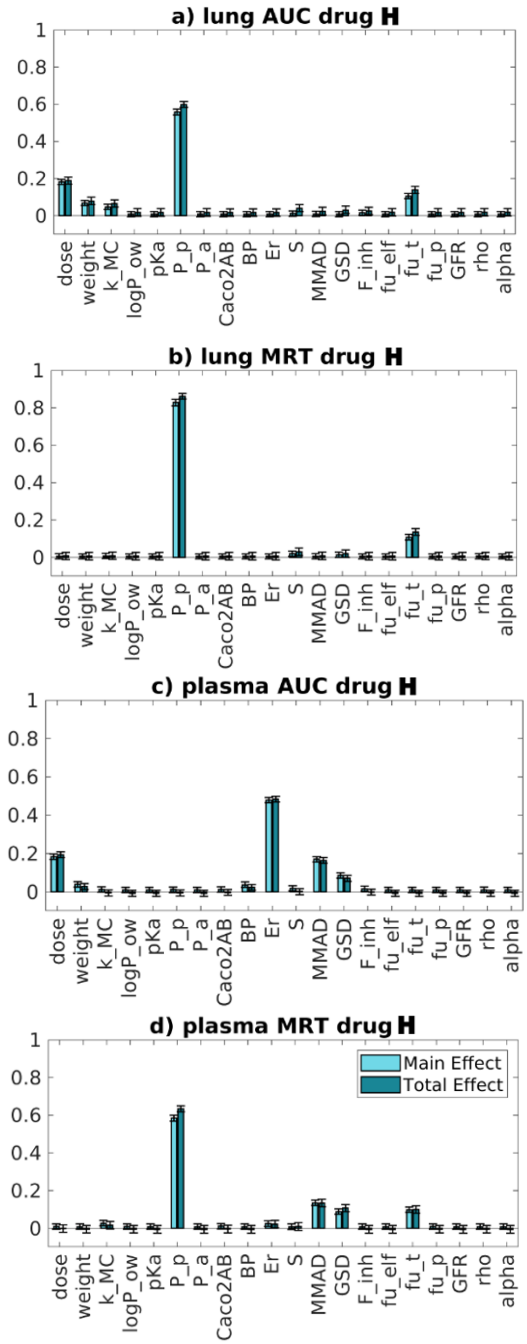

Figure C-5 the sensitivity indices for the selected outputs for compound H.

However, it should be noted that the uncertainty associated with the passive permeability is higher with respect to those associated with other parameters. The passive permeability is still the most important parameter when whole lung MRT was considered. The reasons seem to be very similar to those discussed for both metrics in the *inter-compound* analysis section. Plasma AUC variability is mainly explained by the extraction ratio and, to a minor extent, by the dose, MMAD and GSD variabilities. These results highlight that the elimination process plays a major role in determining plasma AUC variability. Concerning plasma MRT, the most important parameter is passive permeability. This probably happens because the drug is slowly absorbed from the lungs into the systemic circulation.

Compound D

The distribution of drug whole lung and plasma AUC and MRT and the sensitivity indices are reported in Figure C-6 and Figure C-7, respectively.

The parameter that mostly explains compound D whole lung AUC and MRT variation is the passive permeability. This probably happens because compound D has a lower permeability and higher solubility with respect to the other compounds of interest, thus, the absorption rate is probably permeability limited. Moreover, as explained for compound H, with respect to all the other parameters, the permeabilities have a greater associated uncertainty, thus, it is more likely that they have a relevant impact in explaining the AUC variation.

Concerning the plasma AUC, the most important parameters are the dose and the extraction ratio, followed by rat weight and BP. As for compound H, the elimination process is more important than the distribution or absorption processes in determining the AUC variation. The most important parameter in explaining the MRT

variance is the passive permeability. As for compound H, this probably happens because the drug is slowly absorbed from the lungs into the systemic circulation.

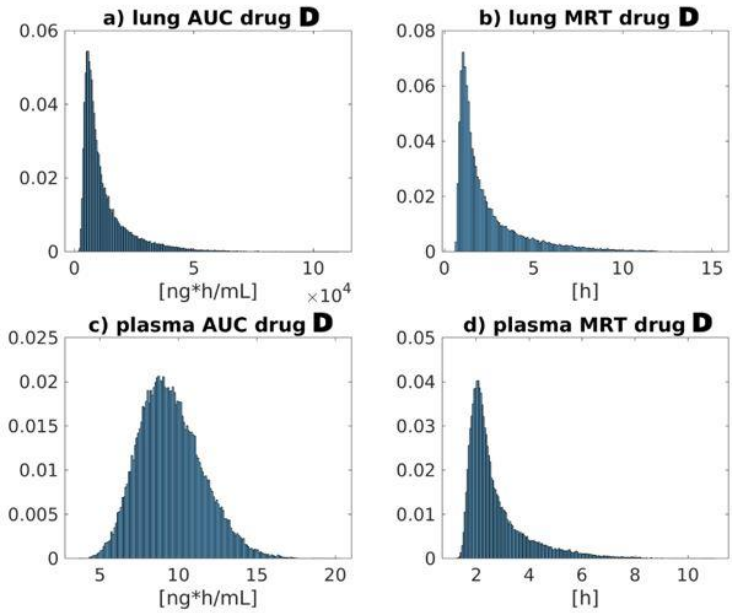

Figure C-6 The distribution of drug whole lung and plasma AUC and MRT for compound D.

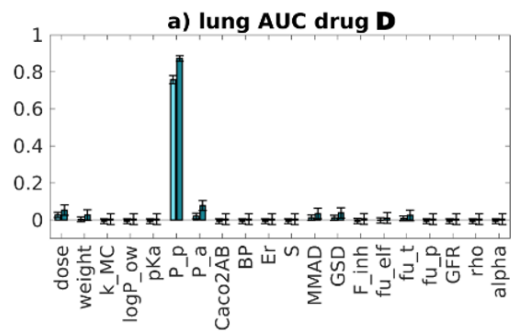

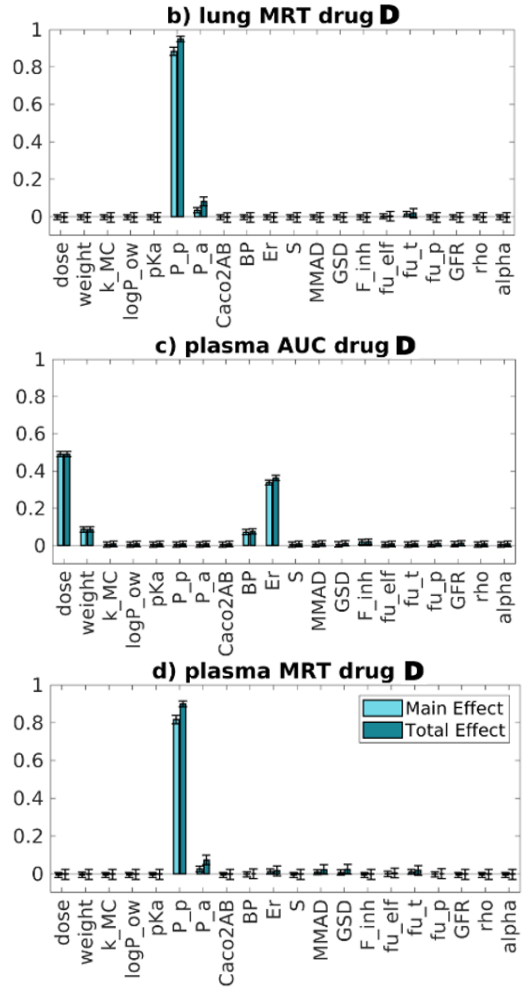

Figure C-7 the sensitivity indices for the selected outputs for compound D.

Compound I

The distribution of plasma and whole lung AUC and MRT and the sensitivity indices relative to compound I are reported in Figure C-8 and in Figure C-9.
For both whole lung AUC and MRT, the parameter that with its variation mainly explains their variability is the passive permeability. The reasons are probably similar to

those reported for compounds H and D. Moreover, compound I has a higher solubility, but lower permeability than compound H and, together with a low fraction unbound, this could explain the slightly higher importance of the passive permeability with respect to compound H. Concerning plasma AUC, the parameters that mainly explain its variation are the dose and the extraction ratio, followed by the passive permeability, rat weight and BP. These results highlight that probably, for this drug, the elimination process has a greater role in determining the AUC variability with respect to the distribution or absorption. Concerning the plasma MRT, the situation resembles the one of compound H.

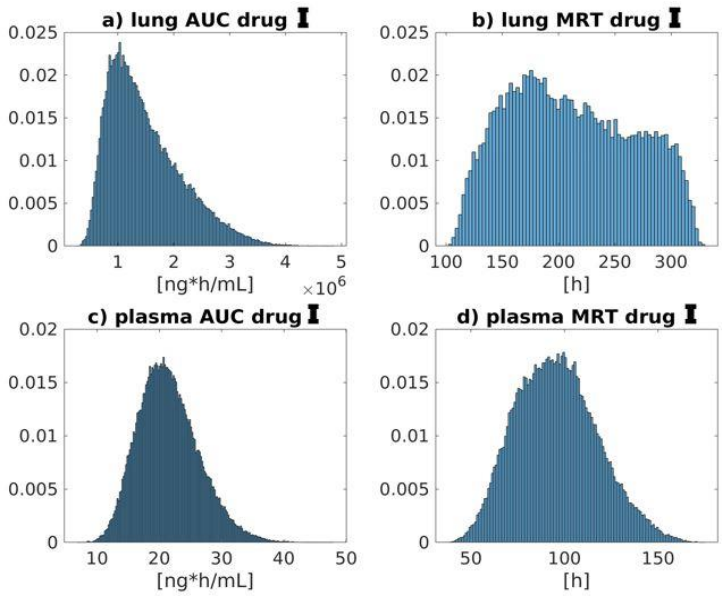

Figure C-8 The distribution of drug plasma and whole lung AUC and MRT for compound I.

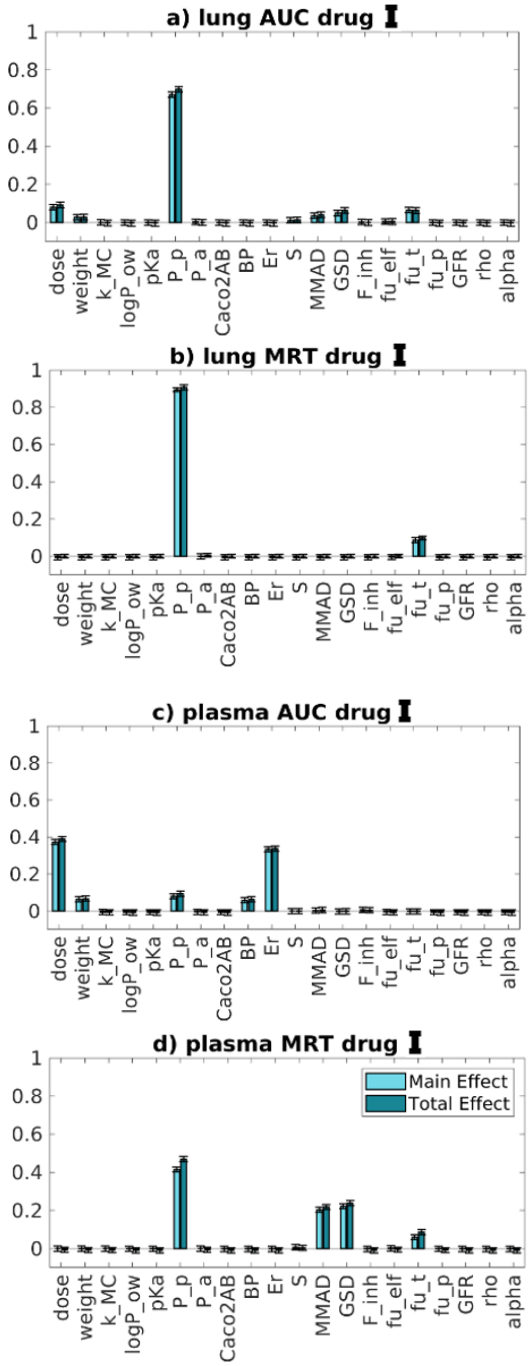

Figure C-9 the sensitivity indices for the selected outputs for compound I.

Discussion

In this Section, has been shown how GSA techniques were used to assess model behaviors and support the development of a mechanistic model describing pulmonary absorption for orally inhaled compounds. Two ways of performing a GSA have been identified, that differ in the aims and thus, in the considered parameters variability: *inter-compounds* and *intra-compound*. Both the approaches helped in understanding different model aspects.

The *inter-compounds* GSA was performed for the absorption model decoupled from the distribution PBPK. In particular, this analysis can be performed in more "homogeneous" sub-spaces of the whole parameter space, as has been done distinguishing HS from PS compounds. Looking at the model output distributions gives the possibility of assessing the extent of the *inter-compound* variability of the metrics of interest and then its relevance. Then, GSA helps in understanding which are the parameters that mostly determine the observed variation of the output predictions between different compounds. For example, from Figure C-2 and Figure C-3, it is possible to appreciate the difference in the model behavior and in the impact of the model parameter variability between HS and PS compounds. It has been found that inter-compound GSA is particularly useful during the process of model development. In fact, this analysis can help in understanding if the model behaves as expected and, in case of discrepancies between the expected and the actual model behavior, GSA gives useful information that helps in identifying the reasons. Theoretically, if the model structure and the physiological and inter-compound parameter variabilities are correctly identified and fixed, this analysis can be performed just once (e.g., when the model is firstly presented or at the platform release).

The *intra*-compound GSA was instead performed for three representative compounds on the whole body PBPK model. The parameters variation was defined to represent

the uncertainties associated with their values for a specific compound. With this analysis it is possible to know how much the model output variation is apportioned to the uncertainty of the parameters. When doing this analysis, it is useful to look at the output distribution, to determine if it is narrow enough to be considered acceptable. If not, GSA helps in selecting which parameters should be known with less degree of uncertainty in order to give a more accurate prediction. For example, we believe that the uncertainty associated with compound H lung MRT is too high. So, if one is interested in using this model for lung MRT predictions (e.g. for different dosages or species), from the GSA results we know that a better characterization of the passive permeability is needed in order to reduce uncertainties of the considered metrics. This situation probably does not happen for compound H lung AUC, given that the uncertainty associated with this metrics can be considered low. Differently from inter-compound GSA, intra-compounds GSA should be performed each time the model (or the PBPK platform) is used for a specific drug.

In our experience, GSA showed some criticisms. For example, in certain situations determining the uncertainty or variability ranges was not an easy task, in particular for the intra-compound GSA. In fact, due to the lack of available data, it was sometimes difficult (and arbitrary) to appropriately quantify the parameters degree of uncertainty. In these cases, expert opinion has to be used to fill the gap.

In conclusion, it is suggested the use of GSA during the model development and evaluation, especially for the development of (complex) mechanistic models. GSA increases the knowledge of the model, it helps in finding errors, sensitive assumptions and it identifies the parameters that must be known with higher confidence if one is interested in reducing the model prediction uncertainties.

References

[1] L. J. Lesko, M. Rowland, C. C. Peck, and T. F. Blaschke, "Optimizing the science of drug development: opportunities for better candidate selection and and accelerated evaluation in humans," *Eur. J. Pharm. Sci.*, pp. 803–814, 2000.

[2] M. J. Ratain and W. K. J. Plunkett, "Principles of Pharmacokinetics," in *Holland-Frei Cancer Medicine, 6th edition*, D. Kufe, R. Pollock, R. Weichselbaum, R. C. J. Bast, T. S. Gansler, J. F. Holland, and E. Frei, Eds. Hamilton (ON): BC Decker Inc., 2003.

[3] S. Singh, "Preclinical pharmacokinetics: an approach towards safer and efficacious drugs," *Curr. Drug Metab.*, vol. 7, no. 2, pp. 165–182, 2006.

[4] J. P. Hughes, S. S. Rees, S. B. Kalindjian, and K. L. Philpott, "Principles of early drug discovery," *Br. J. Pharmacol.*, vol. 162, no. 6, pp. 1239–1249, 2011.

[5] J. A. DiMasi, H. G. Grabowski, and R. W. Hansen, "Innovation in the pharmaceutical industry: New estimates of R&D costs," *J.*

Health Econ., vol. 47, pp. 20–33, 2016.

[6] I. Kola and J. Landis, "Can the pharmacutical industry reduce attrition rates?," *Nat. Rev. Drug Discov.*, vol. 3, pp. 711–715, 2004.

[7] S. Marshall *et al.*, "Model-Informed Drug Discovery and Development: Current Industry Good Practice and Regulatory Expectations and Future Perspectives," *CPT Pharmacometrics Syst. Pharmacol.*, vol. 8, no. 2, pp. 87–96, 2019.

[8] S. F. Marshall *et al.*, "Good Practices in Model-Informed Drug Discovery and Development: Practice, Application, and Documentation," *CPT Pharmacometrics Syst. Pharmacol.*, vol. 5, no. 3, pp. 93–122, 2016.

[9] Y. Wang, H. Zhu, R. Madabushi, Q. Liu, S. M. Huang, and I. Zineh, "Model-Informed Drug Development: Current US Regulatory Practice and Future Considerations," *Clin. Pharmacol. Ther.*, vol. 105, no. 4, pp. 899–911, 2019.

[10] A. E. Cooper, D. Ferguson, and K. Grime, "Optimisation of DMPK by the Inhaled Route: Challenges and Approaches," *Curr. Drug Metab.*, vol. 13, no. 4, pp. 457–473, 2012.

[11] N. R. Labiris and M. B. Dolovich, "Pulmonary drug delivery. Part I: Physiological factors affecting therapeutic

effectiveness of aerosolized medications," *Br. J. Clin. Pharmacol.*, vol. 56, no. 6, pp. 588–599, 2003.

[12] C. A. Fernandes and R. Vanbever, "Preclinical models for pulmonary drug delivery," *Expert Opin. Drug Deliv.*, vol. 6, no. 11, pp. 1231–1245, 2009.

[13] "Asthma," *U.S. Department of Health & Human Services, National Hearth, Lung and Blood Instituted*, 2014. [Online]. Available: https://www.nhlbi.nih.gov/health-topics/asthma. [Accessed: 08-Mar-2019].

[14] "COPD," *U.S. Department of Health & Human Services, Nartional Hearth, Lung and Blood Institute*, 2014. [Online]. Available: https://www.nhlbi.nih.gov/health-topics/copd. [Accessed: 08-Mar-2019].

[15] K. S. Khan, I. Hayes, and D. J. Buggy, "Pharmacology of anaesthetic agents II: Inhalation anaesthetic agents," *Contin. Educ. Anaesthesia, Crit. Care Pain*, vol. 14, no. 3, pp. 106–111, 2014.

[16] A. Nokhodchi and G. P. Martin, Eds., *Pulmonary Drug Delivery Advances and Challenges*, First. John Wiley & Sons, 2015.

[17] B. K. Rubin, "Secretion properties, clearance, and therapy in airway disease," *Transl. Respir. Med.*, vol. 2, no. 1, pp. 1–7,

2014.

[18] M. Ball and D. Padalia, “Anatomy, Airway,” *StatPearls Publishing LLC*, 2019. [Online]. Available: https://www.ncbi.nlm.nih.gov/books/NBK459258/. [Accessed: 12-Mar-2019].

[19] ICRP, *ICRP Publication 66. Human Respiratory Tract Model for Radiological Protection*. SAGE Publishing, 1994.

[20] L. P. Gartner and J. L. Hiatt, *Istologia*, Third Edit. Naples: EdiSES, 2009.

[21] F. X. Mccormack and J. A. Whitsett, “Innate defenses in the lung The pulmonary collectins , SP-A and SP-D , orchestrate innate immunity in the lung,” vol. 109, no. 6, pp. 707–712, 2002.

[22] J. S. Patton and P. R. Byron, “Inhaling medicines: Delivering drugs to the body through the lungs,” *Nat. Rev. Drug Discov.*, vol. 6, no. 1, pp. 67–74, 2007.

[23] “How does the blood circulatory system work?” [Online]. Available: https://www.ncbi.nlm.nih.gov/books/NBK279250/. [Accessed: 25-Mar-2019].

[24] R. R. Mercer, M. L. Russell, V. L. Roggli, and J. D. Crapo, “Cell Number and Distribution in Human and Rat Airways,” *Am. J. Respir. Cell Mol. Biol.*, vol. 10, no. 6, pp. 613–624, 1994.

[25] A. L. Patra, “Comparative anatomy of

mammalian respiratory tracts: The nasopharyngeal region and the tracheobronchial region," *J. Toxicol. Environ. Health*, vol. 17, no. 2–3, pp. 163–174, 1986.

[26] R. Sarangapani *et al.*, "PHYSIOLOGICALLY BASED PHARMACOKINETIC MODELING OF STYRENE AND STYRENE OXIDE RESPIRATORY-TRACT DOSIMETRY IN RODENTS AND HUMANS OF STYRENE AND STYRENE OXIDE RESPIRATORY-TRACT DOSIMETRY IN RODENTS AND," *Inhal. Toxicol.*, vol. 14, no. 8, pp. 789–834, 2002.

[27] B. Kandala and G. Hochhaus, "Pharmacometrics in Pulmonary Diseases," in *Applied Pharmacometrics*, S. Schmidt and H. Derendorf, Eds. Springer, 2014, pp. 349–381.

[28] D. D. Sin and S. F. P. Man, "Corticosteroids and adrenoceptor agonists: The compliments for combination therapy in chronic airways diseases," *Eur. J. Pharmacol.*, vol. 533, no. 1–3, pp. 28–35, 2006.

[29] K. P. O'Donnell and H. D. C. Smyth, "Macro- and Microstructure of the Airways for Drug Delivery," in *Controlled Pulmonary Drug Delivery*, H. D. C. Smyth and A. J. Hickey, Eds. Springer, 2011, pp. 1–19.

[30] R. Aalbers and H. S. Park, “Positioning of long-acting muscarinic antagonists in the management of asthma,” *Allergy, Asthma Immunol. Res.*, vol. 9, no. 5, pp. 386–393, 2017.

[31] Z. Xu and A. J. Hickey, “The Physics of Aerosol Droplet and Particle Generation from Inhalers,” in *Controlled Pulmonary Drug Delivery*, H. D. C. Smyth and A. J. Hickey, Eds. Springer, 2011, pp. 75–100.

[32] J. M. Borghardt, B. Weber, A. Staab, and C. Kloft, “Pharmacometric Models for Characterizing the Pharmacokinetics of Orally Inhaled Drugs,” *AAPS J.*, vol. 17, no. 4, pp. 853–870, 2015.

[33] W. C. Hinds, Ed., “Uniform Particle Motion,” in *Aerosol technology Properties, Behavior, and Measurement of Airborne Particles*, Second., John Wiley & Sons Inc., 1999, pp. 42–74.

[34] H. D. C. Smyth and A. J. Hickey, *Controlled Pulmonary Drug Delivery*. Springer, 2011.

[35] F. Kazmi *et al.*, “Lysosomal sequestration (trapping) of lipophilic amine (cationic amphiphilic) drugs in immortalized human hepatocytes (Fa2N-4 cells),” *Drug Metab. Dispos.*, vol. 41, no. 4, pp. 897–905, 2013.

[36] E. Bäckström, E. Boger, A. Lundqvist, M. Hammarlund-Udenaes, and M. Fridén, “Lung Retention by Lysosomal Trapping of

Inhaled Drugs Can Be Predicted In Vitro With Lung Slices," *J. Pharm. Sci.*, vol. 105, no. 11, pp. 3432–3439, 2016.

[37] A. Ufuk *et al.*, "In vitro and in silico tools to assess extent of cellular uptake and lysosomal sequestration of respiratory drugs in human alveolar macrophages," *Mol. Pharm.*, vol. 14, no. 4, pp. 1033–1046, 2017.

[38] B. Forbes *et al.*, "Challenges in inhaled product development and opportunities for open innovation," *Adv. Drug Deliv. Rev.*, vol. 63, no. 1–2, pp. 69–87, 2011.

[39] P. Bäckman, S. Arora, W. Couet, B. Forbes, W. de Kruijf, and A. Paudel, "Advances in experimental and mechanistic computational models to understand pulmonary exposure to inhaled drugs," *Eur. J. Pharm. Sci.*, no. October, pp. 0–1, 2017.

[40] H. M. Jones and K. Rowland-Yeo, "Basic Concepts in Physiologically Based Pharmacokinetic Modeling in Drug Discovery and Development," *CPT Pharmacometrics Syst. Pharmacol.*, vol. 2, no. 8, p. e63, 2013.

[41] M. Germani *et al.*, "Evaluation of a basic physiologically based pharmacokinetic model for simulating the first-time-in-animal study," *Eur. J. Pharm. Sci.*, vol. 31, no. 3–4, pp. 190–201, 2007.

[42] M. Jamei, "Recent Advances in

Development and Application of Physiologically-Based Pharmacokinetic (PBPK) Models: a Transition from Academic Curiosity to Regulatory Acceptance," *Curr. Pharmacol. Reports*, vol. 2, no. 3, pp. 161–169, 2016.

[43] M. Rowland, C. Peck, and G. Tucker, "Physiologically-Based Pharmacokinetics in Drug Development and Regulatory Science," *Annu. Rev. Pharmacol. Toxicol.*, vol. 51, no. 1, pp. 45–73, 2011.

[44] S. K. B. Sy, X. Wang, and H. Derendorf, "Introduction to Pharmacometrics and Quantitative Pharmacology with an Emphasis on Physiologically Based Pharmacokinetics," in *Applied Pharmacometrics*, Springer, 2014, pp. 1–57.

[45] S. Grandoni, N. Cesari, G. Brogin, and P. Puccini, "Building in-house PBPK modelling tools for oral drug administration from literature information," *Admet Dmpk*, vol. 7, no. 1, pp. 4–21, 2019.

[46] L. B. Sheiner, "Population modelling in drug development," *Stat. Methods Med. Res.*, vol. 8, pp. 183–193, 1999.

[47] R. Hendrickx *et al.*, "Translational model to predict pulmonary pharmacokinetics and efficacy in man for inhaled bronchodilators," *CPT Pharmacometrics Syst. Pharmacol.*, no. November, pp. 1–11, 2017.

[48] M. Caniga *et al.*, “Preclinical Experimental and Mathematical Approaches for Assessing Effective Doses of Inhaled Drugs, Using Mometasone to Support Human Dose Predictions.,” *J. Aerosol Med. Pulm. Drug Deliv.*, vol. 29, no. 4, pp. 362–377, 2016.

[49] E. Boger *et al.*, “Systems Pharmacology Approach for Prediction of Pulmonary and Systemic Pharmacokinetics and Receptor Occupancy of Inhaled Drugs,” *CPT Pharmacometrics Syst. Pharmacol.*, vol. 5, no. 4, pp. 201–210, 2016.

[50] E. Boger and M. Fridén, “Physiologically Based Pharmacokinetic/Pharmacodynamic Modeling Accurately Predicts the Better Bronchodilatory Effect of Inhaled Versus Oral Salbutamol Dosage Forms,” *J. Aerosol Med. Pulm. Drug Deliv.*, vol. 32, no. 1, pp. 1–12, 2018.

[51] S. Goldstein, “ Clinical efficacy and safety of anticholinergic therapies in pediatric patients ,” *Ther. Clin. Risk Manag.*, vol. Volume 15, pp. 437–449, 2019.

[52] E. Boger and O. Wigström, “A Partial Differential Equation Approach to Inhalation Physiologically Based Pharmacokinetic Modeling,” *CPT Pharmacometrics Syst. Pharmacol.*, vol. 7, no. 10, pp. 638–646, 2018.

[53] CERTARA, “Simulating Drug Absorption

Using the Simcyp Simulator." [Online]. Available: https://www.certara.com/software/physiologically-based-pharmacokinetic-modeling-and-simulation/simcyp-simulator/absorption/?ap%5B0%5D=PBPK. [Accessed: 23-May-2019].

[54] H. M. Jones, N. Parrott, K. Jorga, and T. Lavé, "A novel strategy for physiologically based predictions of human pharmacokinetics," *Clin. Pharmacokinet.*, vol. 45, no. 5, pp. 511–542, 2006.

[55] H. M. Jones, I. B. Gardner, and K. J. Watson, "Modelling and PBPK Simulation in Drug Discovery," *AAPS J.*, vol. 11, no. 1, pp. 155–166, 2009.

[56] A. N. Edginton, F. P. Theil, W. Schmitt, and S. Willmann, "Whole body physiologically-based pharmacokinetic models: their use in clinical drug development," *Expert Opin. Drug Metab. Toxicol.*, vol. 4, pp. 1143–1152, 2008.

[57] Y. S. Jeong, C. S. Yim, H. M. Ryu, C. K. Noh, Y. K. Song, and S. J. Chung, "Estimation of the minimum permeability coefficient in rats for perfusion-limited tissue distribution in whole-body physiologically-based pharmacokinetics," *Eur. J. Pharm. Biopharm.*, vol. 115, pp. 1–17, 2017.

[58] P. Poulin and F.-P. Theil, "Prediction of Pharmacokinetics Prior to In Vivo Studies.

II. Generic Physiologically Based Pharmacokinetic Models of Drug Disposition," *J. Pharm. Sci.*, 2002.

[59] S. A. Peters, *Physiologically-based pharmacokinetic (PBPK) modeling and simulations : principles, methods, and applications in the pharmaceutical industry*. Hoboken, New Jersey: John Wiley & Sons, Inc., 2012.

[60] B. Agoram, W. S. Woltosz, and M. B. Bolger, "Predicting the impact of physiological and biochemical processes on oral drug bioavailability," *Adv. Drug Deliv. Rev.*, vol. 50, no. SUPPL. 1, 2001.

[61] R. P. Brown, M. D. Delp, S. L. Lindstedt, L. R. Rhomberg, and R. P. Beliles, "PHYSIOLOGICAL PARAMETER VALUES FOR PHYSIOLOGICALLY BASED PHARMACOKINETIC MODELS," *Toxicol. Ind. Health*, vol. 13, no. 4, pp. 407–484, 1997.

[62] U. S. Environmental Protection Agency (EPA), "Approaches for the Application of Physiologically Based Pharmacokinetic (PBPK) Models and Supporting Data in Risk Assessment," 2006.

[63] B. Davies and T. Morris, "Physiologically Parameters in Laboratory Animals and Humans," *Pharm. Res.*, vol. 10, no. 7, pp. 1093–1095, 1993.

[64] R. Kawai, D. Mathew, C. Tanaka, and M.

Rowland, “Physiologically Based Pharmacokinetics of Cyclosporine A: Extension to Tissue Distribution Kinetics in Rats and Scale-up to Human,” *J. Pharmacol. Exp. Ther.*, vol. 287, no. 2, pp. 457–468, 1998.

[65] M. D. Delp, R. O. Manning, J. V Bruckner, and R. B. Armstrong, “Distribution of cardiac output during diurnal changes of activity in rats.,” *Am. J. Physiol.*, vol. 261, no. 5 Pt 2, pp. H1487-93, 1991.

[66] A. Rostami-Hodjegan, “Physiologically based pharmacokinetics joined with in vitro-in vivo extrapolation of ADME: A marriage under the arch of systems pharmacology,” *Clin. Pharmacol. Ther.*, vol. 92, no. 1, pp. 50–61, 2012.

[67] X. J. H. Pepin, T. R. Flanagan, D. J. Holt, A. Eidelman, D. Treacy, and C. E. Rowlings, “Justification of drug product dissolution rate and drug substance particle size specifications based on absorption PBPK modeling for lesinurad immediate release tablets,” *Mol. Pharm.*, vol. 13, no. 9, pp. 3256–3269, 2016.

[68] R. J. Hintz and K. C. Johnson, “The effect of particle size distribution on dissolution rate and oral absorption,” *Int J Pharm*, vol. 51, no. 1, pp. 9–17, 1989.

[69] S. A. Peters, “Evaluation of a Generic Physiologically Based Pharmacokinetic Model for Lineshape Analysis,” *Clin*

Pharmacokinet, vol. 47, no. 4, pp. 261–275, 2008.

[70] M. Gertz, A. Harrison, J. B. Houston, and A. Galetin, "Prediction of Human Intestinal First-Pass Metabolism of 25 CYP3A Substrates from In Vitro Clearance and Permeability Data ABSTRACT :," vol. 38, no. 7, pp. 1147–1158, 2010.

[71] J. Yang, M. Jamei, K. R. Yeo, G. T. Tucker, and A. Rostami-Hodjegan, "Prediction of intestinal first-pass drug metabolism.," *Curr. Drug Metab.*, vol. 8, no. 7, pp. 676–684, 2007.

[72] P. Poulin and F. P. Theil, "Prediction of pharmacokinetics prior to in vivo studies. 1. Mechanism-based prediction of volume of distribution," *J. Pharm. Sci.*, 2002.

[73] T. Rodgers, D. Leahy, and M. Rowland, "Physiologically based pharmacokinetic modeling 1: Predicting the tissue distribution of moderate-to-strong bases," *J. Pharm. Sci.*, vol. 94, no. 6, pp. 1259–1276, 2005.

[74] T. Rodgers and M. Rowland, "Physiologically-based Pharmacokinetic Modeling 2: Predicting the tissue distribution of acids, very weak bases, neutrals and zwitterions," *J. Pharm. Sci.*, vol. 96, no. 11, pp. 3153–3154, 2007.

[75] G. R. Wilkinson and D. G. Shand, "Commentary: a physiological approach to

hepatic drug clearance," *Clin. Pharmacol. Ther.*, pp. 377–390, 1975.

[76] R. S. Obach, "Prediction of human clearance of twenty-nine drugs from hepatic microsomal intrinsic clearance data: An examination of in vitro half-life approach and nonspecific binding to microsomes," *Drug Metab. Dispos.*, vol. 27, no. 11, pp. 1350–1359, 1999.

[77] J. E. Sager, J. Yu, I. Ragueneau-Majlessi, and N. Isoherranen, "Physiologically Based Pharmacokinetic (PBPK) Modeling and Simulation Approaches: A Systematic Review of Published Models, Applications, and Model Verification.," *Drug Metab. Dispos.*, vol. 43, no. 11, pp. 1823–37, 2015.

[78] European Medicines Agency, "Guideline on the reporting of physiologically based pharmacokinetic (PBPK) modelling and simulation," London (UK), 2018.

[79] Food and Drug Administration (FDA) and Center for Drug Evaluation and Research (CDER), "Physiologically Based Pharmacokinetic Analyses — Format and Content Guidance for industry," 2018.

[80] I. Kocic *et al.*, "A case study on the in silico absorption simulations of levothyroxine sodium immediate-release tablets," *Biopharm. Drug Dispos.*, vol. 33, no. 3, pp. 146–159, 2012.

[81] A. Stojkovic, J. Parojcic, Z. Djuric, and O.

I. Corrigan, “A Case Study of In Silico Modelling of Ciprofloxacin Hydrochloride/Metallic Compound Interactions,” *AAPS PharmSciTech*, vol. 15, no. 2, pp. 270–278, 2014.

[82] R. H. Manzo, M. E. Olivera, G. L. Amidon, V. P. Shah, J. B. Dressman, and D. M. Barends, “Biowaiver Monographs for Immediate Release Sold Oral Dosage Forms: Amitriptyline Hydrocloride,” *J. Pharm. Sci.*, vol. 95, no. 5, pp. 966–973, 2006.

[83] S. K. Gupta, J. Shah, D. Guinta, and S. Hwang, “Multiple-dose pharmacokinetics and pharmacodynamics of OROS and immediate-release amitriptyline hydrochloride formulations,” *J. Clin. Pharmacol.*, vol. 38, no. 1, pp. 60–67, 1998.

[84] M. V. S. Varma *et al.*, “Physicochemical space for optimum oral bioavailability: Contribution of human intestinal absorption and first-pass elimination,” *J. Med. Chem.*, vol. 53, no. 3, pp. 1098–1108, 2010.

[85] M. F. Rasool, F. Khalil, and S. Läer, “Predicting stereoselective disposition of carvedilol in adult and pediatric chronic heart failure patients by incorporating pathophysiological changes in organ blood flows-A physiologically based pharmacokinetic approach,” *Drug Metab. Dispos.*, vol. 44, no. 7, pp. 1103–1115, 2016.

[86] P. Paixão, L. F. Gouveia, and J. A. G. Morais, “Prediction of the in vitro permeability determined in Caco-2 cells by using artificial neural networks,” *Eur. J. Pharm. Sci.*, vol. 41, no. 1, pp. 107–117, 2010.

[87] V. Law *et al.*, “DrugBank 4.0: Shedding new light on drug metabolism,” *Nucleic Acids Res.*, vol. 42, no. D1, pp. 1091–1097, 2014.

[88] M. Davies *et al.*, “ChEMBL web services: Streamlining access to drug discovery data and utilities,” *Nucleic Acids Res.*, vol. 43, no. W1, pp. W612–W620, 2015.

[89] S. G. Dahl and R. E. Strandjord, “Pharmacokinetics of chlorpromazine after single and chronic dosage,” *Clin. Pharmacol. Ther.*, vol. 21, no. 4, pp. 437–448, 1977.

[90] L. M. Berry, C. Li, Z. Zhao, and B. E. T. Al, “Species Differences in Distribution and Prediction of Human Vss from Preclinical Data,” *Drug Metab. Dispos.*, vol. 39, no. 11, pp. 2103–2116, 2011.

[91] B. Ledergerber, J. D. Bettex, B. Joos, M. Flepp, and R. Lüthy, “Effect of standard breakfast on drug absorption and multiple-dose pharmacokinetics of ciprofloxacin,” *Antimicrob. Agents Chemother.*, vol. 27, no. 3, pp. 350–352, 1985.

[92] P. Glue, C. Gale, D. B. Menkes, and N.

Hung, “Evaluation of bioequivalence between clozapine suspension and tablet formulations: A multiple-dose, fed and fasted study,” *Clin. Drug Investig.*, vol. 32, no. 11, pp. 723–727, 2012.

[93] S. Neuhoff, K. R. Yeo, Z. Barter, M. Jamei, D. B. Turner, and A. Rostami-Hodjegan, “Application of permeability-limited physiologically-based pharmacokinetic models: Part I-digoxin pharmacokinetics incorporating P-glycoprotein-mediated efflux,” *J. Pharm. Sci.*, vol. 102, no. 9, pp. 3145–3160, 2013.

[94] D. Moj *et al.*, “Clarithromycin, Midazolam, and Digoxin: Application of PBPK Modeling to Gain New Insights into Drug–Drug Interactions and Co-medication Regimens,” *AAPS J.*, vol. 19, no. 1, pp. 298–312, 2017.

[95] T. Rodgers and M. Rowland, “Mechanistic approaches to volume of distribution predictions: Understanding the processes,” *Pharm. Res.*, vol. 24, no. 5, pp. 918–933, 2007.

[96] A. Loffreda *et al.*, “Bioequivalence assessment of two different tablet formulations of diltiazem after single and repeated doses in healthy subjects,” *Curr Med Res Opin*, vol. 15, no. 1, pp. 53–61, 1999.

[97] T. Legg, E. Paluch, and S. Jayawardena, “Single- and Multiple-Dose

Pharmacokinetics of Immediate-Release/Extended-Release Ibuprofen Tablets," *Clin. Pharmacol. Drug Dev.*, vol. 6, no. 1, pp. 36–43, 2017.

[98] V. Lukacova, W. S. Woltosz, and M. B. Bolger, "Prediction of Modified Release Pharmacokinetics and Pharmacodynamics from In Vitro, Immediate Release, and Intravenous Data," *AAPS J.*, vol. 11, no. 2, pp. 323–334, 2009.

[99] F. Fenneteau, P. Poulin, and F. Nekka, "Physiologically Based Predictions of the Impact of Inhibition of Intestinal and Hepatic Metabolism on Human Pharmacokinetics of CYP3A Substrates," *J. Pharm. Sci.*, vol. 99, no. 1, pp. 486–514, 2009.

[100] H. H. T. Kupferschmidt, H. R. Ha, W. H. Ziegler, P. J. Meier, and S. Krahenbuhl, "Interaction between grapefruit juice and midazolam in humans," *Clin. Pharmacol. Ther.*, vol. 58, no. 1, pp. 20–28, 1995.

[101] P. Crevat-Pisano, S. Dragna, C. Granthil, P. Coassolo, J. P. Cano, and G. Francois, "Plasma concentrations and pharmacokinetics of midazolam during anaesthesia," *J. Pharm. Pharmacol.*, vol. 38, no. 8, pp. 578–582, 1986.

[102] J. Y. Dupuis, H. J. Nathan, and S. Laganiere, "Intravenous nifedipine for prevention of myocardial ischaemia after coronary revascularization," *Can. J.*

Anaesth., vol. 39, no. 10, pp. 1012–1022, 1992.

[103] L. M. Almond *et al.*, "Prediction of drug-drug interactions arising from CYP3A induction using a physiologically based dynamic models," *Drug Metab. Dispos.*, vol. 44, no. 6, pp. 821–832, 2016.

[104] C. Wagner, K. Thelen, S. Willmann, A. Selen, and J. B. Dressman, "Utilizing in vitro and PBPK tools to link ADME characteristics to plasma profiles: Case example nifedipine immediate release formulation," *J. Pharm. Sci.*, vol. 102, no. 9, pp. 3205–3219, 2013.

[105] K. Thelen, E. Jantratid, J. B. Dressman, J. Lippert, and S. Willmann, "Analysis of Nifedipine Absorption from Soft Gelatin Capsules Using PBPK Modeling and Biorelevant Dissolution Testing," *J. Pharm. Sci.*, vol. 99, no. 6, pp. 2899–2904, 2010.

[106] T. Heimbach, B. Xia, T. Lin, and H. He, "Case Studies for Practical Food Effect Assessments across BCS/BDDCS Class Compounds using In Silico, In Vitro, and Preclinical In Vivo Data," *AAPS J.*, vol. 15, no. 1, pp. 143–158, 2013.

[107] A. Villiger, C. Stillhart, N. Parrott, and M. Kuentz, "Using Physiologically Based Pharmacokinetic (PBPK) Modelling to Gain Insights into the Effect of Physiological Factors on Oral Absorption in Paediatric Populations," *AAPS J.*, vol. 18, no. 4, pp.

933–947, 2016.

[108] P. J. Bungay, S. Tweedy, D. C. Howe, K. R. Gibson, H. M. Jones, and N. M. Mount, “Preclinical and Clinical Pharmacokinetics of PF-02413873 , a Nonsteroidal Progesterone Receptor Antagonist ABSTRACT :,” vol. 39, no. 8, pp. 1396–1405, 2011.

[109] R. Jayaraman *et al.*, “Preclinical metabolism and disposition of SB939 (pracinostat), an orally active histone deacetylase inhibitor, and prediction of human pharmacokinetics,” *Drug Metab. Dispos.*, vol. 39, no. 12, pp. 2219–2232, 2011.

[110] L. I. Kajosaari, J. Laitila, P. J. Neuvonen, and J. T. Backman, “Metabolism of repaglinide by CYP2C8 and CYP3A4 in vitro: Effect of fibrates and rifampicin,” *Basic Clin. Pharmacol. Toxicol.*, vol. 97, no. 4, pp. 249–256, 2005.

[111] Z. Mandić and V. Gabelica, “Ionization, lipophilicity and solubility properties of repaglinide,” *J. Pharm. Biomed. Anal.*, vol. 41, no. 3, pp. 866–871, 2006.

[112] M. Niemi, L. I. Kajosaari, M. Neuvonen, J. T. Backman, and P. J. Neuvonen, “The CYP2C8 inhibitor trimethoprim increases the plasma concentrations of repaglinide in healthy subjects,” *Br. J. Clin. Pharmacol.*, vol. 57, no. 4, pp. 441–447, 2004.

[113] Z. W. Gao *et al.*, "Preclinical pharmacokinetics of TPN729MA, a novel PDE5 inhibitor, and prediction of its human pharmacokinetics using a PBPK model," *Acta Pharmacol. Sin.*, vol. 36, no. 12, pp. 1528–1536, 2015.

[114] G. Allan *et al.*, "Pre-clinical pharmacokinetics of UK-453,061, a novel non-nucleoside reverse transcriptase inhibitor (NNRTI), and use of in silico physiologically based prediction tools to predict the oral pharmacokinetics of UK-453,061 in man," *Xenobiotica*, vol. 38, no. 6, pp. 620–640, 2008.

[115] J. McEwen, C. Durnin, M. E. T. McMurdo, and T. A. Moreland, "Sustained-Release Verapamil: Multiple-Dose Pharmacokinetic Comparison of 120-mg and 240-mg Tablets and the Effect of Halving a 240-mg Tablet," *J. Cardiovasc. Pharmacol.*, pp. 57–59, 1989.

[116] T. M. Ludden, "Non linear pharmacokinetics: clinical implications," *Clin. Pharmacokinet.*, vol. 20, pp. 429–446, 1991.

[117] C. Y. Wu and L. Z. Benet, "Predicting drug disposition via application of BCS: Transport/absorption/ elimination interplay and development of a biopharmaceutics drug disposition classification system," *Pharm. Res.*, vol. 22, no. 1, pp. 11–23, 2005.

[118] E. Boger and M. Fridén, “Physiologically Based Pharmacokinetic/Pharmacodynamic Modeling Accurately Predicts the Better Bronchodilatory Effect of Inhaled Versus Oral Salbutamol Dosage Forms,” *J. Aerosol Med. Pulm. Drug Deliv.*, vol. 32, no. 1, pp. 1–12, 2018.

[119] S. Grandoni, N. Cesari, N. Melillo, G. Brogin, P. Puccini, and P. Magni, “Development and evaluation of a PBPK model to study the pharmacokinetics of inhaled drugs in rats,” *PAGE. Abstr. Annu. Meet. Popul. Approach Gr. Eur.*, p. Abstr 9047, 2019.

[120] S. Grandoni, N. Cesari, G. Brogin, P. Puccini, and P. Magni, “Evaluating the inclusion of the particle size distribution in the lung dissolution model of a WB-PBPK model to describe the pharmacokinetics of inhaled polydisperse drugs,” *PAGE. Abstr. Annu. Meet. Popul. Approach Gr. Eur.*, p. Abstr 8549, 2018.

[121] N. Melillo, S. Grandoni, N. Cesari, G. Brogin, P. Puccini, and P. Magni, “Global sensitivity analysis of a physiologically based pulmonary absorption model,” *PAGE. Abstr. Annu. Meet. Popul. Approach Gr. Eur.*, p. Abstr 9072, 2019.

[122] J. P. Mitchell and M. W. Nagel, “Cascade Impactors for the Size Characterization of Aerosols from Medical Inhalers: Their Uses and Limitations,” *J. Aerosol Med.*, vol. 16,

no. 4, pp. 341–377, 2004.

[123] M. Stefani *et al.*, “Development of an In Vitro Solubility Test as a Tool for Predicting Lung Retention of Poorly Water Soluble Compounds,” *Drug Delivery to the Lungs*. Edinburgh, 2018.

[124] B. Forbes and C. Ehrhardt, “Human respiratory epithelial cell culture for drug delivery applications,” *Eur. J. Pharm. Biopharm.*, vol. 60, no. 2, pp. 193–205, 2005.

[125] C. Meindl, S. Stranzinger, N. Dzidic, and S. Salar-behzadi, “Permeation of Therapeutic Drugs in Different Formulations across the Airway Epithelium In Vitro,” pp. 1–19, 2015.

[126] N. R. Mathias, J. Timoszyk, P. I. Stetsko, J. R. Megill, and R. L. Smith, “Permeability Characteristics of Calu-3 Human Bronchial Epithelial Cells : In Vitro – In Vivo Correlation to Predict Lung Absorption in Rats,” vol. 10, no. 1, pp. 31–40, 2002.

[127] C. Bosquillon, M. Madlova, N. Patel, N. Clear, B. Forbes, and B. Forbes, “Comparison of Drug Transport in Pulmonary Absorption Models : Isolated Perfused rat Lungs , Respiratory Epithelial Cell Lines and Primary Cell Culture,” pp. 2532–2540, 2017.

[128] M. Madlova, C. Bosquillon, D. Asker, P. Dolezal, and B. Forbes, “In-vitro respiratory

drug absorption models possess nominal functional P-glycoprotein activity," pp. 293–301, 2009.

[129] W. Hofmann and B. Asgharian, "The effect of lung structure on mucociliary clearance and particle retention in human and rat lungs," *Toxicol. Sci.*, vol. 73, no. 2, pp. 448–456, 2003.

[130] J. Campbell *et al.*, "A preliminary regional PBPK model of lung metabolism for improving species dependent descriptions of 1,3-butadiene and its metabolites," *Chem. Biol. Interact.*, vol. 238, pp. 102–110, 2015.

[131] R. F. Phalen and O. G. Raabe, "The evolution of inhaled particle dose modeling: A review," *J. Aerosol Sci.*, vol. 99, pp. 7–13, 2016.

[132] M. D. S. Mendes, S. Neuhoff, H. Burt, C. Uk, and S. Division, "The MechP model - Mechanistic modelling of in- vitro bidirectional permeability studies and in vivo absorption of metoprolol," in *PAGE meeting 2018*, 2018.

[133] J. Eriksson, E. Sjögren, H. Thörn, K. Rubin, P. Bäckman, and H. Lennernäs, "Pulmonary absorption – estimation of effective pulmonary permeability and tissue retention of ten drugs using an ex vivo rat model and computational analysis," *Eur. J. Pharm. Biopharm.*, vol. 124, no. November 2017, pp. 1–12, 2018.

[134] K. R. Korzekwa, S. Nagar, J. Tucker, E. A. Weiskircher, S. Bhoopathy, and I. J. Hidalgo, “Models to predict unbound intracellular drug concentrations in the presence of transporters,” *Drug Metab. Dispos.*, vol. 40, no. 5, pp. 865–876, 2012.

[135] M. Sakagami, “In vivo, in vitro and ex vivo models to assess pulmonary absorption and disposition of inhaled therapeutics for systemic delivery,” *Adv. Drug Deliv. Rev.*, vol. 58, no. 9–10, pp. 1030–1060, 2006.

[136] B. Olsson *et al.*, “Pulmonary Drug Metabolism, Clearance, and Absorption,” in *Controlled Pulmonary Drug Delivery*, H. D. C. Smyth and A. J. Hickey, Eds. Springer, 2011, pp. 21–50.

[137] J. E. Hastedt *et al.*, “Scope and relevance of a pulmonary biopharmaceutical classification system AAPS/FDA/USP Workshop March 16-17th, 2015 in Baltimore, MD,” *AAPS Open*, vol. 2, no. 1, p. 1, 2016.

[138] N. A. Miller, M. B. Reddy, A. T. Heikkinen, V. Lukacova, and N. Parrott, “Physiologically Based Pharmacokinetic Modelling for First-In-Human Predictions: An Updated Model Building Strategy Illustrated with Challenging Industry Case Studies,” *Clin. Pharmacokinet.*, vol. 58, no. 6, pp. 727–746, 2019.

[139] C. Wagner *et al.*, “Application of physiologically based pharmacokinetic

(PBPK) modeling to support dose selection: Report of an FDA public workshop on PBPK," *CPT Pharmacometrics Syst. Pharmacol.*, vol. 4, no. 4, pp. 226–230, 2015.

[140] European Medicines Agency Committee for Medicinal Products for Human Use, "Guideline on strategies to identify and mitigate risks for first-in-human and early clinical trials with investigational medicinal products." London, 2018.

[141] J. Muddle *et al.*, "Predicting the Fine Particle Fraction of Dry Powder Inhalers Using Artificial Neural Networks," *J. Pharm. Sci.*, vol. 106, no. 1, pp. 313–321, 2017.

[142] "Budesonide/Formoterol Teva Annex I - Summary of Product Characteristics." European Commisison Union Register of medicinal products, 2016.

[143] L. Garcia-Contreras, "In Vivo Animal Models for Controlled-Release Pulmonary Drug Delivery," in *Controlled Pulmonary Drug Delivery*, H. D. C. Smyth and A. J. Hickey, Eds. Springer, 2011, p. 452.

[144] Z. E. Barter *et al.*, "Scaling Factors for the Extrapolation of In Vivo Metabolic Drug Clearance From In Vitro Data : Reaching a Consensus on Values of Human Micro-somal Protein and Hepatocellularity Per Gram of Liver," pp. 33–45, 2007.

[145] (CDER) Food and Drug Administration (FDA) and Center for Drug Evaluation and Research, “Physiologically Based Pharmacokinetic Analyses — Format and Content Guidance for industry,” 2018.

[146] A. Saltelli, S. Tarantola, F. Campolongo, and M. Ratto, *Sensitivity Analysis in Practice: A Guide to Assessing Scientific Models*. John Wiley & Sons Inc., 2004.

[147] U. S. Environmental Protection Agency (EPA), “Uncertainty and Variability.” [Online]. Available: https://www.epa.gov/expobox/uncertainty-and-variability. [Accessed: 10-Sep-2019].

[148] A. Saltelli *et al.*, *Global Sensitivity Analysis. The Primer*. John Wiley & Sons Inc., 2008.

[149] A. Saltelli, “Making best use of model evaluations to compute sensitivity indices,” *Comput. Phys. Commun.*, vol. 145, pp. 280–297, 2002.

[150] I. M. Sobol, “Sensitivity Estimates for Nonlinear Mathematical Models,” *Math. Model. Comput. Exp.*, vol. 1, pp. 407–414, 1993.

[151] N. Melillo, L. Aarons, P. Magni, and A. S. Darwich, “Variance based global sensitivity analysis of physiologically based pharmacokinetic absorption models for BCS I–IV drugs,” *J. Pharmacokinet. Pharmacodyn.*, vol. 46, no. 1, pp. 27–42,

2019.

[152] A. Fioni *et al.*, “Investigation of Lung Pharmacokinetic of the Novel PDE4 Inhibitor CHF6001 in Preclinical Models: Evaluation of the PreciseInhale Technology,” *J. Aerosol Med. Pulm. Drug Deliv.*, vol. 31, no. 1, pp. 61–70, 2018.

[153] G. E. B. Archer, A. Saltelli, and I. M. Sobol, “Sensitivity measures, anova-like techniques and the use of bootstrap,” *J. Stat. Comput. Simul.*, vol. 58, no. 2, pp. 99–120, 1997.

[154] R. L. Iman and S. C. Hora, “A Robust Measure of Uncertainty Importance for Use in Fault Tree System Analysis,” *Risk Anal.*, vol. 10, no. 401–406, 1990.

[155] N. Teuscher, “Mean Residence Time (MRT): Understanding How Long Drug Molecules Stay in the Body,” *The Certara Blog: PK/PD Modeling & Simulation*, 2013. .

[156] G. L. Amidon, H. Lennernäs, V. P. Shah, and J. R. Crison, “A Theorethical Bases for a Biopharmaceutic Drug Classification: The Correlation of in Vitro Drug Product Dissolution and in Vivo Bioavailability,” *Pharm. Res.*, vol. 3, 1995.

[157] B. Srinivasan *et al.*, “TEER measurement techniques for in vitro barrier model systems,” *J. Lab. Autom.*, vol. 20, no. 2, pp. 107–126, 2015.

[158] "Clinical Pharmacokinetic Noncompartmental Data Analysis Plan for A Phase 1 Clinical Trial to Evaluate the Plasma Pharmacokinetics, Safety, and Tolerability of a Single Oral Dose of Zoliflodacin in Healthy Male and Female Subjects," Rockville, Maryland USA, 2018.

[159] J. Gabrielsson and D. Weiner, "Non Compartmental Analysis," in *Journal of Computational Toxicology: Volume I, Methods in Molecular Biology*, B. Reisfeld and A. N. Mayeno, Eds. Springer, 2012, pp. 377–389.

List of Publications

Articles in peer reviewed journals

- **Grandoni S.**, N. Cesari, G. Brogin, P. Puccini and Magni P., "*Building in-house PBPK modelling tools for oral drug administration from literature information*," Admet & Dmpk, vol. 7, no. 1, pp. 4–21, 2019.

Articles submitted for publication

- **Grandoni S.**, Cesari N., Melillo N., Brogin G., Puccini P. and Magni P., "*Development and evaluation of a PBPK modelling framework for inhaled drugs PK studies from the early stages of drug development*" (2019), ready to submit for publication.

- Melillo N., **Grandoni S.**, Cesari N., Brogin G., Puccini P. and Magni P., *Global Sensitivity Analysis of a physiological model for pulmonary absorption of inhaled compounds* (2019), ready to submit, ready to submit for publication.

Contributions to conference proceedings

- **Grandoni S.**, Bigoni G., Cesari N., Puccini P., Brogin G. and Magni P., "*Evaluation of a minimal WB-PBPK platform supporting*

different routes of administration", PAGE Meeting 2017.

- **Grandoni S.**, Cesari N., Brogin G., Puccini P., Magni P., "*Evaluating the inclusion of the particle size distribution in the lung dissolution model of a WB-PBPK model to describe the pharmacokinetics of inhaled polydisperse drugs*", PAGE Meeting 2018.

- Bartolucci R., Lavezzi S.M., Tosca E.M, Melillo N., **Grandoni S.**, Borella E., Pasotti L., De Nicolao G., Magni P., "*Evaluation of software tools for Bayesian estimation on population models: an update based on current software version*", PAGE Meeting 2018.

- **Grandoni S.**, Cesari N., Brogin G., Puccini P., Magni P., "*Simulating pharmacokinetic profiles in different species through PBPK modelling: assessment of a MATLAB-based platform",* National Bioengineering Congress (GNB) 2018.

- **Grandoni S.**, Cesari N., Melillo N., Brogin G., Puccini P., Magni P., "*Development and evaluation of a PBPK model to study the pharmacokinetics of inhaled drugs in rats*", congress PAGE meeting 2019.

- Melillo N., **Grandoni S.**, Cesari N., Brogin G., Puccini P., Magni P., "*Global sensitivity analysis of a physiologically based pulmonary absorption model"*, congress PAGE meeting 2019.

- Bartolucci R., **Grandoni S.**, Melillo N., Nicora G., Sauta E., Tosca E.M., Magni P., *"Artificial intelligence and machine learning: just a hype or a new opportunity for Pharmacometrics?",* congress PAGE meeting 2019.

- Melillo N., **Grandoni S.**, Cesari N., Brogin G., Puccini P. and Magni P., "*Variance based global sensitivity analysis of a mechanistic model for the pharmacokinetics of inhaled compounds in rats*", Ninth International Conference on Sensitivity Analysis of Model Output (SAMO), 2019.

Silvia Grandoni
silvia.grandoni01@universitadipavia.it

Università degli Studi di Pavia
via Ferrata, 5
27100 Pavia, Italy